E-Glider: Active Electrostatic Flight for Airless Body Exploration[1]

Phase I Final Report - January 2017

by Marco B. Quadrelli[2]

Henry Garrett
Julie Castillo
Adrian Stoica
Hiro Ono
Hanspeter Schaub
Caleb Christianson
Shota Kikuchi

Dario Lusso
Simone Fasiello

FINAL REPORT

Early Stage Innovation

NASA Innovative Advanced Concepts (NIAC)

E-Glider: Active Electrostatic Flight for Airless Body Exploration[3]

Marco B. Quadrelli (Principal Investigator, JPL)

Co-Investigators: Henry Garrett, Julie Castillo,
Adrian Stoica, Hiro Ono (Jet Propulsion Laboratory)
Hanspeter Schaub (University of Colorado Boulder)

Interns: Caleb Christianson (UCSD), Shota Kikuchi (University of Tokyo,
Japan), Dario Lusso (Polytechnic of Torino, Italy), Simone Fasiello
(Polytechnic of Torino, Italy)

Jet Propulsion Laboratory
California Institute of Technology

January 2017

Acknowledgements

Executive Summary

The environment near the surface of asteroids, comets, and the Moon is electrically charged due to the Sun's photoelectric bombardment and lofting dust, which follows the Sun illumination as the body spins. Charged dust is ever present, in the form of dusty plasma, even at high altitudes, following the solar illumination. If a body with high surface resistivity is exposed to the solar wind and solar radiation, sun-exposed areas and shadowed areas become differentially charged. The E-Glider (Electrostatic Glider) is an enabling capability for operation at airless bodies, a solution applicable to many types of in-situ mission concepts, which leverages the natural environment. With the E-Glider, we transform a problem (spacecraft charging) into an enabling technology, i.e. a new form of mobility in microgravity environments using new mechanisms and maneuvering based on the interaction of the vehicle with the environment. Consequently, *the vision of the E-Glider is to enable global scale airless body exploration with a vehicle that uses, instead of avoids, the local electrically charged environment.* This platform directly addresses the "All Access Mobility" Challenge, one of the NASA's Space Technology Grand Challenges. Exploration of comets, asteroids, moons and planetary bodies is limited by mobility on those bodies. The lack of an atmosphere, the low gravity levels, and the unknown surface soil properties pose a very difficult challenge for all forms of know locomotion at airless bodies. This E-Glider levitates by extending thin, charged, appendages, which are also articulated to direct the levitation force in the most convenient direction for propulsion and maneuvering. The charging is maintained through continuous charge emission. It lands, wherever it is most convenient, by retracting the appendages or by firing a cold-gas thruster, or by deploying an anchor. The wings could be made of very thin Au-coated Mylar film, which are electrostatically inflated, and would provide the lift due to electrostatic repulsion with the naturally charged asteroid surface. Since the E-glider would follow the Sun's illumination, the solar panels on the vehicle would constantly charge a battery. Further articulation at the root of the lateral strands or inflated membrane wings, would generate a component of lift depending on the articulation angle, hence a selective maneuvering capability which, to all effects, would lead to electrostatic (rather than aerodynamic) flight. Preliminary calculations indicate that a 1 kg mass can be electrostatically levitated in a microgravity field with a 2 m diameter electrostatically inflated ribbon structure at 19kV, hence the need for a "balloon-like" system. Due to the high density and the photo-electron sheath and associate small Debye length, significant power is required to levitate even a few kilograms. The power required is in the kilo-Watt range to maintain a constant charge level.

TABLE OF CONTENTS

LIST OF FIGURES

LIST OF TABLES

Summary Chart

E-Glider: Active Electrostatic Flight for Airless Body Exploration

Marco Quadrelli[1], Henry Garrett[1], Hiro Ono[1], Adrian Stoica[1], Julie Castillo[1], Hanspeter Schaub[2]
[1]Jet Propulsion Laboratory,[2]U. of Colorado

Concept The environment near the surface of airless bodies (asteroids, comets, moons) is electrically charged due to Sun's photoelectric bombardment. Charged dust is ever present, even at high altitudes (dust fountains), following the Sun's illumination. We envisage the global scale exploration of airless bodies by a gliding vehicle that levitates by experiencing electrostatic lift by its interaction with the naturally charged particle environment. This Electrostatic Glider (E-Glider) lifts off by extending thin, charged, appendages (like some flying spiders on Earth), which are also articulated to direct the levitation force in the most convenient direction for propulsion and maneuvering. It lands, wherever it is most convenient, by retracting the appendages or by thruster/anchor.

Benefits This study will:
1. Open new avenues for low-cost, persistent, reconnaissance of airless bodies without interacting with the surface for locomotion, leading to effective prospecting of mineral-rich asteroids;
2. Provide a framework for the effective use of the coupling between the naturally existing electrostatic environment and gossamer extended surfaces as a novel mechanism for locomotion and exploration in airless bodies;
3. Enable new sampling techniques for in-situ spatial and temporal sensing of the environment on airless bodies, and
4. Lead to new concepts for robotic exploration of planets, natural satellites, and other bodies by taking advantage of existing natural plasma and charge distributions.

Study Approach: Analyze a mission scenario involving an electrostatic glider maneuvering above the surface of a reference asteroid, such as Itokawa:
(1) Study the known environmental conditions of the electrostatics of the lofting dust on the surface of airless bodies;
(2) Determine E-glider vehicle configurations, and specific methods for energy harvesting, mobility, communication, survivability, and instruments for in-situ sampling of dust and surface regolith; and
(3) Explore the possibility of generating (in Phase II) physical simulations with approximate models of the E-glider, including their energy harvesting, mobility, and comm. mechanisms.

Artist view of E-Glider on airless body

Evaluation Notes

1. Introduction

The E-Glider (Electrostatic Glider) is an enabling capability for exploration of airless bodies, a solution applicable to many types of in-situ mission concepts, which leverages, instead of avoiding, the natural environment.   We envisage the global scale exploration of airless bodies by a gliding vehicle that experiences its own electrostatic lift by its interaction with the naturally charged particle environment near the surface. This E-Glider levitates by extending thin, charged, appendages (like some flying spiders on Earth), which are also articulated to direct the levitation force in the most convenient direction for propulsion and maneuvering. It lands, wherever it is most convenient, by retracting the appendages or by firing a cold-gas thruster, or by deploying an anchor. See Figure 1. With the E-Glider, we transform a problem (spacecraft charging) into an enabling technology, i.e. a new form of mobility in microgravity environments using new mechanisms and maneuvering based on the interaction of the vehicle with the environment. Consequently, the vision of the E-Glider is to *enable global scale airless body exploration with a vehicle that uses, instead of avoids, the local electrically charged environment*.

The use of electrostatic levitation for circumnavigating a Solar System body is still unexplored. A mission based on an E-Glider would truly be a very exciting one, as it would be the first asteroid circumnavigation of an airless body by electrostatic forces, opening new avenues for low-cost, persistent, reconnaissance of airless bodies, leading to effective global scale prospecting of mineral-rich asteroids.
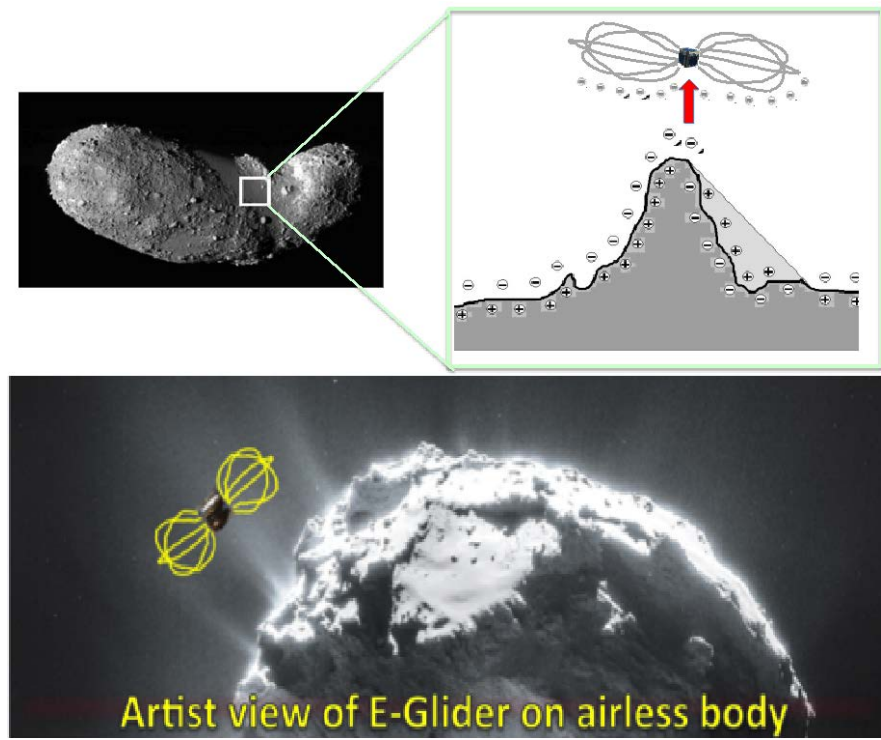
Figure 1. *The E-Glider (electrostatic Glider) is a small vehicle that levitates above the surface of an asteroid after extending strands of metallic film, forming the wings, so that it becomes "airborne", but in the electrostatic vacuum lofting around the asteroid. By articulating the wings, the E-Glider can now hover, and maneuver around, without touching the surface. It is the first circumnavigation of an airless body by electrostatic forces, opening new avenues for low-cost, persistent, reconnaissance of airless bodies, leading to effective global scale prospecting of mineral-rich asteroids.*

To our knowledge, the E-Glider concept has never been explored, and no other previous NIAC task has explored a concept similar to the E-Glider. Another NIAC task on the *Electrostatic Sail* (Heliopause Electrostatic Rapid Transit System (HERTS), 2014), which leverages electrostatics for interplanetary trajectory propulsion (like a solar sail), shares some similarities, whereas the E-Glider is focused on a new form of locomotion at airless bodies. NIAC 2005 *Analysis of a Lunar Base Electrostatic Radiation Shield Concept* and NIAC 2014 *Meeting the Grand Challenge of Protecting Astronaut's Health: Electrostatic Active Space Radiation Shielding for Deep Space Missions* explored the use of electrostatic fields for radiation shielding, but not for locomotion. NIAC 2004 *Optimal*

Navigation in a Plasma Medium proposed an innovative way to navigate in the space plasma using magnetic fields, but not electrostatically inflated structures. NIAC 2006 *Tailored Force Fields* included electrostatic forces as manipulation technology for space construction, but not for locomotion.

1.1 Benefits

Locomotion in micro-gravity is currently done with hoppers, or micro-gripper locomotion, which depend on having sufficient friction against the unknown surface [Yoshida2009, Quadrelli2012, Parness2011, Seeni2010]. Except for hoppers and micro-grippers, which use momentum exchange or mechanical forces to move, no other solutions exist at the present time. E-Glider uses the local environment to its advantage, and keeps the vehicle safe while it conducts its science mission away from the surface. The E-Glider lifts off by extending its electrostatic wings, i.e. thin, charged, appendages, which like the spiders on Earth, mimics Nature, harvests and uses the electrostatic energy abundantly present in the local environment, and it starts the new era of "Solar System exploration by electrostatic flight". The use of electro-static levitation for circumnavigating a Solar System body is still unexplored. Our vision is to develop an enabling capability for operation at airless bodies, a solution applicable to many types of in-situ mission concepts, which leverages the natural environment. A mission based on an E-Glider would truly be a very exciting one, as it would be the first asteroid circumnavigation of an airless body by electrostatic forces, opening new avenues for low-cost, persistent, reconnaissance of air-less bodies, leading to effective global scale prospecting of mineral-rich asteroids.

Exploration of comets, asteroids, and moons (e.g., Phobos, Deimos, Enceladus) is limited by mobility on those bodies [Quadrelli2013]. Current robotic [Seeni2010] and human systems [Abell2012] cannot safely traverse a number of prevalent surface terrains, and travel slowly, requiring detailed oversight and planning activities. Consequently, these systems are often limited to exploring areas close to their original landing site. The lack of an atmosphere, the low gravity levels, and the unknown surface soil properties pose a very difficult challenge for all forms of know locomotion. Small body mobility concerns spatial surface coverage on planetary bodies with substantially reduced gravitational fields for the purpose of science and human exploration. This includes mobility on irregular-shaped objects such as NEOs (Near Earth Objects), asteroids, comets, and planetary moons (e.g., Phobos, Deimos, Enceladus).

The National Research Council [Decadal2011] has designated technologies for small body mobility as a high priority for NASA given its destination potential for human spaceflight, which would likely require precursor robotic missions. Specific technology needs include novel mobility systems together with associated control techniques and novel localization techniques. For science missions, in-situ spatially extended exploration of small bodies would address key priority questions in the Building New Worlds theme. In addition, a variety of observations have recently shed new light on the astrobiological relevance of small bodies, as a source of organics to Earth and/or as potentially habitable objects [Castillo2012]. Surface mobility platforms for small bodies differ from their planetary counterparts because the microgravity environment largely influences their design. Microgravity can be leveraged as an asset for mobility, as in the case of hopping platforms, or overcome as a challenge, as in the case of anchoring systems. Microgravity mobility could include hoppers, wheeled, legged, and hybrids, but so far no electrostatic solution has been proposed. While there have been several attempts at small body surface mobility, to date, no such system has been designed for the large scale exploration of small bodies. Microgravity environments pose many challenges not only for mobility and manipulation, but also for control, localization, and navigation. Recent observations from both space mission and ground-based telescopes have revealed a more diverse landscape on small body surfaces than previously thought. Small body surfaces can range from areas covered with a thick layer of fine regolith and ones that have boulders and protruded regions, thus making locomotion based on surface interaction very problematic. The E-Glider concept directly addresses the "All Access Mobility" Challenge, one of the NASA's Space Technology Grand Challenges [Decadal20111], specifically aimed at enabling robotic operations and mobility, in the most challenging environments of our solar system.

At the time of writing this report, the NASA Discovery program has selected one proposal for a mission to a metallic asteroid, Psyche[4]. The Psyche mission would explore the origin of planetary cores by studying the metallic asteroid Psyche. This asteroid is likely the survivor of a violent hit-and-run with another object that stripped off the outer, rocky layers of a protoplanet. 16 Psyche is one of the ten most-massive asteroids in the asteroid belt, over 200 kilometers in diameter and contains a little less than 1% of the mass of the entire asteroid belt. It is thought to be the exposed iron core of a protoplanet. The studies conducted in this

---

[4] http://www.jpl.nasa.gov/news/news.php?feature=6713

report would apply to this type of metallic asteroid, and could be useful to arrive at innovative ways to collect science around them.

1.2 Contributions to space technologies

The effort contributes to TA04, Robotics and Autonomous Systems, because in all respects E-Gliders are a new class of robots/autonomous systems, with capabilities beyond the projections of the Roadmap, as they are a new form of locomotion in airless and microgravity environments. By the end of the Phase I, we have assessed the basic elements of the E-Glider concept, in the context of various relevant mission concept scenarios. *From a science perspective*, the E-Glider concept will open new frontiers of exploration and scientific discovery in the Solar System in missions involving circumnavigation. *From a robotic control perspective*, we will have explored a new form of propulsion and locomotion in microgravity. *From a systems perspective*, Phase I developed a preliminary feasibility assessment of the innovative distributed sensing and actuation, and maneuvering in microgravity environments around very irregular bodies within a charged environment.

1.3 Technical challenges and Risks

There are several challenges, with potential risks (denoted by R#) to the development of the E-Glider. In this section, we address some of these, and propose an associated mitigation plan (denoted by M#).

- R1: Vehicle will become electrically neutral and unable to levitate. M1: Use electron emitters on top side, while bottom side facing ground have opposite charge to surface. A detailed levitation analysis is described in Sections 12 and 13.

- R2: There might be too much uncertainty in dust density and electrostatic potential distribution. How accurate does the electric field map need to be? M2: We will map the surrounding field during the reconnaissance phase. We will also refine this measure around the vehicle during flight (we'll do "electrostatic cartography tracking" in flight, like (TRN) Relative Navigation on Mars [Johnson], but electrostatically). A detailed description of alternative differential charging mechanisms is described in Section 9, and a description of the approach for autonomy is described in Section 10.

- R3: Which sensor(s) might provide the potential map around the vehicle? Will this sensor exist? M3: we are envisioning an array of Langmuir probes for distributed potential sensing around the vehicle. More details are in Section 9.

- R4: There might be a serious internal charging problem due to internal charge generation, or an adverse charging problem in charged dust, or an insufficient electric field that will jeopardize the planned mission performance. M4: One solution to a depleting electric field might be to enhance or control it by shooting a charge pellet to the surface, thus dislodging the top layer of soil, and producing more charged dust. The vehicle will then operate inside the Debye length of the local plasma, move inside its own charged cloud, and thus avoid arcing or similar problems. Some of these issues are addressed in Section 4, 7, and 9.
- R5: How much fuel for thrusters is required for take-off/landing? M5: we assume that the E-Glider never lands, but ejects charged probes, which are the ones to touch the surface of the small body for science data collection and surface locomotion. This is discussed in Section 8.
- R6: Can we actually lift 10 kg (like a cubesat) electrostatically? Where would the extra power come from? M6: We will still have a battery (fuel cell) and solar panels, plus unused charge difference could be harvested from the environment, and stored and released when needed. This is discussed in sections 12, 13, 14, and 15.
- R7: A key question is "at what point do the wings become so large that the electric field is vastly different between the center and tip of the wing, and what is the maximum acceptable size of the wing?" M7: a preliminary sensitivity analysis was conducted in Phase I, and summarized in section 12.

2. Environmental Challenges at Small Bodies

Physics at airless bodies is dominated by four physical fields [Kobrick2014, Quadrelli2013]: a) microgravity, responsible for locomotion; b) cohesion forces, which can dominate particle interactions through van der Waals forces; c) solar radiation, which is constantly acting; and d) electrostatics, which is strongest at terminator where it can lead to significant dust transport. The highly irregular shapes of many asteroid and other small bodies lead to unique modeling and dynamics challenges. In contrast to the gravitational fields of spherical and ellipsoidal bodies, those produced by Near Earth Objects (NEOs) are frequently much more complex. The gravitational fields of these irregular bodies exhibit high levels of variation at both the surface and locations near the bodies. In addition, these

gravitational fields are often orders of magnitude weaker than Earth's. In addition to exhibiting irregular shapes, the gravitational fields produced by small bodies often have milli-G or micro-G order magnitudes. As a result, escape velocities from these bodies are exceptionally low and must be carefully considered when maneuvering landers or spacecraft. Another consequence of these low gravitational magnitudes is that the rotational period, some times as fast as a fraction of minute, may impact spacecraft motion. It may be possible to take advantage of this behavior to aid in motion between surface locations on a small body. This could potentially be achieved by applying an impulse to the lander such that it hops away from the surface without an orbital velocity component while the small body continues to rotate. This maneuver would lead to a change in position when gravity pulls the lander back to the surface. As the topics examined illustrate, it is necessary to understand the impacts of both small gravitational magnitudes and irregular gravitational field shapes to ensure successful spacecraft interactions with small bodies.
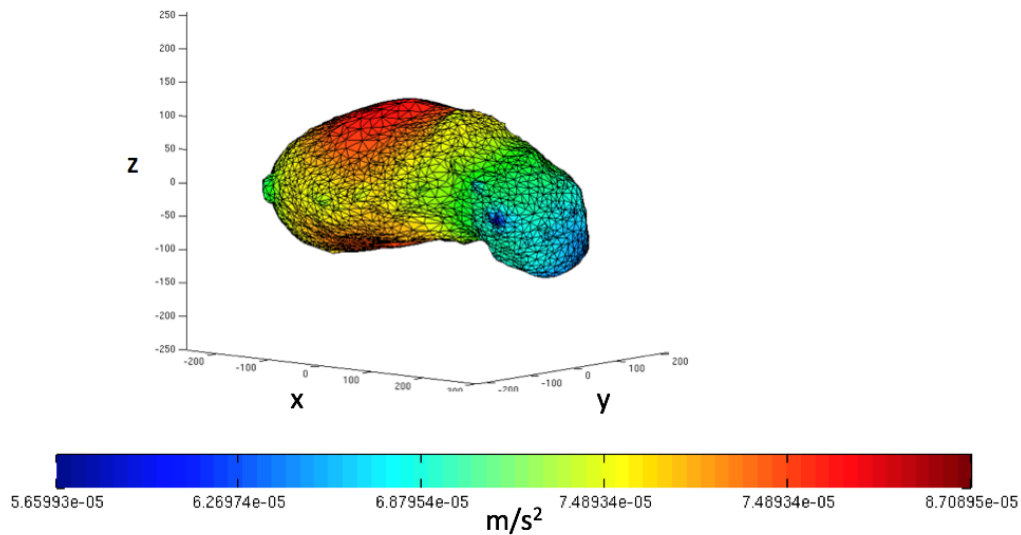
Figure 2. *Surface acceleration at Itokawa [Quadrelli2012].*
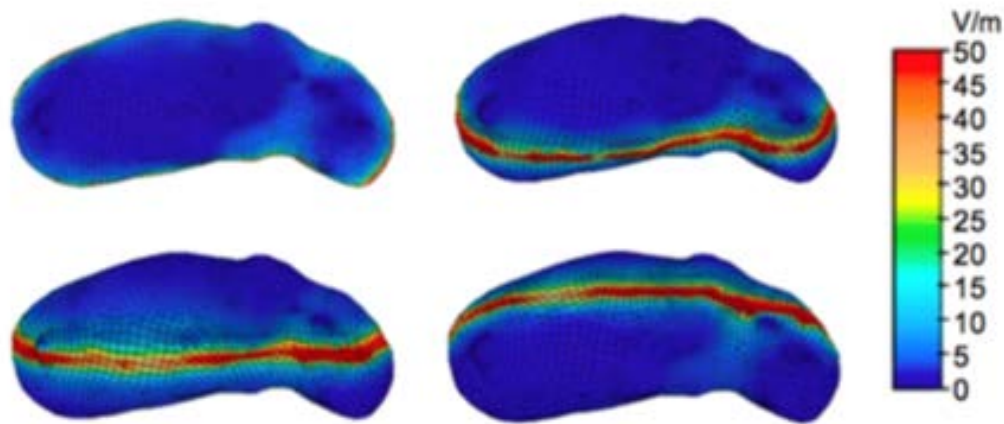
Figure 3. *Electric field at terminator of Itokawa [Aplin2011].*

The environment near the surface of airless bodies (asteroids, comets, Moon) is electrically charged due to interactions with the solar wind plasma and UV radiation. Charged dust is ever present, in the form of dusty plasma [Vladimirov2005]. Comets have a gas tail and a second electrostatic tail. This environment is also largely unexplored. Electrostatically levitating dust grains have been hypothesized to exist above 10's of meters above the dayside surface [Harzell2011, Harzell2013, Lee1996]. If a body with high surface resistivity is exposed to the solar wind and solar radiation, sun-exposed areas and shadowed areas become differentially charged (see Fig. 3). Charging on the dayside surface is dominated by photoelectrons emitted due to solar UV radiation that create a positive surface potential, while the shadowed side accumulates electrons and acquires a negative surface potential. Recent work [Harzell2013, Renno2008, Stubbs2005] shows that, on the Moon, soft solar X-rays with wavelengths smaller than 25 Å can remove electrons with energies of 500 to 1500 eV from the surface and create cm-scale electric fields which may reach levels of ~50-150 kV/m. The spokes in Saturn's rings are most likely clouds of particles electrostatically levitated from the surfaces of larger bodies in the rings [Goertz1989], and electrostatic dust transport processes have been proposed on the surface of Mercury [Ip1986] and comets [Mendis1981, Miyamoto2007]. Asteroid electric charge has never been measured, but simple estimates predict that an electric potential difference of ~1 kV can be attained on the dark side compared to the sunlit side, which becomes slightly positively charged by photoelectron emission. These differences are enhanced further at the terminator (the day/night boundary),

when fields could reach ~100-300 kV/m ([Aplin2011], also Figure 1, with results obtained by simulation). Millimeter-size particles can be most easily lifted from the surface of Itokawa [Harzell2011]. As these particles are lifted, they dislodge smaller particles that are harder to lift due to their strong cohesive forces [Harzell2013]. Once separated from the surface, grains can either travel on ballistic trajectories, escape from the asteroid, or levitate. During these migrations the larger particles can get trapped in topographic lows, as observed in [Miyamoto2007]. As a surface element on a resistive asteroid rotates into and out of view of the sun, electrostatic levitation may agitate its uppermost particulate layer. Larger levitated particles remaining gravitationally bound to the asteroid are redistributed across its surface following local electrostatic and gravity gradients. Consequently, the study of levitating dust is relevant in that it provides some insight into the plasma environment and confirms the possibility of levitation. An intriguing example from nature discussed in [Gorham2013], refers to existing observations and the physics of spider silk in the presence of the Earth's static atmospheric electric field (-120 V/m negative) to indicate a potentially important role for electrostatic forces in the flight of Gossamer spiders. A compelling example is analyzed in detail, motivated by the observed "unaccountable rapidity" in the launching of such spiders from the vessel H.M.S. Beagle, recorded by Charles Darwin during his famous voyage, on a day without wind, and far away from the shore [Gorham2013]. It is believed that such spiders are able to emit threads that are either pre-loaded with a static electric charge, so that the presence of this charge will lead both to mutual repulsion among the emitted threads, and an additional overall induced electrostatic force on the spider, providing a component of lift that is in-dependent of convection or aerodynamic effects. The E-Glider biomorphically behaves like one of these spiders, greatly favored by the charged environment, in absence of aerodynamics and convection, and in the microgravity fields at small bodies.

3. Proposed Science Instrumentation

Many science objectives can be addressed at small bodies, such as NEOs, also shown in Figure 4. Figure 5 maps Decadal science priorities to small instrument availability for science to be conducted at NEOs. Thanks to recent advances in miniaturization, several science-grade instruments are becoming available for implementation on small vehicles such

as Cubesats. Some of these instruments, which could be suitable for use on the E-Glider, are [Kobrick2014]: quadrupole ion trap spectrometers (2.5 kg, with isotopic accuracy < 1%), snow and water imaging spectrometers (with high-throughput, low-polarization, high-uniformity, in the 350-1700 nm spectral range), Advanced infrared photodetectors (thermal sensitivity 0.2 degrees), high-resolution visible camera (used for science, optical navigation, and Autonomous Navigation demonstration), and micro-seismometers.

Objectives	Observations	Measurements	Architecture
Determine surface mechanical properties	Soil competence, granularity at all scales, gravity	High resolution imaging, gradiometer, mechanical tester	Reconnaissance with orbiter, track rover's motion and interaction with dust
Search for in-situ resources	Chemical and mineralogical composition	NIR, GRaND, APXS	Remote sensing from orbiter, in-situ characterization at selected sites
Characterize risk and search for mitigation approaches	Waves and fields (e.g., electrostatic field), dust dynamics	UV imaging, high-res imaging	In situ
Understand and simulate human activities in low-gravity environment	Simulate digging, sampling	Performance	In situ

Figure 4. *Science objectives at NEOs.*

THEME	MEASUREMENTS	OPPORTUNITY FOR CUBESAT/SMALLSAT	INSTRUMENTS
Building New Worlds	Isotopic, elemental, mineralogical composition	In situ, extreme environments	APXS, TLS, IR Spec, Submm Spec, UV Spec, Gamma Ray/ NeutronSpec, Dust Spec, MassSpec
		Returned sample (small bodies)	Sample Return Capsule (possibly Acquisition as well)
Planetary Habitats Ocean Worlds	Composition (volatiles, organics) endogenic activity, heat budget, environment	In situ	MassSpec, Micro-XRF, Imaging, IR Spec, Seismometer, heat probe, radar
Processes	Atmospheric structure, fields, plasma, dust	Close proximity, in situ, multiple data points	Imaging, IR Spec, Mag, Transponders, Langmuir probes, Mass Spec, TLS, Plasma Spec.
Human Exploration	Dust, fields, radiations, Gravity field, orbital properties Regolith mechanical properties ISRU (composition)	Close proximity, in situ, risky environments	Dust Counter, Neutron, Geophysics Inst., IR Spec, APXS, Transponders, radiations spec, Surface perturbation, radar, seismometer

Color code: Green = exists; Blue = in developmentt; Red = does not exist yet

Figure 5. *Decadal Science [Decadal2011] mapping and instrument availability*

4. E-Glider Physics

The E-Glider charging is maintained through continuous charge emissions of either electrons or ions, depending on the desired polarity to achieve a repulsive force with the local asteroid surface E-field. Therefore, we need to consider the interaction with the plasma. In a plasma environment, an oppositely charged sheath forms about a charged space object. The electron Debye Length is defined as:

$$\lambda_D = \sqrt{\frac{\epsilon_0 \kappa T_e}{n_e e_c^2}},$$

(1)

Assuming the object's potential is small compared to the plasma temperature, the potential about a sphere drops off as:

$$\Phi(r) = \frac{V_A R_A}{r} e^{-(r-R_A)/\lambda_D}.$$

(2)

If the spacecraft potential is large compared to the ambient plasma temperature, then the Debye length be multiples larger [Seubert2014]. The E-field is the gradient of the potential, and is about a sphere as expressed as [Seubert2014, Whipple1981]:

$$E(r) = -\nabla_r \Phi(r) = \frac{V_A R_A}{r^2} e^{-(r-R_A)/\lambda_D} \left(1 + \frac{r}{\lambda_D}\right)$$

(3)

The Debye Shielding increases the local gradient of the potential, and thus can increase the capacitance of the surface. This can yield a strong E field, thus force, near a surface, but at some distance the shielding dominates:

$$F = \frac{V_A R_A q_B}{d^2} e^{-(d-R_A)/\lambda_D} \left(1 + \frac{d}{\lambda_D}\right)$$

(4)
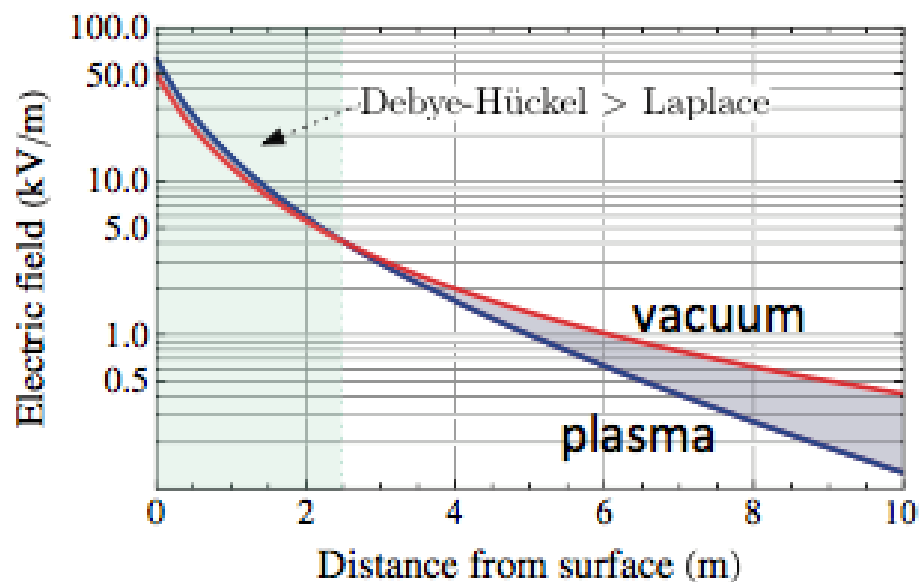
Figure 6. *Electric field on 1 meter diameter sphere with 4 meter Debye length [35].*

[Aplin2011] shows that electric fields of E~100-300 kV/m could take place on Itokawa, and Figure 3 shows expected Itokawa surface E-fields around 5-50V/m. As a comparison, an electric field of E=-10 V/m has been measured on the surface of the Moon under full Sun's illumination. Therefore a wide range of E is to be considered in this study.
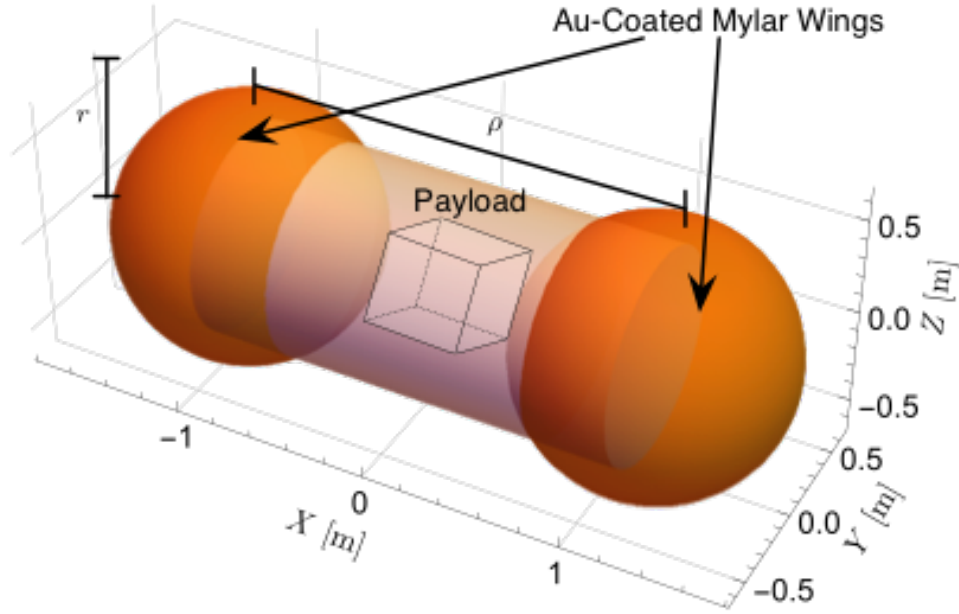
Figure 7. *Electrostatic lifting capability as a function of wing radius.*

A simplified E-Glider model is shown in Figure 7 where r is the Au-coated Mylar wing radius, and ρ is the center to center separation. Here $\rho = 2r + 0.5m$ is used to allow for a payload between the Mylar wings. Using the Multi-Sphere-Method (MSM) [Chow2016] assuming two charged spheres, the self-capacitance is given by

$$C_s = 4\pi\varepsilon_0 \frac{2r\rho}{r+\rho}$$

(5)

where ε_0 is the permittivity of vacuum. To estimate the Debye sheath modified capacitance about a sphere or radius is approximated by [Seubert2014]

$$C = 4\pi\varepsilon_0 r_{eff}\left(1 + \frac{r_{eff}}{\lambda_D}\right)$$

(6)

where λ_D is the effective Debye sheath. The plasma shield increases the objects capacitance, but will also partially shield the E-field experienced due to a neighboring charged object. The effective radius of the single-sphere representation is found using

$$r_{eff} = \frac{C_s}{4\pi\epsilon_0}$$

(7)

The Debye sheath reduced local E-Field is obtained assuming E_0 is the surface E-field of a locally flat plate (good assumption is asteroid is much larger the E-Glider), and the sheath causes an exponential E-field drop [Whipple1981]

$$E(h) = E_0 \, e^{-h/\lambda_D}$$

(8)

where h is the height above the asteroid surface. In this study this is set to $h = r + 1m$ to cause the E-Glider to have a 1 meter height above the surface, regardless of the Mylar wing size. Finally, let ϕ be the Glider potential that is maintained through active charge emission. A rough order of magnitude mass estimate that can be levitated is given by

$$m = \frac{C(r) \, \phi \, E(r)}{g}$$

(9)

The local gravitational acceleration level of g=10-5 m/s2 is typical of asteroids such as Itokawa.
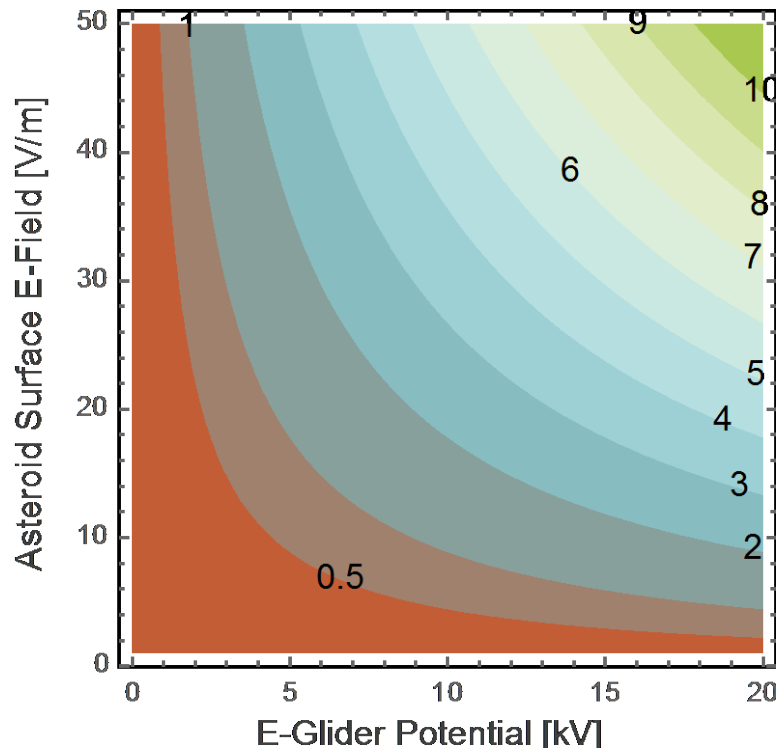
Figure 8. *Levitated mass estimates in kg assuming massless Mylar wings of radius 1m, an effective Debye length of 2.5 meters.*

The resulting rough estimates of levitated masses are shown in Figure 8 assuming an effective Debye length of 2.5 meters. If the asteroid surface E-fields are low around 5V/m, it would take about 19kV to levitate 1kg of mass. In contrasts, considering the terminator regions shown in Figure 3 with 50V/m of E-fields, the 1kg mass can be levitated using only 2kV.
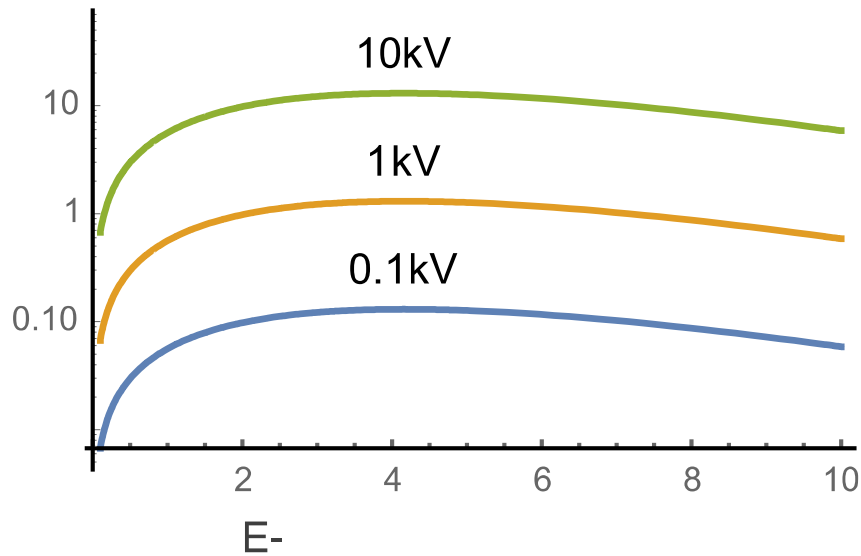
Figure 9. *Levitated mass estimates considering a range of wing radii and, an effective Debye length of 2.5 meters.*

Next the impact of the wing radius is investigated. Figure 9 illustrates the levitated mass estimates of three Glider potential levels. As the wing radius increases, so does it's capacitance, and levitated mass becomes larger. However, as an increase wing radius requires the Glider to hover further from the surface to maintain the 1m separation, the local E field is reduced exponentially through the Debye sheath. As a result, Figure 9 illustrates that there are optimal wing sizes that provide the largest payload mass for a given E-Glider potential. Note that these results assume a fixed local gravitational acceleration value. Naturally, as the asteroid shape is non-spherical, the *g* values will vary across the surface. The rough order of magnitude mass levitation estimates are performed making several strong assumptions and simplifications. However, the resulting values look promising as only kV levels of charge are required. Such charging potentials are commonly achieved on GEO and deep space objects with their natural interaction with the space weather.

5. Power Consideration

To estimate how much electrical power is required to levitate a certain mass off the asteroid surface, the local plasma conditions must be taken into account. We are assuming the e-Glider is hovering on the sun lit side of the asteroid. Here the photo-electron current or sheath is the stronger influence compared to the free space plasma Debye length [Han2015]. With a 0deg incidence angle the Debye length can be as small as 1.35 meters. This assumes an electron density of 64 particles per cm^3. To avoid the worst case condition and consider rather a more nominal sun-light asteroid photo-electron sheath condition, a density value of $n_e = 20$ particles/cm^3 is assumed. The expected electron temperature is set to T_e= 2.2 eV. This results in a photo-electro sheath Debye length of 2.5 meters, same as in the earlier analysis above.

The E-Glider is flying in a positive E field of the asteroid. To achieve levitation, the vehicle must charge to a positive value by continuously emitting electrons. The electrons must be emitted with an energy level that is at least as large as the spacecraft potential ϕ. Given this electron emission I_{eGun} which result in a positive current onto the craft, the charge balance equation is modeled by [Schaub2014]:

$$I_e + I_{eGun} = 0$$

(10)

Note that the photo-electro current of the sunlight hitting the metallic spacecraft surface doesn't need to be included here as this current is very weak, and it fully returns to the positively charged e-Glider. The collection of plasma electrons onto a positively charged spacecraft from the surrounding plasma is given by [Pfau2001]:

$$I_e = -\frac{A\, q\, n_e\, w_e}{4}\left(1 + \frac{\phi}{T_e}\right)$$

(11)

where $A = 4\pi R_{eff}^2$ is the projected surface area of the craft and

$$w_e = \sqrt{\frac{8T_e}{\pi\, m_e}}$$

(12)

is the thermal velocity of the local plasma electrons. Given an electron gun current value, and substituting Eq. (11) into Eq. (10), the resulting equilibrium spacecraft potential can be solved for.

$$\phi = \left(\frac{4 \, I_{eGun}}{A \, q \, n_e \, w_e} - 1 \right) T_e$$

(13)

The minimum electrical power required to achieve this potential is

$$P = \phi \, I_{eGun}$$

(14)

The electrons must be emitted from the spacecraft with an energy level that is at least as large as the spacecraft potential. Otherwise the positive spacecraft potential will attract them back to the spacecraft, yielding no net charging. Substituting Eq. (13) into (14) and solving for the spacecraft potential, a formula is developed that maps the minimum electrical power to the resulting spacecraft potential.

$$\phi = -\frac{T_e}{2} + \sqrt{\frac{4PT_e}{A \, q \, n_e \, w_e} + \frac{T_e^2}{4}}$$

(15)

As the electron temperatures are rather low, this formula can be approximated as

$$\phi = \sqrt{\frac{4PT_e}{A \, q \, n_e \, w_e}}$$

(16)

Figure 10 illustrates both spacecraft potentials evaluated with the full and simplified answer. With the asteroid photo electron current only have energies of about 2-3 eV, this assumption is very valid for the scenarios considered.
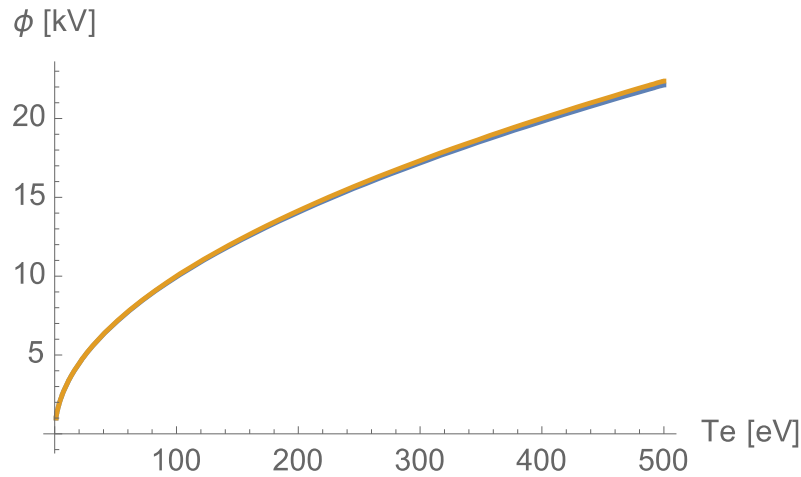
Figure 10. *Comparison of Eqs. (15) (brown) and (16) (blue), illustrating the validity of the simplification.*

Finally, the power to spacecraft potential relationship in Eq. (16) can be substituted in the estimated levitated mass function in Eq. (9) to study what power levels will cause what mass to levitate, all as a function of the asteroid surface E-field values. The resulting trade-space is illustrated in Figure 11. Due to the high density and the photo-electron sheath and associate small Debye length, significant power is required to levitate even a few kilo-grams. The power requirement are in the kilo-Watt range to maintain a constant charge level.
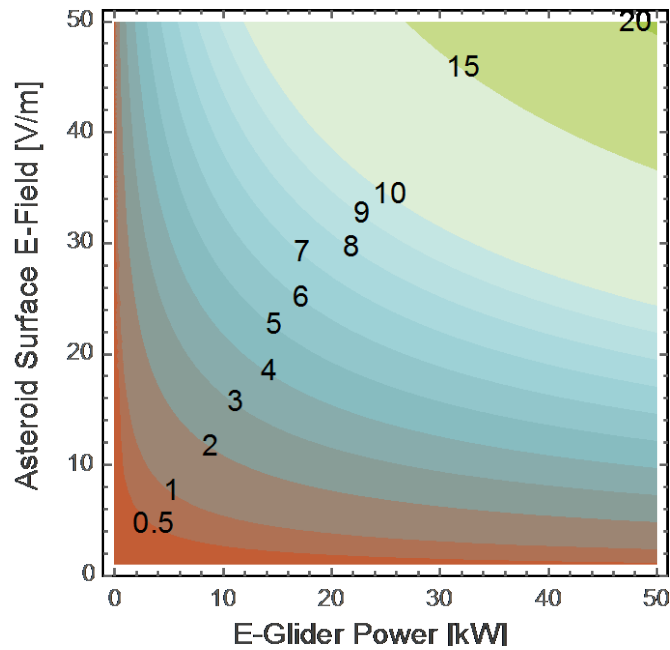
Figure 11. *Levitated mass estimates in kg assuming massless Mylar wings of radius 1m, an effective Debye length of 2.5 meters.*

6. E-Glider Dynamics and Control Model

The E-glider concept proposes a novel flight mechanism around asteroids, taking the advantage of the unique dynamical environment around them. Because of the weak gravitational force, the motion in the vicinity of an asteroid is strongly perturbed by non-gravitational forces, such as solar radiation pressure (SRP) [Scheeres1994, Scheeres1999]. In addition, asteroids have irregular shapes in general, and thus, irregular gravitational fields are formed around the asteroids, leading to additional perturbing effects [Scheeres1994, Scheeres1998]. For these reasons, the dynamics around asteroids exhibits intriguing characteristics that cannot be observed in the conventional two- and three-body problems. Another unique characteristic arises from a lack of air around asteroids. Due to the airless condition, the surfaces of asteroids are constantly radiated by the sun light, which induces the photoelectric effect. As a result of the interaction between the emitted photoelectrons and the solar wind particles, electric fields are formed around asteroids. Previous research has

been revealed that the electric field induces electrostatic force on dust particles, and it can levitate the particles above the surface of an asteroid [Lee1996, Nitter1998, Colwell2005].

While these characteristics have been of interest from the perspective of science, it poses difficulty in the operation of a spacecraft around an asteroid. The strongly perturbed environment around an asteroid disturbs the motion of a spacecraft and can lead to the impact or escape in the worst case. One solution to this problem is hovering operation, in which a spacecraft constantly maintains its relative position with respect to an asteroid and the sun [Broschart2005, Kominato2006]. This type of operation is very simple, and thus, this strategy may be the easiest option for asteroid mission concepts. However, hovering operation on the dayside requires frequent thrusting and thus large amounts of fuel, because an equilibrium point close to the asteroid exists only on the nightside due to the SRP effect.

Another option for the operation around an asteroid is the use of periodic orbits, which ideally do not require any fuel. It has been revealed that several types of periodic orbits can actually be achieved even under the strongly perturbed environment. Well-known examples are terminator orbits, which have simple orbital shapes and provide long-term stability [Scheeres1999, Scheeres2007, Broschart2010]. However, this type of orbits must lie close to the terminator plane with displacement in the anti-sun direction, and therefore, the orbits exist on the nightside of asteroids, posing a considerable disadvantage for optical observation. Other types of periodic orbits have also been proposed as alternatives to terminator orbits [Broschart2010, Broschart2013, Giancotti2014]; nevertheless, their coverage around the sub-solar point remains limited, and also, their orbital shapes are generally complex.

In order to overcome these disadvantages inherent in the hovering and orbiting operation, this study proposes the novel maneuvering method around asteroids utilizing electrostatic force. The basic idea is that a spacecraft with electrically charged appendages induces electrostatic force via an ambient electric field to control its motion, as shown in Figure 10. Spacecraft flight mechanics utilizing electrostatic force has been of interest in recent years, and various applications have been proposed, including formation flying, collision avoidance, and rendezvous docking [Schaub2003, King2002a, King2002b, Seubert2014]. These studies proposed to make use of the electrostatic force interacted between two spacecraft via artificially generated electric fields. By contrast, the E-Glider concept is novel in that it leverages the natural environment around an asteroid and utilizes the electrostatic force interacted between a spacecraft and an ambient electric field.
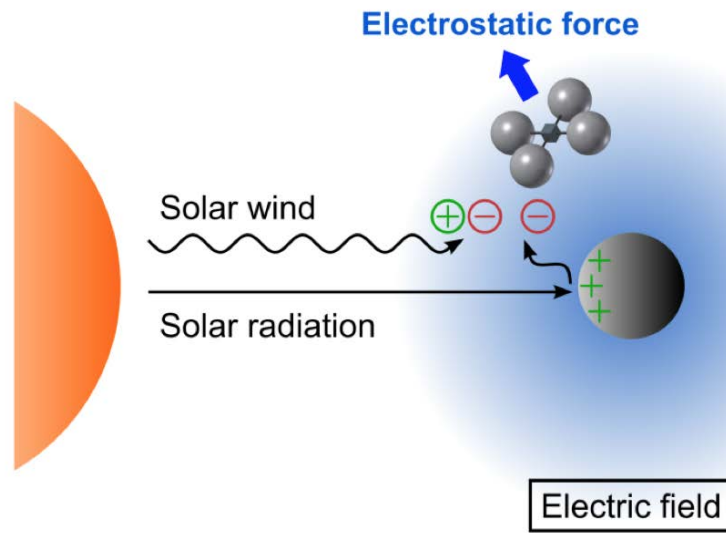
Figure 10. E-glider concept.
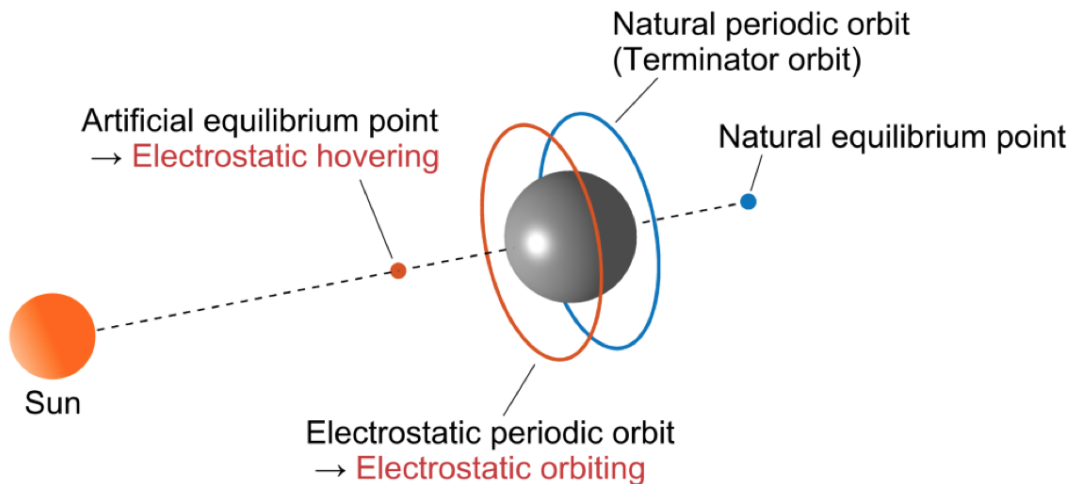
Figure 11.Electrostatic orbiting and electrostatic hovering.

This study proposes the two distinct types of operations for an E-Glider, namely electrostatic hovering and electrostatic orbiting. The basic strategy of the electrostatic hovering is to create artificial equilibrium points by inducing repulsive electrostatic force. These artificial equilibrium points are present not only on the nightside but also on the dayside unlike natural equilibrium points, as illustrated in Figure 11. Therefore, the proposed method can potentially achieve fuel-free hovering on the dayside without experiencing eclipse. On the other hand,

the utilization of electrostatic force offers advantages for orbiting operation as well. This section identifies a new class of periodic orbits around asteroids using electrostatic force, which are called *electrostatic periodic orbits*. In contrast to the natural terminator orbits, these orbits are displaced from the terminator plane in the sun direction, as depicted in Figure 11, enabling the observation of the sun-lit side of an asteroid. Besides, the electrostatic periodic orbits are sun-synchronous, and thus, they ensure constant illumination from the sun. Another advantage of the electrostatic orbiting is that it only requires a small amount of power; for example, some of the electrostatic periodic orbits consume only few watts of electricity.

As mentioned above, the electrostatic hovering and the electrostatic orbiting method using an E-Glider allow the dayside operation without requiring any fuel, and thus, the proposed methods are advantageous for mass budget, optical observation, solar power generation, and thermal design. By virtue of these characteristics, the E-Glider enables asteroid mission concepts with lower cost and higher scientific value; for example, an E-Glider can be used as a daughter spacecraft for proximity operation around an asteroid. In addition to these practical advantages, this study is also intriguing in that completely new aspects of astrodynamics are revealed. This section presents unique dynamical structure behind the complex environment around an asteroid involving the interaction between irregular gravitational force, SRP force, and electrostatic force. Consequently, this research expands the possibility of flight mechanics in space.

This section begins with a description of the dynamical model used in this study. Then, the electrostatic field around an asteroid is computed numerically, which is an essential part to analyze the motion of an E-Glider. Based on the simulated electrostatic field, the general theories of the dynamics of electrostatic hovering and electrostatic orbiting are discussed. Finally, the effects of shape irregularity of an asteroid, including the irregular gravitational field and the irregular electrostatic field, are formulated and evaluated. This report clarifies that electrostatic flight using an E-Glider is useful for asteroid missions and exhibits unique and valuable dynamic characteristics.
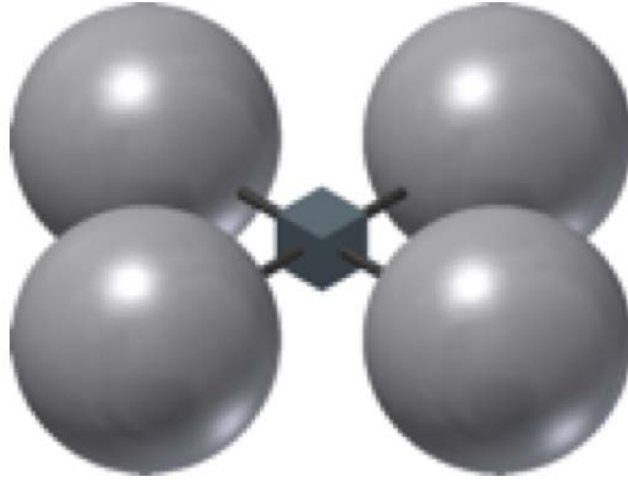
Figure 12. E-glider model.

6.1 Spacecraft and Asteroid Model

The preliminary CAD model and the physical parameters of an E-Glider are presented in Figure 12 and Table 1, respectively. The E-Glider is assumed to have charged spheres made of thin film, and the mass is small as a CubeSat, which is given as 1 kg in this study. Other possible options for the design, structure, and material of an E-Glider are discussed in detail in the past study [Quadrelli2017]. The number of spheres is denoted by N_{sp}, and the number of spheres exposed to the sun light is denoted by $N_{sp}^*(\leq N_{sp})$. It is also assumed that the size of the body of the E-Glider, which is illustrated as the cube in Figure 12, is negligible compared with that of the spheres. The capacitance of an E-Glider is given by the equation below.

$$C = N_{sp} \cdot 4\pi\varepsilon_0 r_{sp}$$

(17)

where ε_0 is the vacuum permittivity. The cross sectional area exposed to the solar radiation is calculated from the following equation.

$$A = N_{sp}^* \cdot \pi r_{sp}^2$$

(18)

C_s, C_d, and C_a denote optical constants of the E-Glider surface that correspond to the modes of specular reflection, diffuse reflection, and absorption, respectively, which satisfy $C_s + C_d + C_a = 1$. The optical constants provided in Table 1 are based on a spacecraft mounting solar array paddles [Ono2016], and it should be noted that these parameters would exhibit less absorptive property if the spheres of an E-Glider are made of a specular material. The emissivity ε_{sc} is given to calculate the photoemission effect on the surface of an E-Glider, and it is identical to that of an asteroid in this study. Throughout this section, the motion of an E-Glider is analyzed by treating the spacecraft as a point mass.

The physical parameters for an asteroid are given in Table 2. The body is assumed to be moving in a circular orbit, with a radius of 1 AU, around the sun. The most of the analyses in this study are performed by modelling the asteroid as a sphere with a diameter of 100 m, while the shape irregularity effects are also discussed in Section 15 by modelling the asteroid as a homogeneous triaxial ellipsoid. The density of an asteroid is given based on the value of Itokawa, which is an S-type asteroid [Fujiwara2006]. It is also assumed that the emissive property of the surface of an asteroid is the same as the lunar surface, as explained in detail in the Appendix.

Table 1. E-glider parameters

Item	Symbol	Value
Mass	M	1 kg
Radius of a sphere	r_{sp}	25 cm
Number of spheres	N_{sp}, N_{sp}^*	4, 2
Optical constants	C_s, C_d, C_a	0.01, 0.08, 0.91
Emissivity	ε_{sc}	1

Table 2. Asteroid parameters

Item	Symbol	Value
Distance from the sun	d	1 AU
Diameter	D	100 m
Density	ρ	2 g/cm^3
Emissivity	ε_{ast}	1

6.2   Plasma Model

In order to estimate the electrostatic force applied to an E-glider, the plasma environment around an asteroid must be modelled appropriately. The plasma consists of three types of charged particles, namely solar wind ions, solar wind electrons, and photoelectrons emitted from the surface of an asteroid. The distributions of the solar wind particles can be illustrated as shown in Figure 13. Given the fact that the mass of an electron is much smaller than that of an ion, the solar wind electrons possess larger thermal velocity, resulting in a wide velocity distribution. By contrast, the solar wind ions can be regarded to have an identical velocity, which is equal to the drifting velocity of the solar wind. Therefore, the solar wind ions, the solar wind electrons, and the photoelectrons can be modelled, respectively, as a mono-energetic beam, a drifting Maxwellian distribution, and a stationary Maxwellian distribution [Nitter1998, Jeong2008, Harzell2008].
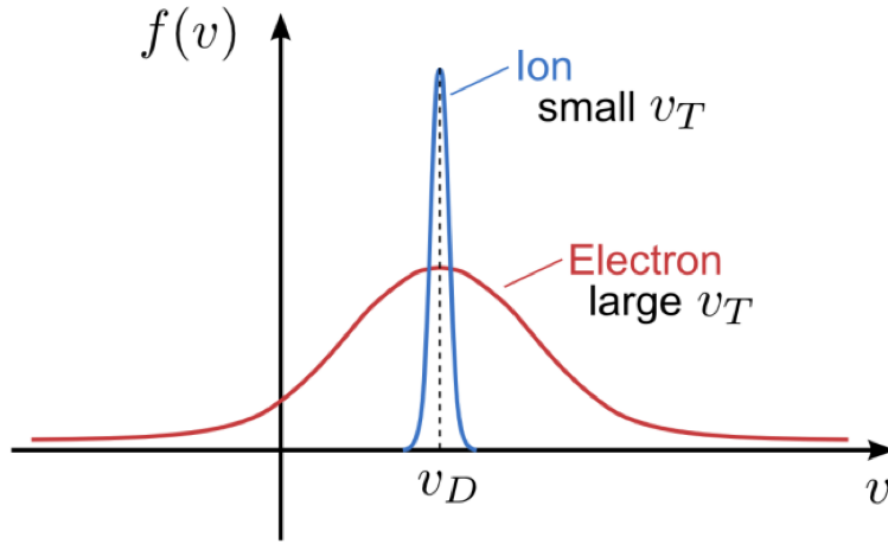
Figure 13. Distribution of solar wind parameters [Jeong2008].

Table 3. Plasma parameters [Nitter1998]

Item	Symbol	Value
Solar wind Mach number	$\mathcal{M}$	10 [-]
Solar wind electron temperature	T_e	15 eV
Photoelectron temperature	T_p	1.47 eV
Ion number density	$n_{i,\infty}$	5×10^6 /m^3

Let $v_{T,i}$, $v_{T,e}$, and $v_{T,p}$ denote the thermal velocity of the solar wind ions, the solar wind electrons, and the photoelectrons, respectively, and v_D denotes the drifting velocity of the solar wind. Here, $v_{T,i} \ll v_D \ll v_{T,e}$ holds from the assumption mentioned above. The drifting velocity can also be expressed as the solar wind Mach number by the following equation:

$$\mathcal{M} = \frac{v_D}{v_B}, \qquad v_B = \sqrt{\frac{k_B\, T_e}{m_i}}$$

(19)

where v_B is the Bohm velocity. $\mathcal{M} = 10$ is given here on the basis of past research [Nitter1998]. On the other hand, the thermal velocity of particles can be converted to the temperature by using the equation below.

$$T_\xi = \frac{m_\xi v_{T,\xi}^2}{2k_B}$$

(20)

where m_ξ is the mass of a particle and k_B is the Boltzmann constant. The temperature of solar wind electrons and photoelectrons are presented in Table 3. Finally, the number density of solar wind ions at infinity is given as $n_{i,\infty} = 5{\times}10^6$ /cm^3.

6.3 Equations of Motion

The orbital motion is analyzed by treating the spacecraft as a point mass. The orbital motion of a spacecraft in the proximity of an asteroid moving in a circular orbit around the sun can be modelled using Hill's equation below [Scheeres2002].

$$\ddot{\boldsymbol{r}} + 2\boldsymbol{\omega}{\times}\dot{\boldsymbol{r}} + \boldsymbol{\omega}{\times}(\boldsymbol{\omega}{\times}\boldsymbol{r}) = |\boldsymbol{\omega}|^2\big(3(\hat{\boldsymbol{d}} \cdot \boldsymbol{r})\hat{\boldsymbol{d}} - \boldsymbol{r}\big) + \boldsymbol{a}_G + \boldsymbol{a}_E + \boldsymbol{a}_{SRP}$$

(21)

where $\boldsymbol{r}$ is the position vector of a spacecraft; $\boldsymbol{\omega}$ is the angular velocity vector of an asteroid about the sun; $\hat{\boldsymbol{d}}$ is the unit vector pointing from the sun to an asteroid. The second, third, and fourth terms on the right hand side of Eq.(21) represent the gravitational, electrostatic, and SRP acceleration.

The gravitational acceleration is calculated from the equation below.

$$\boldsymbol{a}_G = \frac{\partial U_G(\boldsymbol{r})}{\partial \boldsymbol{r}}$$

(22)

The gravitational potential of a spherical asteroid is given by the following equation, and that of an ellipsoidal asteroid is given in Section 15:

$$U_G = \frac{\mu}{r}$$

(23)

where μ is the gravitational constant and $r \equiv |\boldsymbol{r}|$ is the distance from the center of an asteroid. Next, the electrostatic acceleration can be expressed as

$$\boldsymbol{a}_E = \frac{\boldsymbol{F}_E}{m} = \frac{Q}{m}\frac{\partial \phi(\boldsymbol{r})}{\partial \boldsymbol{r}}$$

(24)

where $\boldsymbol{F}_E$ is the electrostatic force; Q is the charge of an E-Glider; and ϕ is the electrostatic potential, which is described in another section. Finally, the SRP acceleration is obtained from the following equation.

$$\boldsymbol{a}_{SRP} = a_{SRP} \cdot \hat{\boldsymbol{d}} = \frac{(1+\xi)P_0 A}{d^2 M}\hat{\boldsymbol{d}}$$

(25)

where $P_0 \simeq 1\times10^{17}$ kg $\cdot$ m/s^2 is the solar flux constant [Scheeres2012]; d is the distance from the sun expressed in AU; and $\xi \equiv C_s + 2/3C_d$ is the reflectivity of the surface of a spacecraft. This model, which is so called cannonball model, assumes that a spacecraft has a spherical shape and the SRP force consists of only a radial component. It should be also noted that the effect of solar eclipse is not included in this SRP model.

The orbital motion is described in the sun-asteroid rotating frame illustrated in Figure 14, which is also referred to as the Hill coordinate. The origin is at the center of an asteroid. The x axis points in the anti-sun direction, the z axis is perpendicular to the ecliptic plane, and the y axis completes a right-handed Cartesian coordinate system. The equation of motion, Eq. (21) is expressed in the Hill coordinate as follows:

$$\ddot{x} - 2n\dot{y} = -\frac{\mu}{r^3}x + 3n^2 x + a_{E,x} + a_{SRP}$$
$$\ddot{y} + 2n\dot{x} = -\frac{\mu}{r^3}y + a_{E,y}$$
$$\ddot{z} = -\frac{\mu}{r^3}z - n^2 z + a_{E,z}$$

(26)

Here, $n = |\boldsymbol{\omega}|$ denotes the mean motion of an asteroid.
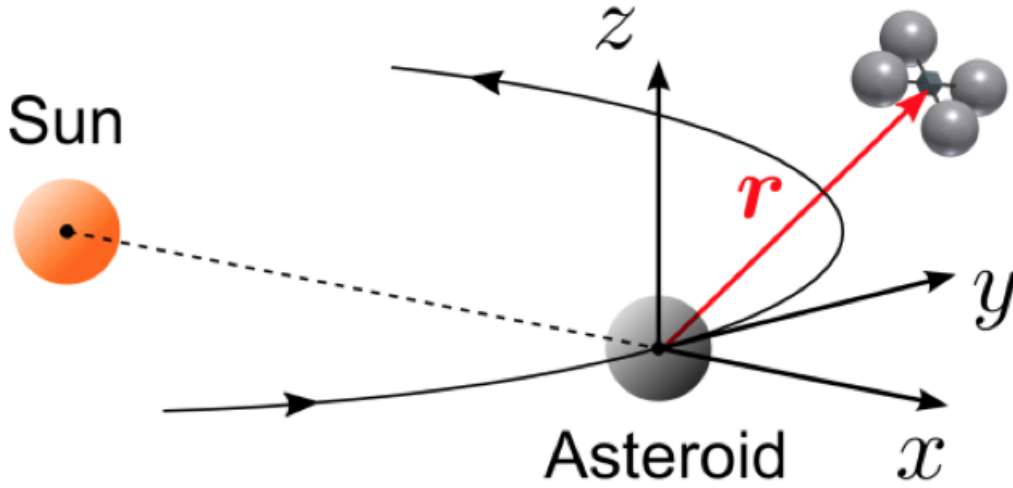
Figure 14. Coordinate System.

6.4 Numerical Model of the Electrostatic Potential

In order to describe the complex plasma environment around an asteroid, a numerical non-monotonic sheath model is used in this study. The possible plasma potential profiles A, B, and C are illustrated in Figure 15. The sheath A possesses a minimum potential value at an altitude $h = h_m$. The electrostatic potentials at $h = 0$, h_m, and ∞ are denoted as ϕ_0, ϕ_m, and $\phi_\infty (= 0)$, respectively. For sheath B, $h_m = \infty$ and $\phi_m = \phi_\infty$. For sheath C, $h_m = 0$ and $\phi_m = \phi_0$.

The electrostatic potential profile is calculated from the Poisson's equation, by assuming the distribution of charged particles n_i, n_e, and n_p. In the current model, the solar wind ions, the solar wind electrons, and the photoelectrons are modelled, respectively, as a mono-energetic beam, a drifting Maxwellian distribution, and a stationary Maxwellian distribution [Nitter1998, Jeong2008, Harzell2008]. To calculate the number densities of these particles, the following parameters must be specified: the number density of solar wind ions and electrons at infinity $n_{i,\infty}$ and $n_{e,\infty}$; and the number density of photoelectrons at the surface of an asteroid $n_{p,0}$. Here, $n_{i,\infty}$ is given as a parameter in Table 3. $n_{e,\infty}$ is given such that a boundary condition is satisfied, and $n_{p,0}$ is given by the equation below.

$$n_{p,0} = \begin{cases} \varepsilon_{ast} \dfrac{J_0 \cos\theta}{d^2 e} \sqrt{\dfrac{2\pi m_e}{k_B T_p}} & (\theta < 90 \text{ deg}) \\ 0 & (\theta \geq 90 \text{ deg}) \end{cases}$$

(27)

where $J_0 = 4.5 \times 10^{-6}$ A/m^2 is the current density at 1 AU, which was observed from the lunar surface particles [Nitter1998]; d is the distance from the sun expressed in AU; and ε_{ast} is the photoemissivity of an asteroid. In this research, it is assumed that the emissivity of an asteroid is the same as that of the lunar surface, yielding $\varepsilon_{ast} = 1$.
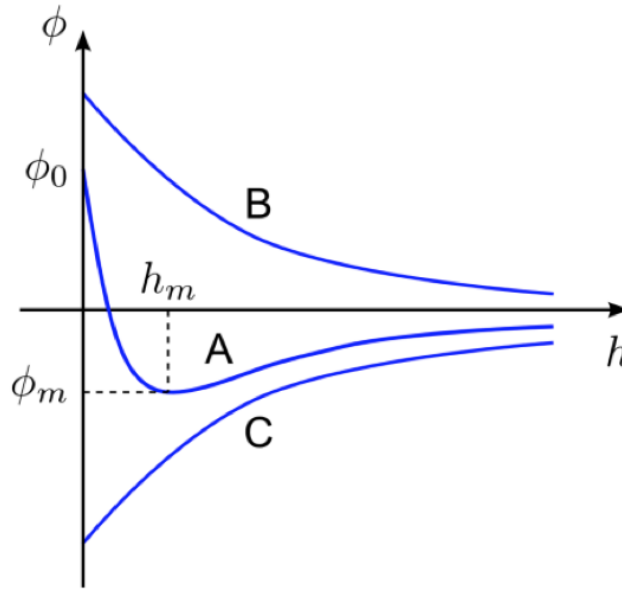
Figure 15. Shape of the electrostatic potentials [Nitte1998].

Let $\hat{\phi}$ denote the normalized electrostatic potential defined by the equation below.

$$\hat{\phi} = \frac{e}{k_B T_p} \phi$$

(28)

Then, by using this normalized electrostatic potential, the number densities of the plasma particles are given by the equation below.

$$n_i = n_{i,\infty} \left(1 - \frac{2\hat{\phi}}{\alpha \mathcal{M}_\theta^2} \right)^{-\frac{1}{2}}$$

$$n_e = \begin{cases} \dfrac{n_{e,\infty}}{2} \exp\left(\dfrac{\hat{\phi} - \hat{\phi}_\infty}{\alpha}\right) \left\{ 1 - \mathrm{erf}\left(\sqrt{\dfrac{\hat{\phi} - \hat{\phi}_m}{\alpha}} - \eta \right) \right\} & (h < h_m) \\[4mm] \dfrac{n_{e,\infty}}{2} \exp\left(\dfrac{\hat{\phi} - \hat{\phi}_\infty}{\alpha}\right) \left\{ 1 + \mathrm{erf}\left(\sqrt{\dfrac{\hat{\phi} - \hat{\phi}_m}{\alpha}} - \eta \right) + 2\,\mathrm{erf}\,\eta \right\} & (h \geq h_m) \end{cases}$$

$$n_p = \begin{cases} \dfrac{n_{p,0}}{2} \exp(\hat{\phi} - \hat{\phi}_0) \left\{ 1 + \mathrm{erf}\left(\sqrt{\hat{\phi} - \hat{\phi}_m} \right) \right\} & (h < h_m) \\[4mm] \dfrac{n_{p,0}}{2} \exp(\hat{\phi} - \hat{\phi}_0) \left\{ 1 - \mathrm{erf}\left(\sqrt{\hat{\phi} - \hat{\phi}_m} \right) \right\} & (h \geq h_m) \end{cases}$$

(29)

where $\alpha = T_e/T_p$; $\mathcal{M}_\theta = \max(1, \mathcal{M} \cos\theta)$; $\eta = v_D/v_{T,e}$; and $\mathrm{erf}\,x$ is the error function defined as follows:

$$\mathrm{erf}\,x = \frac{2}{\sqrt{\pi}} \int_0^x e^{-t^2} dt$$

(30)

The Poisson's equation can be written as

$$\lambda_D^2 \frac{\partial^2 \hat{\phi}}{\partial h^2} = -\frac{1}{\tilde{n}} \left(n_i - n_e - n_p \right)$$

(31)

where the Debye length λ_D and the characteristic number density $\tilde{n}$ are given by the following equations:

$$\lambda_D = \sqrt{\frac{\varepsilon_0 k_B T_p}{\tilde{n} e^2}}$$

$$\tilde{n} = n_{p,0} + \frac{n_{e,\infty}}{\alpha}$$

(32)

Consequently, the seconder order differential equation in terms of h, Eq.(37), can be solved numerically. To solve the differential equation, three unknown parameters $\hat{\phi}_0$, $\hat{\phi}_m$, and $n_{e,\infty}$

must be specified. These parameters can be obtained by numerically solving the following three equations:

$$\left.\frac{\partial \hat{\phi}}{\partial h}\right|_{h=\infty} = 0$$

(33)

$$\left.\frac{\partial^2 \hat{\phi}}{\partial h^2}\right|_{h=\infty} = 0$$

(34)

$$n_{i,\infty}\mathcal{M}_\theta \sqrt{2\pi\alpha\frac{m_e}{m_i}} + n_{p,0}\exp\left(\hat{\phi}_m - \hat{\phi}_0\right)$$
$$- {}_{e,\infty}\sqrt{\alpha}\left[\exp\left\{-\left(\sqrt{-\frac{\hat{\phi}_m}{\alpha}} + \eta\right)^2\right\} - \sqrt{\pi}\eta\,\mathrm{erfc}\left(\sqrt{-\frac{\hat{\phi}_m}{\alpha}} + \eta\right)\right] = 0$$

(35)

The first equation is the condition of zero electrostatic field at infinity; the second equation is the condition of quasi-neutrality at infinity; and the third equation is the condition of zero net current at infinity [Nitter1998].

Once the normalized potential $\hat{\phi}$ is computed, the electrostatic potential $\phi(h,\theta)$ can be immediately obtained from Eq. (37). As a result, the electrostatic force applied to a spacecraft can be calculated.

7. Plasma Dynamics

7.1 Electrostatic Potential and Electrostatic Force

Airless bodies, such as asteroids, are exposed to the solar wind plasma. Due to the interaction between the surface of an asteroid and the plasma, a plasma sheath is formed above the asteroid, leading to the existence of an electrostatic field. In addition, the solar radiation on the sunlit surface causes the photoelectric effect, which charges the surface

positively and expels photoelectrons. Consequently, the distributions of these charged particles (solar wind ions, solar wind electrons, and photoelectrons) dominate the complex electrostatic field around an asteroid.

The relationship between the particle densities and the electrostatic potential is described by Poisson's equation. Given that the asteroid has spherical shape and the particle distribution is symmetry about the sub-solar line, the electrostatic potential is expressed as a function of the altitude h and the solar incident angle θ defined by the equations below.

$$
\begin{aligned}
h &= r - R \\
\theta &= \cos^{-1}\left(-\frac{x}{r}\right)
\end{aligned}
$$

$$(36)$$

Here, $R = D/2$ is the radius of an asteroid. Then, the electrostatic potential around the asteroid is modelled using the following Poisson's equation, which is expressed as a seconder order differential equation in terms of h [Nitter1998, Jeong2008, Harzell2008]:

$$
\frac{\partial^2 \phi(h,\theta)}{\partial h^2} = -\frac{e}{\varepsilon_0}\left(n_i - n_e - n_p\right)
$$

$$(37)$$

where e is the elementary charge; ε_0 is the vacuum permittivity; and n_i, n_e, and n_p are number densities of the solar wind ions, the solar wind electrons, and the photoelectrons, respectively. Assuming that the solar wind ions are modelled as a mono-energetic beam, and the solar wind electrons and the photoelectrons follow Maxwellian distributions, n_i, n_e, and n_p are given by analytical expressions, as presented in the previous section. Based on this assumption, $\phi(h,\theta)$ can be solved numerically as described above.

Given that there is the direct relationship between (h,θ) and the position vector $\boldsymbol{r}$, the electrostatic potential can also be expressed in the Cartesian coordinate as $\phi(\boldsymbol{r})$. Therefore, the electrostatic force acting on a spacecraft with the charge Q is calculated from the equation below.

$$
\boldsymbol{F}_E = Q \cdot \boldsymbol{E}(\boldsymbol{r}) = -Q\frac{\partial \phi(\boldsymbol{r})}{\partial \boldsymbol{r}}
$$

$$(38)$$

Here, $\boldsymbol{E}(\boldsymbol{r})$ denotes the local electrostatic field.

7.2   Spacecraft Charging

The power supply voltage for charging a spacecraft, which is regarded as the electrostatic potential of the spacecraft relative to the ambient plasma potential, is given by the equation below.

$$V_{sc} = \frac{Q}{C}$$

(39)

The spacecraft in the plasma environment around an asteroid collects charged particles. Besides, the spacecraft itself is also exposed to the solar radiation and emits photoelectrons. As a result, the charge of the spacecraft varies due to the current flux from/to the ambient plasma, as expressed by the equation below [Nitter1998, King2002b].

$$\frac{dQ}{dt} = I_i - I_e - I_p + I_{p,sc}$$

(40)

where I_i, I_e, and I_p are the currents from the solar wind ions, the solar wind electrons, and the photoelectrons emitted from the asteroid surface; and $I_{p,sc}$ is the photoelectron current from the spacecraft. These currents can be expressed as follows [Nitter1998, Havnes1987, Hirata2012]:

$$I_i = \begin{cases} N_{sp} \cdot \pi r_{sp}^2 e n_i v_i \left(1 - \dfrac{2eV_{sc}}{m_i v_i^2}\right) & \left(V_{sc} < \dfrac{m_i v_i^2}{2e}\right) \\[2em] 0 & \left(V_{sc} \geq \dfrac{m_i v_i^2}{2e}\right) \end{cases}$$

$$I_e = \begin{cases} N_{sp} \cdot \pi r_{sp}^2 e n_e \sqrt{\dfrac{8k_B T_e}{\pi m_e}} \exp\left(\dfrac{eV_{sc}}{k_B T_e}\right) & (V_{sc} < 0) \\[2em] N_{sp} \cdot \pi r_{sp}^2 e n_e \sqrt{\dfrac{8k_B T_e}{\pi m_e}} \left(1 + \dfrac{eV_{sc}}{k_B T_e}\right) & (V_{sc} \geq 0) \end{cases}$$

$$I_p = \begin{cases} N_{sp} \cdot \pi r_{sp}^2 e n_p \sqrt{\dfrac{8k_B T_p}{\pi m_e}} \exp\left(\dfrac{eV_{sc}}{k_B T_p}\right) & (V_{sc} < 0) \\[2em] N_{sp} \cdot \pi r_{sp}^2 e n_p \sqrt{\dfrac{8k_B T_p}{\pi m_e}} \left(1 + \dfrac{eV_{sc}}{k_B T_p}\right) & (V_{sc} \geq 0) \end{cases}$$

$$I_{p,sc} = \begin{cases} N_{sp}^* \cdot \pi r_{sp}^2 \dfrac{\varepsilon_{sc} J_0}{d^2} & (V_{sc} < 0) \\[2em] N_{sp}^* \cdot \pi r_{sp}^2 \dfrac{\varepsilon_{sc} J_0}{d^2} \exp\left(-\dfrac{eV_{sc}}{k_B T_p}\right) & (V_{sc} \geq 0) \end{cases}$$

(41)

where k_B is the Boltzmann constant; $v_i \equiv (v_D^2 - 2e\phi/m_i)^{1/2}$ is the velocity of the solar wind ions; T_e, and T_p are the temperatures of the solar wind electrons and photoelectrons, respectively; m_i and m_e are the masses of an ion and an electron, respectively; ε_{sc} is the photoemissivity of a spacecraft; $J_0 \equiv 4.5 \times 10^{-6}$ A/m^2 is the photoemission current density at 1 AU [Nitter1998]; and d is the distance of an asteroid form the sun expressed in AU. These equations indicate that a positively charged spacecraft attracts more electrons, while a negatively charged spacecraft attracts more ions. The last equation , derived based on the assumption that $v_{T,i} \ll v_D \ll v_{T,e}$, shows that the photoelectric effect is less likely to occur for a positively charged spacecraft.

Since the charge of the spacecraft is affected by the ambient plasma, the spacecraft must emit current constantly in order to maintain the charge level [King2002b]. The emitted current I_{sc} is given by the following equation:

$$\frac{dQ}{dt} = I_i - I_e - I_p + I_{p,sc} + I_{sc} = 0$$
$$\therefore \ I_{sc} = -I_i + I_e + I_p - I_{p,sc}$$

(42)

Several solutions for emitting current from a spacecraft have been proposed in previous research [Quadrelli2017, Schaub2003, King2002b]. Consequently, the required power for electrostatic levitation with a constant charge Q is calculated as follows:

$$P = |V_{sc}I_{sc}|$$

(43)

The flow chart to calculate the required power is described in Figure 16.
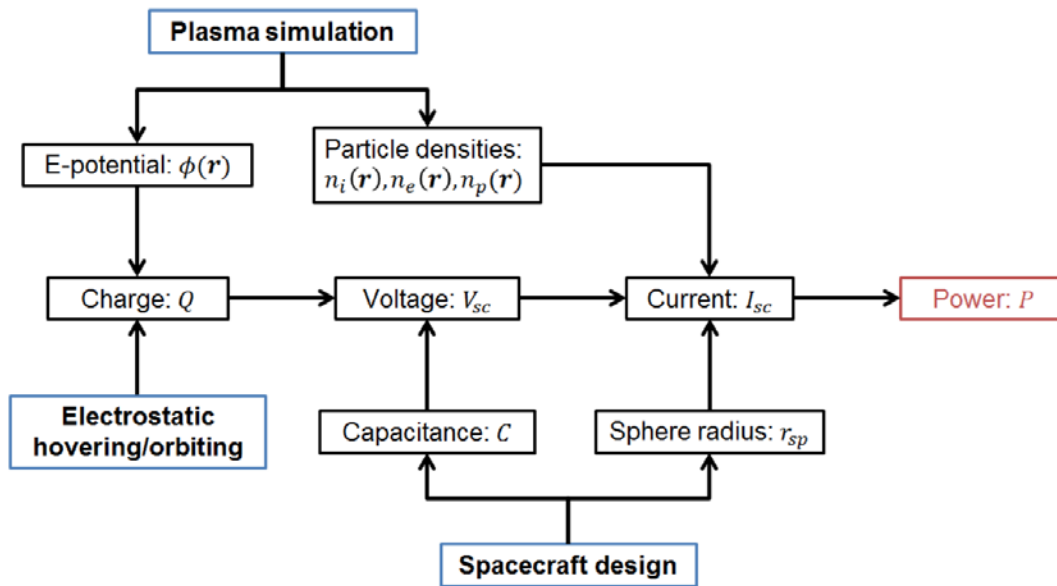
Figure 16. Flow chart of power calculation.

7.3   Simulation of the Plasma Environment

This subsection presents several simulation results of the plasma environment around the asteroid. Figure 17 depicts the electrostatic potential profiles computed from Eq. (37) for several different solar incident angles. It can be observed that the surface of the asteroid is positively charged when the solar incident angle is small (i.e. near the sub-solar region), while the surface is negatively charged when the solar incident angled is large (i.e. near the terminator region). The enlarged view in Figure 18 also shows that non-monotonic sheath profiles appear in some cases, which implies that plasma structure around an asteroid is complex. Figure 19 shows the relationship between the solar incident angle and the Debye

49

length λ_D. The Debye length is an index of how far from the asteroid surface the electrostatic effects can exert influence, and thus, this figure implies that the electrostatic force obtained in the terminator region is much stronger than that of the sub-solar region.

Figure 20 illustrates the distributions of the charged particles along the sub-solar line ($\theta = 0$ deg). One of the remarkable features is that the number density of photoelectrons is considerably large near the surface. This dense photoelectron layer on the dayside involves strong screening effect, and thus, the Debye length near the sub-solar point is comparatively short as shown in Figure 20. It is also shown in Figure 20 that, when the altitude increases, the density of the net electrons approaches that of solar wind ions, which indicates that the plasma is in a quasi-neutral state.

Figure 20 illustrates a contour map of the electrostatic potential around the asteroid, which is expressed in the x-y plane. The broken line in the enlarged view corresponds to the potential level of zero volts, and it is evident that the dayside region close to the surface has positive potential; on the other hand, there exists strong negative potential region on the nightside and around the terminator. Note that the wake streams of the solar wind behind the asteroid is not considered in this simulation, which can exert strong influence on the nightside electrostatic potential [Han2016, Yu2016]; however, the current model is regarded to be valid for analysis of plasma structures on the dayside and in the terminator region, which are our major interests as mentioned in the introduction. The visual representation of the electrostatic field is displayed in Figure 21. The direction and magnitude of the electrostatic field are expressed by the arrows and their colors, respectively. This figure is useful to understand the behavior of electrostatic force acting on an E-Glider and to make effective use of it.

These unique characteristics regarding the plasma environment around an asteroid, which are provided in Figure 21, have been revealed in previous studies as well and are consistent with them [Nitter1998, Poppe2011, Han2016, Yu2016]. Consequently, it has been confirmed that the numerical model used in this study is valid to analyze the E-Glider dynamics.
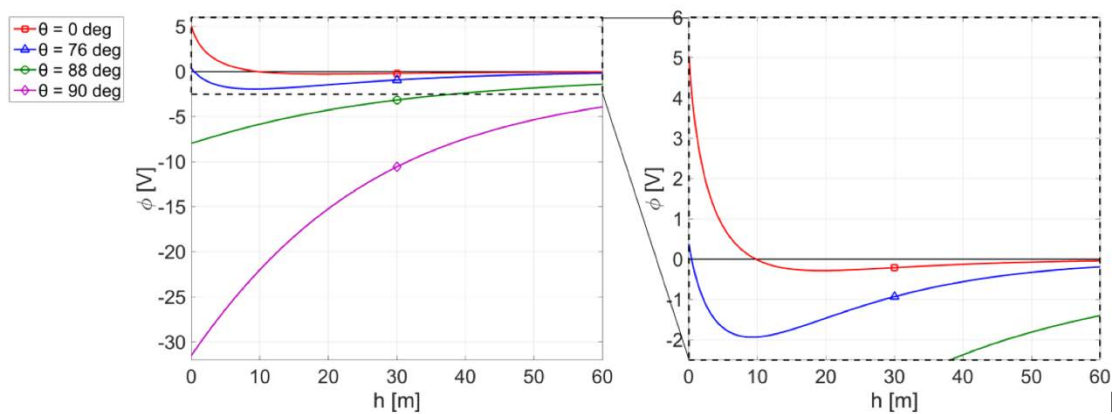
Figure 17. Electrostatic potential profiles for different solar incident angles.
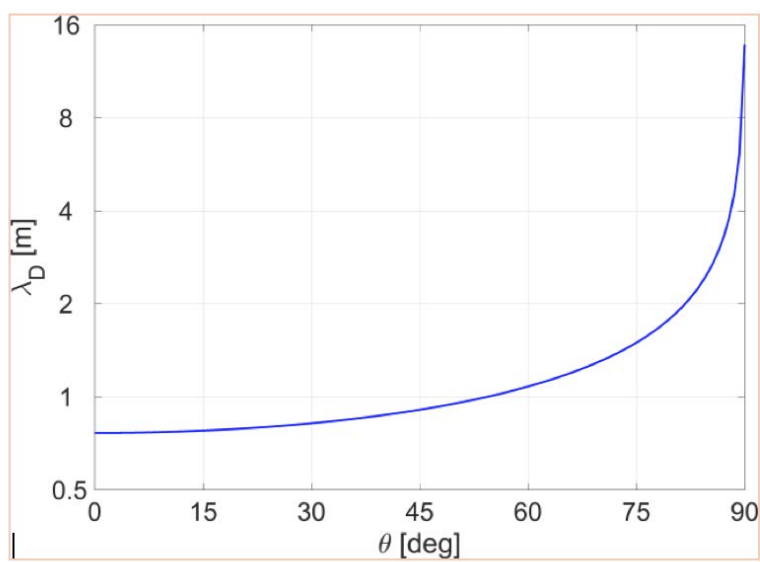
Figure 18. Relationship between the solar incident angle and the Debye length
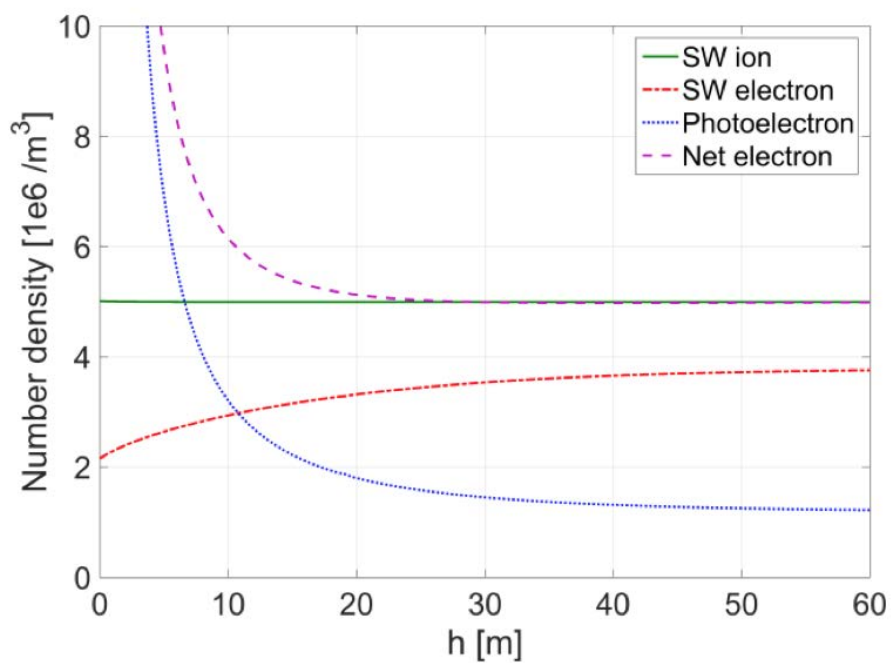
Figure 19. Number densities of charged particles.
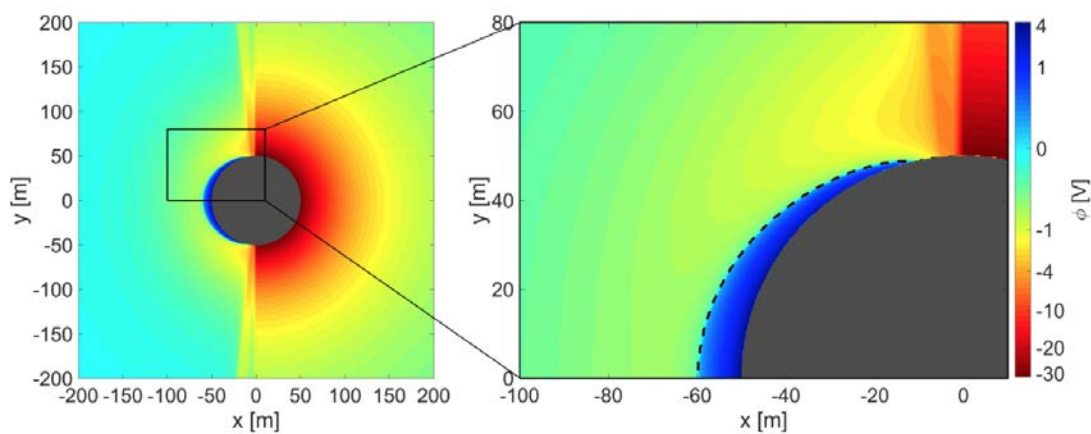
Figure 20. Electrostatic potential around the charged asteroid.
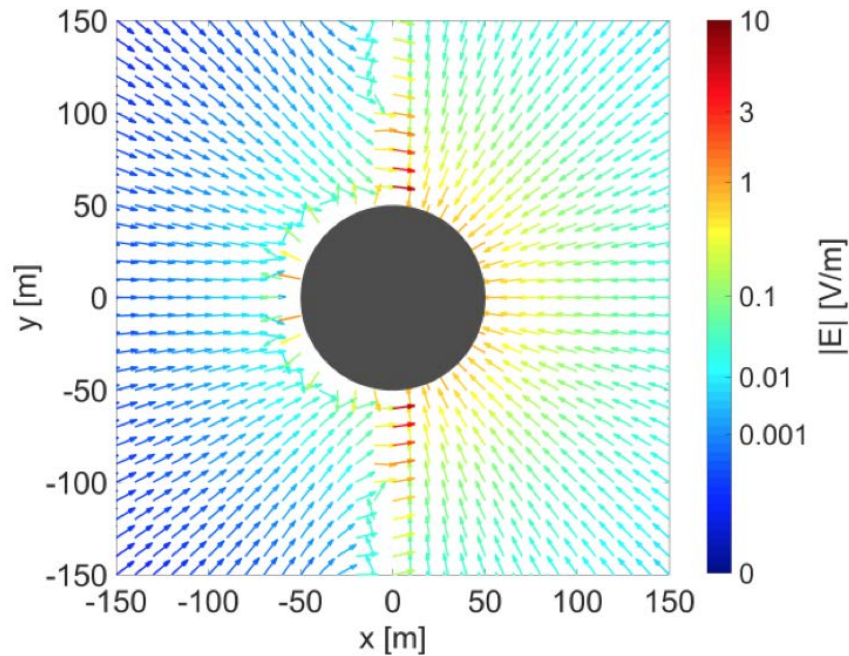
Figure 21. Electrostatic field vector components around the asteroid.

8. E-Glider System Concept

In this section, we describe the EGlider system configuration, and the possibility of ejecting a number of probes to increase the mission success by sampling the surface at multiple sites, while the EGlider remains hovering at a convenient altitude.

8.1 System Configuration

The wings could be made of very thin charged Mylar film, or long charged Mylar strands, which are electrostatically inflated, like in the Earth's Gossamer spider webs, as demonstrated in Figure 22 taken from [Stiles2010, Stiles2011, Stiles2012], and would enable lift via electrostatic repulsion. Since the E-glider follows the Sun illumination, the solar

panels on the vehicle constantly charge a battery. Electron emitter arrays discharge electrons from the surface on the shielded side when a voltage difference in excess of a threshold voltage develops between a field emission array gate and the emitter array due to differential charging of the exposed and shielded sides of the vehicle chassis, which has one side exposed to the Sun's UV photons, and another side shielded from the UV photon exposure [US2013]. The emitted electrons are used to selectively and differentially charge the various surfaces of the glider to match the ambient electrostatic charge level, so that the E-Glider can acquire a specific force/moment distribution to enable the glide, and follow a planned path. Figure 23 shows a CAD model depicting a preliminary design of the E-Glider.
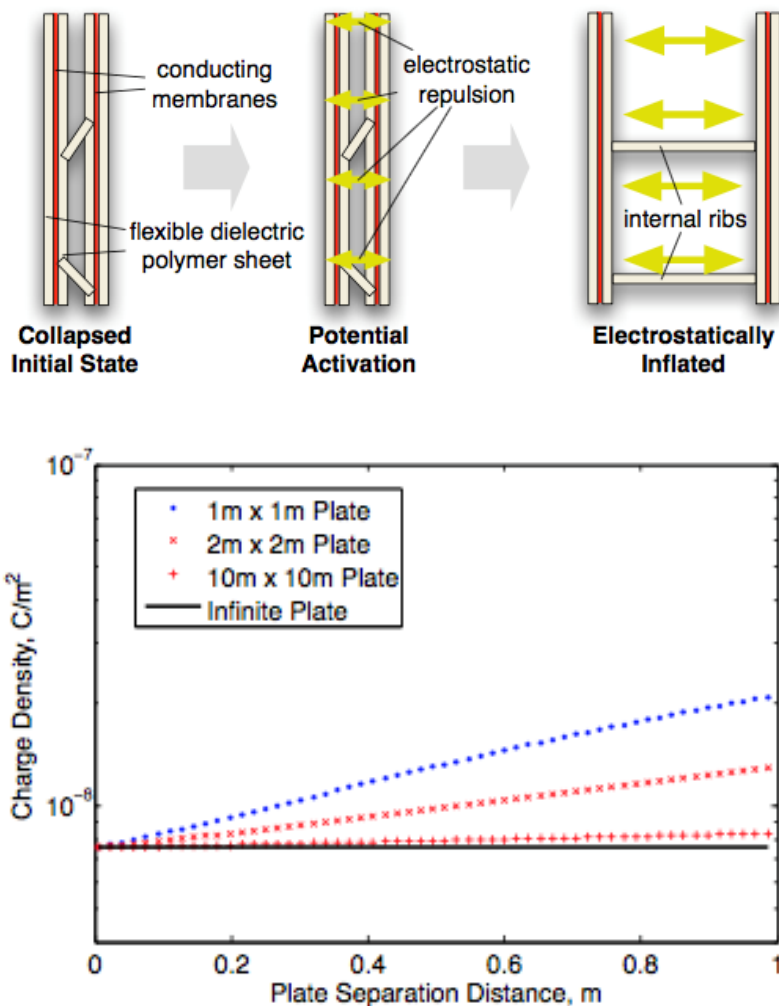
Figure 22. *(top) sample open-ended membrane rib structure undergoing electrostatic inflation [Stiles2012]. (bottom) charge density required to inflate a shell in GEO [Stiles2012].*
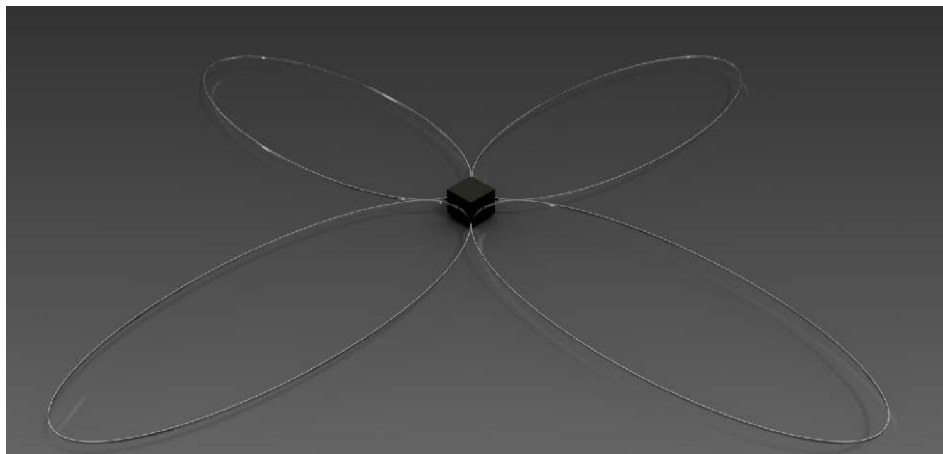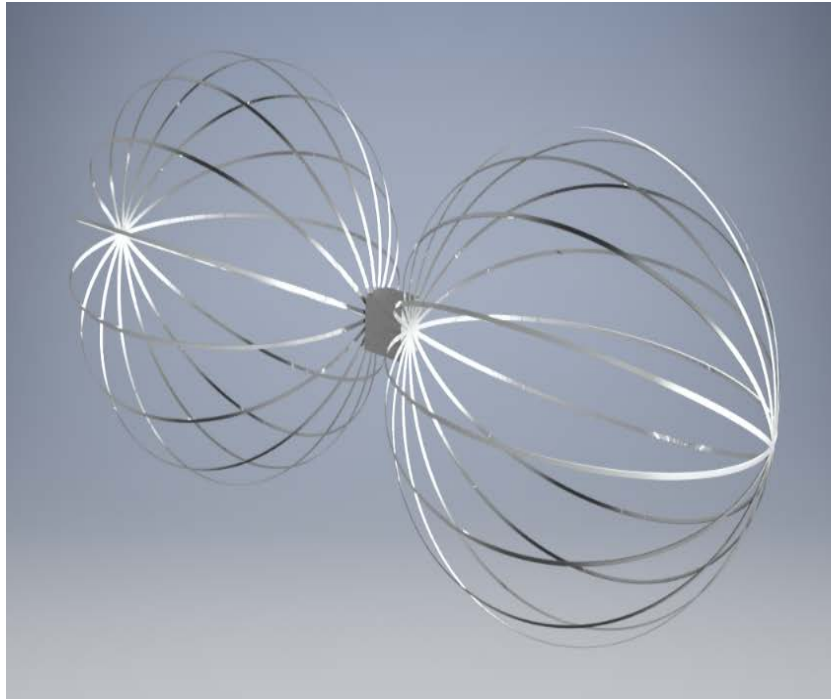
Figure 23. *Preliminary CAD models of E-Glider system design.*
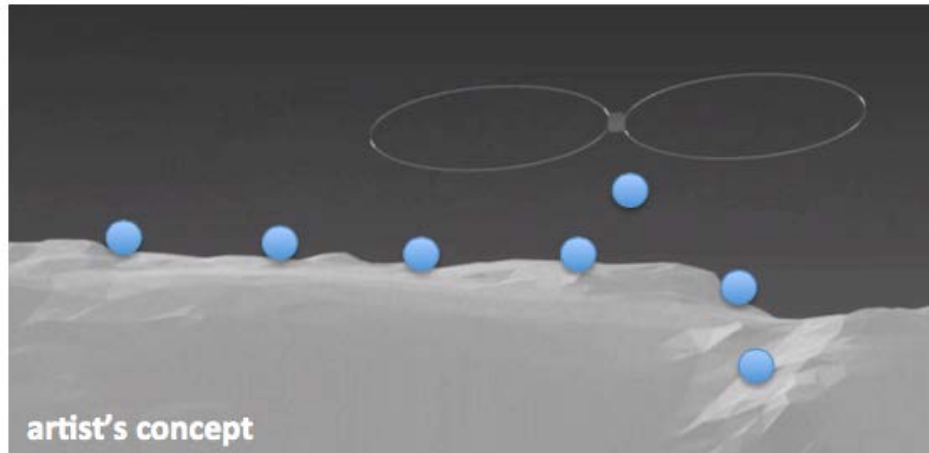
Figure 24. EGlider as mothercraft.

In addition to carrying onboard science instruments, the E-Glider could also serve as a mothership for small rovers that could be ejected from the E-Glider and used for in-situ analysis of the body surface, as shown in Figure 24. For small bodies, the force of gravity is nearly negligible, preventing the use of wheeled or hopping mechanisms for locomotion. A soft, deformable rover, however, may be able to roll around the surface through deformation of the rover body via electroactive polymers and controllable adhesion to the surface via electrostatic attraction. Figure 25 shows the principle of "dielectric rolling", based on bending the shell of the balloon, which acts as a dielectric capacitor. Once there is an offset between the geometric center and the center of "electrostatic pressure", a torque is possible. Certain electroactive polymers have been shown to work in space-like conditions, including under vacuum and down to -100 °C, as shown in Table 4 [Carpi2005]. Each rover would be covered in patches of actuators made of dielectric elastomers. The rover would be inflated pneumatically to a small initial positive pressure to provide a spherical shape. Actuation of the dielectric elastomer patches that are in proximity or in contact with the surface of the body would cause the patches to expand outward, pushing against the surface of the body and causing the rover to roll. In the case of negligible gravity, the skin of the rover could be biased electrically such that the side of the rover that is in contact with the surface could be charged to the opposite polarity of the surface, enabling electrostatic attraction and allowing the rover to roll along the surface of the body.
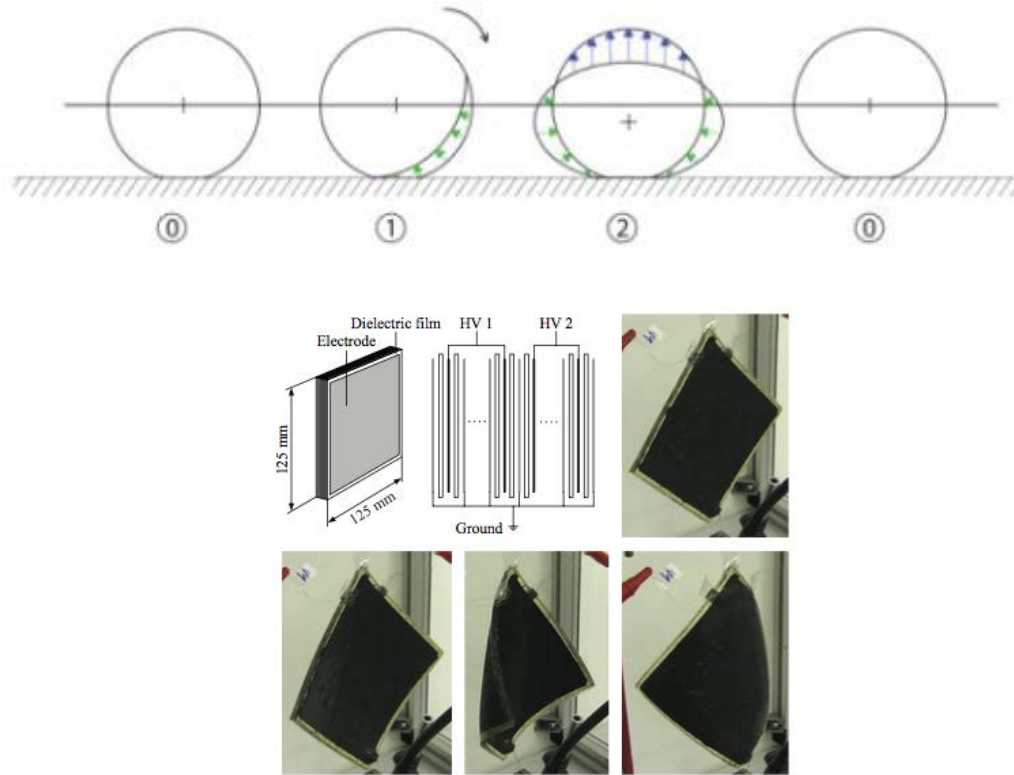
Figure 25. *(top) Principle of "dielectric rolling". (bottom) Bending of dielectric shell [Lochmatter2007].*

8.2 Dielectric elastomeric probes for mobility in low gravity

Controlled moving in low gravity environments presents an interesting challenge in that typical solutions for mobility on Earth rely upon the presence of a substantial gravitational force which can't be relied upon when exploring small bodies. Wheeled systems rely on gravitational attraction to maintain sufficient friction between the wheel and ground to enable lateral motion. lf the gravitational force is too low, then the wheels may not be able to generate enough traction to move. Legged solutions face a similar challenge. In the absence of a sufficient gravitational force, the foot of a legged may not have enough traction for motion. Further, a legged system may risk stepping with too much force and exceeding

the escape velocity of the body. A deformable, soft robot with dielectric elastomer panels that can generate reactionary forces with the ground based on deformations or electric fields may provide a potential solution to mobility in low gravity environments.

Dielectric elastomer actuators (DEAs) are a class of electroactive polymers that can deform due to electric fields [Perline1998], as shown in Figure 26. A dielectric elastomer is sandwiched between a pair of compliant electrodes which are connected to a power supply. As a voltage is applied across the dielectric layer, charges build up in the electrodes. The opposite charges attract, applying Maxwell pressure to the elastomer, compressing it. Since the electrodes are compliant, like charges also repel, inducing a lateral strain in the DEA. The combination of these effects cause the DEA to both compress in thickness while stretching laterally.

Table 4. Environmental compliance of tested EAP materials [Carpi2005].

Material	Elastic down to $-100\,^\circ$C [1]	Elastic down to $-40\,^\circ$C	Temperature dependence of mechanical properties	Temperature dependence of electric properties	Outgassing properties: TML [4] < 1%	Withstand cooling to $-150\,^\circ$C
TC5005	x	✓	weak[2]	strong[2]	x	x
E625	x	✓	weak[2]	weak[2]	x	✓
LR3162	x	✓	weak[2]	weak[2]	✓	✓[5]
RTV567	✓	✓	weak[3]	weak[3]	✓	✓

DEAs have been proposed for mobility systems in space exploration. For example, Carpi et al proposed a Martian jumping rover with a stack of DEAs which would cause the rover to jump due to a change in the center of mass of the system [Carpi2007]. Similarly, Plante et al

developed a DEA-based hopping robot for planetary exploration [Plante2007, Dubowsky2005, Dubowsky2007]. More specifically, Potz et al developed an inflated, spherical, rolling robot using DEA panels to adjust the center of gravity to induce directional motion [Potz2010, Artusi2011]. External panels comprised of DEAs were affixed together and the entire structure was inflated. Electrical activation of a single panel caused a thinning and stretching of that panel, which resulted in a localized bulging in that DEA panel. The bulging offset the center of gravity and/or introduced a force against the ground, causing the rover to roll. In a related example, Wait et al implemented a pneumatically actuated rover comprised of a number of panels attached together in a pattern similar to a soccer ball. Each panel was attached to a pneumatic source, which, when inflated pressed against the ground, causing the rover to achieve directional motion [Menon2009]. The directionality enabled by Wait's design [Wait1010], coupled with the DEA panels for a spherical, rolling rover demonstrated by Potz et al, could lead to a deformable, DEA-based robot capable of articulated motion in low

Dielectric elastomers have been studied for space-based applications and extreme environments. Menon et al demonstrated that dielectric silicone rubbers for DEAs show appreciable strain, even in low vacuum conditions [Menon2009]. De Rossi et al studied the potential of several electroactive polymers under the thermal conditions experienced in space applications and determined that DEAs are possible solutions for actuation in thermal environments ranging from the sun side of the Moon (+ 140 °C) to possibly even shaded regions in deep space (-270 °C) [DeRossi2004].

The E-Glider is expected to operate at low altitudes (in the m to km range), but is not optimized for ground-based, in situ scientific analysis. For contact sampling, probes based on DEA actuators may be deployed from altitude to sample and explore the surface of the body. For example, a number of small, lightweight DEA probes may be carried on the E-Glider as a payload and then ejected towards the surface of the target body during approach. The DEA probe can then translate over the surface of the body to perform the desired scientific mission.

The probe will be comprised of several DEA panels that can be individually actuated. The internal structure of the probe will be inflated pneumatically to a positive pressure to establish the shape of the probe. DE activation will control bulging of the individual DE panels, allowing the probe to roll with directional control. Since the surface of small bodies is expected to be highly charged, the polarity of the external DEA panels can be controlled to

attract (via opposite charge) or repel (via like charges) the surface of the body, as shown in Figure 27. Pneumatic and DEA control will enable the probe to conform to the surface features of the body, enabling conformable contact with the body to maximize surface adhesion/repulsion forces. Since the external structure of the probe is elastomeric, it is expected to be collapsible to a small footprint to maximize storage and packing during transport. At the point of deployment, a small pneumatic source could pressurize the rover to prepare it for mobility. Electroadhesion has been studied for adhering objects, but the effects may be shielded in the presence of the insulating dust that could be found on small bodies. However, electroadhesion can be complemented with electric repulsion, which may provide sufficient torque for inducing a controlled rolling motion in the probe. Figure 28 shows two views of the flight of the inflated E-Glider around Itokawa.

In summary, electroactive polymers have been demonstrated to be viable options for actuating robotic structures for space exploration. In particular, dielectric elastomers may be the most promising for viability in the extreme conditions of space. Mobility systems based upon DEAs have been established by a number of research groups, and this proposal leverages their work into proposing a DEA-based probe that can be launched by the E-Glider to perform in situ, ground-based sampling of small bodies.
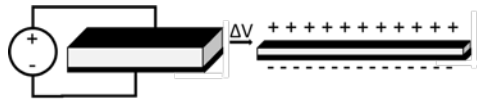
Figure 26. *Principle of dielectric elastomer actuators. Comprised of a dielectric elastomer (shown in white) sandwiched by two compliant electrodes (black) and connected to a voltage source. A change in voltage charges the electrodes, inducing a buildup of charge on the electrodes. Opposite charges then attract, compressing the dielectric elastomer in the vertical direction, while like charges repel, inducing an additional lateral strain.*
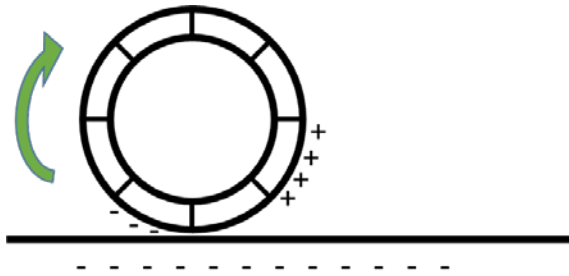
Figure 27. *Rolling via electric forces - for a negatively charged body, positive charges attract while negatively biased*

panels repel, inducing rolling in the DEA probe.
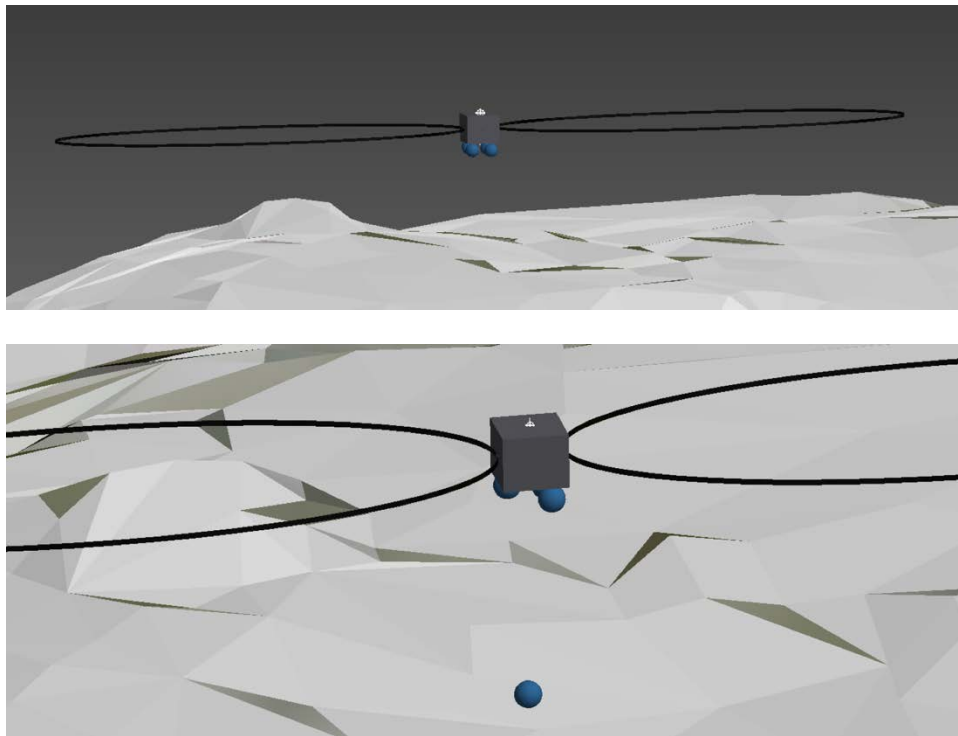
Figure 28. DSENDS views of the E-Glider in flight around Itokawa.

9. Methods for Charging the E-Glider

The overall concept for the E-Glider is to develop a small vehicle/structure that can be charged relative to an asteroid and the resulting electric field differences used to maneuver the object over the immediate surface of the asteroid. A primary requirement for accomplishing this is to be able to control the charge on the object and indeed manipulate the differential potential on its surfaces to allow not only movement over the asteroid but the ability to orient the structure relative to the surface. To do this, the E-Glider must be able to both generate charge and alter that charge in real time on its surfaces. The following briefly reviews and evaluates several possible methods that might be considered for accomplishing this.

9.1 Method 1: Charge Ejection

A standard method for charging/discharging spacecraft is by emitting beams of electrons or positively charged ions. Indeed, the ability to emit neutral beams of ions has been highly developed and is now used for electric propulsion for missions like Deep Space One and Dawn. Typically atomic species such as argon or xenon are ionized and accelerated by high voltage electric fields to provide low thrust but high efficiency propulsion. The emission of only positive ions, however, typically leads to high negative potentials (~kV's) on the emitting vehicle equivalent to the potential on the accelerating grids. Similarly, electron beams can be used to emit negative charge causing the vehicle to go negative. The grounding scheme for the vehicle, the local magnetic or electric fields, or even physical shadowing can all affect the returning beam particles so that isolated (electrically) surfaces can become differentially charged. Given the complex return patterns and resulting differential charging, mono-energetic beams are usually not used to control charging unless the body is totally conducting in which case the absolute potential can be adjusted in real time to the desired level. Instead, the ejected beam is usually "neutralized" in the case of an ion beam by emitting low energy electrons to keep the absolute vehicle potentials as low as possible. Thus while electron and ion beams can be used to control potential on electrically isolated spacecraft surfaces, it is difficult to determine the detailed charging of the overall vehicle accurately given the uncertain return current pathways. Also the systems for generating ion beams in particular can be relatively cumbersome compared to the E-Glider.

9.2 Method 2: Electron field emission devices.

A method that has seen some utilization in controlling surface charging is that associated with electron field emission devices. An example would be a surface consisting of a layer of very small carbide or similar cones etched into the surface. A negative potential on the surface will cause the points to freely emit electrons thereby driving the surface positive. Such devices are available but currently are limited to negative charge emission. They are also typically low potential devices, though they could be used to mimic photoelectron emission currents on shadowed surfaces. The electron emitters would need to be hard mounted on or electrically coupled to the surfaces to be charged. Though typically requiring a power source to actively emit electrons and charge a surface positive, various designers have proposed using such surface emitter in a passive mode to discharge negative surfaces.

9.3 Method 3: Material Selection

Though very much a function of the ambient environment, spacecraft surface materials all have unique photoemission, back scatter, and secondary emission properties. Several well know materials for example emit many times more electrons at very low energies (e.g., ITO coatings) then impact the surface so that the surface will stay near 0 potential. Some materials are profuse photoelectron emitters and will drive surfaces positive (~10 V) in sunlight. Other materials such as aluminum actually emit few secondary electrons and will charge negatively when impacted by electrons. By the selective choice of surface materials (and/or perhaps interchangeable surfaces–a "Lazy Suzanne"), surfaces could be designed to charge to different potentials in the solar wind, when exposed to sunlight, in the asteroid plasma wake, etc. Although basically a passive process, this method of generating differential charging is very dependent on the ambient environment as the sunlight, impacting electrons, and solar wind plasma would be highly variable. In addition, the asteroid would provide a highly variable shield to sunlight and plasma and would have a varying plasmasheath.

9.4 Method 4: Direct Biasing

Differential potentials can be induced on electrically isolate surfaces relative to the spacecraft buss by using active sources to bias the different surfaces. This biasing can be accomplished by batteries/solar cells or by a compact Van De Graff generator. Batteries/solar cells have the advantage of passive components though energy storage needs to be carefully considered. A compact Van De Graff generator could be adapted to produce high surface potentials but

would require moving components (and their resulting torques) such as a small electric motor and the static charging method (moving belt, spinning parallel plates, etc.). Similarly, it would need to be continually powered by a battery or solar cell.

In summary, surfaces in space will naturally charge differentially relative each other in the space environment based on differences in surface materials and exposure conditions. These are typically very low levels (<100 V) and will vary rapidly with the changes in the space environment. Several methods offer the capability to actively charge isolated spacecraft surfaces. All have drawbacks ranging from mechanical complexity (the Van De Graff) to size/power (ion beams). Further, any system will need to be able to rapidly detect the ambient electric field environment and respond appropriately. Of the methods discussed, the simple Van De Graff approach may prove the most reliable. Issues still remain, however, as to the details of the electric fields generated and the effects of return currents and photoemission on surface potential variations. Finally, the sheath of the E-Glider and its interaction with the asteroid's plasma sheath will need to be carefully modeled in real time to allow rapid changes in the E-Glider's surface fields. The latter is a complex but doable problem given current computing power and available models such as NASCAP-2K.

9.5 Approaches for Differential Surface Charging

For small bodies in the interplanetary environment, the main source of surface charging is the Solar Wind plasma and sunlight. Typically surfaces in sunlight are dominated by photoelectron emission currents so that the typical potentials are on the order of ~10 V positive. Given the expected shadowing of the flowing Solar Wind plasma and the insulating nature of the asteroidal material, the plasma wake of asteroid is expected to be largely devoid of Solar Wind plasma leading to differential surface potential variations around the asteroid. The wake region can, in the absence of the Solar Wind plasma, charge negatively with values of -100 V having been observed on shadowed spacecraft surfaces (note: some simulations imply that potentials as high as -1000 V may be possible, however). The sunlight and Solar wind, however, can cause charge neutralization within a fraction of a second on exposed spacecraft surfaces. It will be the same or worse around an asteroid with higher plasma densities expected close to the asteroid and a complex terminator and wake region in the anti-sunward direction. As a result the E-Glider electrostatic inflation and levitation concept will have to provide continual charge emission to control the spacecraft potential relative to the

space environment and asteroid. Here we will describe the characteristics of that charge control system and how the differential charging will be modeled.

Any charge control system will need to maintain the absolute potential of the spacecraft relative to the asteroid to control levitation and be able to generate differential potentials to control attitude. The former can be accomplished by using combinations of small electron (to bias the vehicle positive) or ion (to bias the vehicle negative) current emitting systems such as provided by ion engines or electron beams (more recently electron-emitting surfaces have become available that may also be an option). The large, differential potentials required for attitude control may be produced by a small Van De Graff generator or by battery/solar cell power bias sources. In any case, the complex interactions of these active charge control systems with the ambient plasma and the E-Glider will need to be modeled in real time. Previous work at JPL on the plasma dynamics of a 150 m solar sail [Garrett2004] studied the charging characteristics of large bodies in the Solar Wind and is applicable to the E-Glider concept. To do this, the spacecraft charging analysis program NASCAP-2k was used to model differential potentials of many tens of volts across the thickness of the solar sail membrane and its insulating back in the Solar Wind environments. NASCAP-2k [Mandell2006, Davis2004] is a widely used interactive toolkit for studying such plasma interactions with realistic bodies in three dimensions. It can model interactions that occur in tenuous and in dense plasma environments. Capabilities include surface charging in geosynchronous and interplanetary orbits and sheath and wake structures. The JPL/NASA NASCAP-2k study results demonstrated that the complex charging interactions and differential charging of a large body (a solar sail) and a small spacecraft can be readily modeled. In addition to NASCAP-2k, the Immersed-Finite-Element PIC (IFE-PIC) algorithm [Yu2016] has been developed which allows the modeling of the effects of differential charging on dust particles in space. Using the IFE-PIC algorithm, recent work [Yu2016] has investigated the numerical modeling of dust dynamics around small asteroidal bodies. In that work, a numerical investigation on the charged dust distribution around small spherical asteroids with the implementation of a 3D IFE-PIC plasma-asteroid interaction model and a 3D dust transport model was conducted. In all simulation cases analyzed, charged dust was observed to tend to migrate toward the dayside at high altitudes, with the exception of the ultra fine grain case. Near the surface, there is a preference to gravitate towards the dayside. At large altitudes, gravity would appear to be the dominant player in dust transport, while the electric field has a strong influence on dust dynamics at low

altitudes. An increase in the electrostatic force would be more efficient at perturbing the density profile between the low and high altitude. For smaller grains, solar radiation pressure may have a greater role on dynamics around an asteroid. Figure 29 shows a representative electrostatic field distribution around a spherical asteroidal body applicable to the current study [Yu2016].
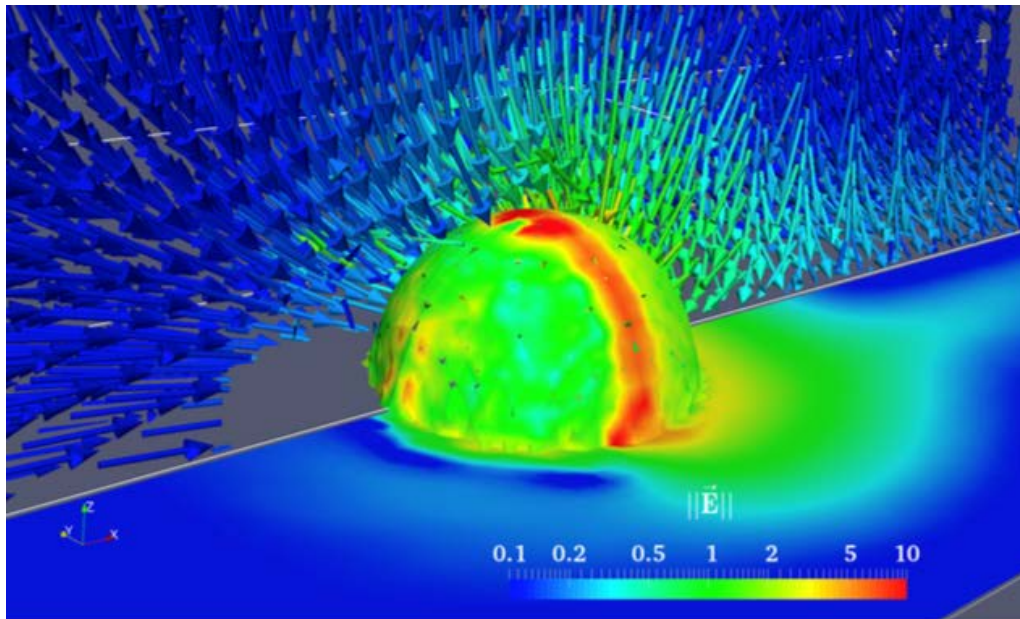
Figure 29. *Electrostatic vector field around spherical asteroidal body, from [Yu2016].*

To summarize, an E-Glider will need to actively control its differential and absolute potentials. Mechanisms exist for producing charged beams and differential surface potentials. While challenging perhaps to fit into the E-Glider mass and power constraints, the real problem will be to calculate the detailed electric fields produced by these systems in real time. To date various spacecraft charging models have been developed that allow detailed estimates of the induced differential potentials (NASCAP-2k) and the charged dust environment (IFE-PIC) around an asteroid and the spacecraft. Thus the technical elements necessary to develop and control differential charging in principle exist though their capability to work together in real time is still to be demonstrated.

9.6 Approaches for Energy Harvesting

A key issue for the E-Glider is how to differentially bias the flyer's surfaces relative to the body being orbited and how to power that differential charging. For small bodies in the interplanetary environment, the main source of surface and differential charging is the Solar Wind plasma and sunlight. Typically surfaces in sunlight are dominated by photoelectron emission currents (a few nA/cm^2 for most surface materials) and the average energy of the photoelectrons (~few eV) so that the potentials are on the order of ~10 V positive. Given the shadowing of the radially flowing Solar Wind plasma and the insulating nature of the asteroidal material, the plasma wake of asteroid is expected to be largely devoid of Solar Wind plasma and sunlight leading to differential surface potential variations around the asteroid. The wake region can, in the absence of the Solar Wind plasma and sunlight, charge negatively with values of -100 V having been observed on shadowed spacecraft surfaces (note: some simulations imply that potentials as high as -1000 V may be possible, however). The sunlight and Solar Wind, however, can cause charge neutralization within a fraction of a second on exposed spacecraft surfaces. It will be the same or worse around an asteroid with higher plasma densities expected close to the asteroid and a complex terminator and wake region in the anti-sunward direction. As a result the E-Glider electrostatic inflation and levitation concept will have to provide continually varing charge emission to control the spacecraft potential relative to the space environment and asteroid. Here we will describe the characteristics of that charge control system, how the differential charging might be modeled, and how to provide the energy necessary to power the flyer.

Any charge control system will need to maintain the absolute potential of the spacecraft relative to the asteroid to control levitation and be able to generate differential potentials to control attitude. To accomplish the former, our study estimates that power levels between 1-10 kW might be required to maintain the potentials necessary to levitate the E-Glider of a few kg on the order of ~1 m. In particular, potentials of 1-10 kV can be accomplished by using combinations of electron (to bias the vehicle positive) or ion (to bias the vehicle negative) current emitting systems such as provided by ion engines or electron beams (more recently electron-emitting surfaces have become available that may also be an option). To attain these potential and power levels, some form of "power harvesting" will be necessary. While we do not yet have a definitive solution, several possibilities present themselves for consideration. First, battery sources or solar arrays are obvious possibilities though both pose potential mass and size issues. For example, at ~1 AU the solar constant

is 1367.7 W/m². Currently photoelectric power systems are ~20% efficient so collection areas of 10's of square meters would be necessary adding substantially to the E-Glider mass. This problem is readily solvable if the spacecraft delivering the EGlider (and remaining in a higher altitude orbit around the small body) collected the power and transmitted (perhaps through RF or laser beam) power to the E-Glider. Such power beaming has been demonstrated and, aside from the added complexity of another orbiter, possible with current technology Another possibility we considered was energy harvesting from the Solar Wind plasma. Table 5 lists the typical properties of the Solar Wind at 1 AU.

Table 5. Nominal Solar Wind Parameter at 1 AU

	MIN	MAX	AVG
FLUX (NO#/CM²-S)	10^8	10^{10}	$2\text{-}3 \times 10^8$
VELOCITY (KM/S)	200	2500	400-500
DENSITY (NO#/CM³)	0.4	80	5-10
T (eV)	0.5	100	20
T_{max}/T_{avg}	1.0*	2.5	1.4
HELIUM RATIO (N_{He}/N_H)	0.0	0.25	0.05
FLOW DIRECTION	±15° from radial;		~2° East
ALFVEN SPEED (KM/S)	30	150	60
B (γ)	0.25	40	6

B VECTOR

    POLAR COMPONENT: AVG IN ECLIPTIC PLANE

    PLANAR COMPONENT: AVG SPIRAL ANGLE ~45°

*isotropic

Electrodynamic tethers in the Solar Wind and around planets have been considered (and at Earth tested) as a possible power source using the Lorentz effect. That is:

$$E = 0.1 \ (v \times B) \ V/m$$

(44)

where for the Solar Wind: E = induced electric field, v ~ 500 km/s, and B ~10^{-4} G. A nominal electric field produced by the Solar Wind would by ~0.05 V/m. This would require a tether of 20 km to give a potential drop of 1 kV. While a possible power source, such a system would clearly be very awkward and the highly variable nature of the Solar Wind would make utilizing it quite difficult—we have to rule this technique out as a viable power source. The power requirements for the differential potentials required for attitude control will be quite modest compared to that required to maintain levitation and may be produced by a small Van De Graff generator or by battery/solar cell powered bias sources. These could be maintained again by broadcast power from a nearby mother ship. The exterior surface of the vehicle can also be used to generate differential potentials by using materials (isolated electrically from each other) that have very different charging characteristics. For example, graphite and aluminum (actually aluminum oxide) surfaces have very different photoelectron emission properties with the aluminum oxide emitting 10 times the photoelectron current of graphite. Finally, a central body surrounded by a grid of electrically isolated wires (for example plated on an inflatable balloon like surface) could be biased in complex patterns to attain a variety of differential patterns. We note that differential potentials as high as 40 kV have been obtained in-situ (e.g., the SPEAR program) though special precautions were necessary to produce such high potentials. No matter what methods are used to produce differential potentials, the complex interactions of these active charge control systems with the ambient plasma and the E-Glider will need to be modeled in real time. As illustrated by Table 5, the Solar Wind parameters are highly variable and will produce a very dynamic environment for the E-Glider. Fortunately, previous work at JPL on the plasma dynamics of a 150 m solar sail [Garrett2014] studied the charging characteristics of large bodies in the Solar Wind and is applicable to the E-Glider concept. In addition to NASCAP-2k, use for the past Solar Sail work, the Immersed-Finite-Element PIC (IFE-PIC) algorithm [Yu2016] has been developed. Both have been discussed in the previous section. In particular, the IFE-PIC algorithm will be used in Phase II for more higher fidelity models and simulation of the E-Glider and of its energy harvesting capability.

To summarize, an E-Glider will need to actively control its differential and absolute potentials given the varying natures of the asteroidal surface and the Solar Wind. Mechanisms exist for producing variable charged beams and differential surface potentials but these will be challenging to fit into the E-Glider mass and power constraints. The best solution currently appears to be to use some form of power beaning from another spacecraft (perhaps the same spacecraft that would deliver the E-Glider to the small body) given the mass issues expected with storage batteries or solar arrays. The real problem will likely be calculating the detailed electric fields produced by these systems in real time. To date various spacecraft charging models have been developed that allow detailed estimates of the induced differential potentials (NASCAP-2k) and the charged dust environment (IFE-PIC) around an asteroid and the spacecraft. Thus the technical elements necessary to develop and control differential charging in principle exist though their capability to work together in real time is still to be demonstrated.

10. Approaches for Autonomy

Figure 30 shows a functional block diagram of the E-Glider autonomy functions. Through an array of Langmuir probes, which measure the spatial distribution of the charges surrounding the vehicle, an "electrostatic map" is thus generated. Once the electric potential has been mapped, the E-glider is able to use this "electrostatic topographic map" for path planning and navigation. Further articulation at the root of the lateral strands or inflated membrane wings, would generate a component of lift depending on the articulation angle, hence a selective maneuvering capability which, to all effects, would lead to electrostatic (rather than aerodynamic) flight. A potential field approach to path planning for navigation [Koren1991, Quadrelli2004a, Quadrelli2004b, Reif1999, Johnson2007] is one candidate to be explored, see Figure 31. The autonomy aspects of guidance, estimation, and control, will be investigated by introducing the possibility of optimizing the trajectory of the E-Glider to a desired science target [Quadrelli2004b, Reif1999], while simultaneously the E-Glider tracks the Sun, communicates with the Earth, and optimally re-allocates control commands to the wings for flight maneuvering. Figure 32 shows a proposed algorithm to estimate the E-Glider electrostatic cartographic map. Once measured by Langmuir probes, the charges are compared to the estimated charges from an on-board model (see Figure 32). The map is the

result of the differentials between the model and the measurements, which is continuously updated in flight.
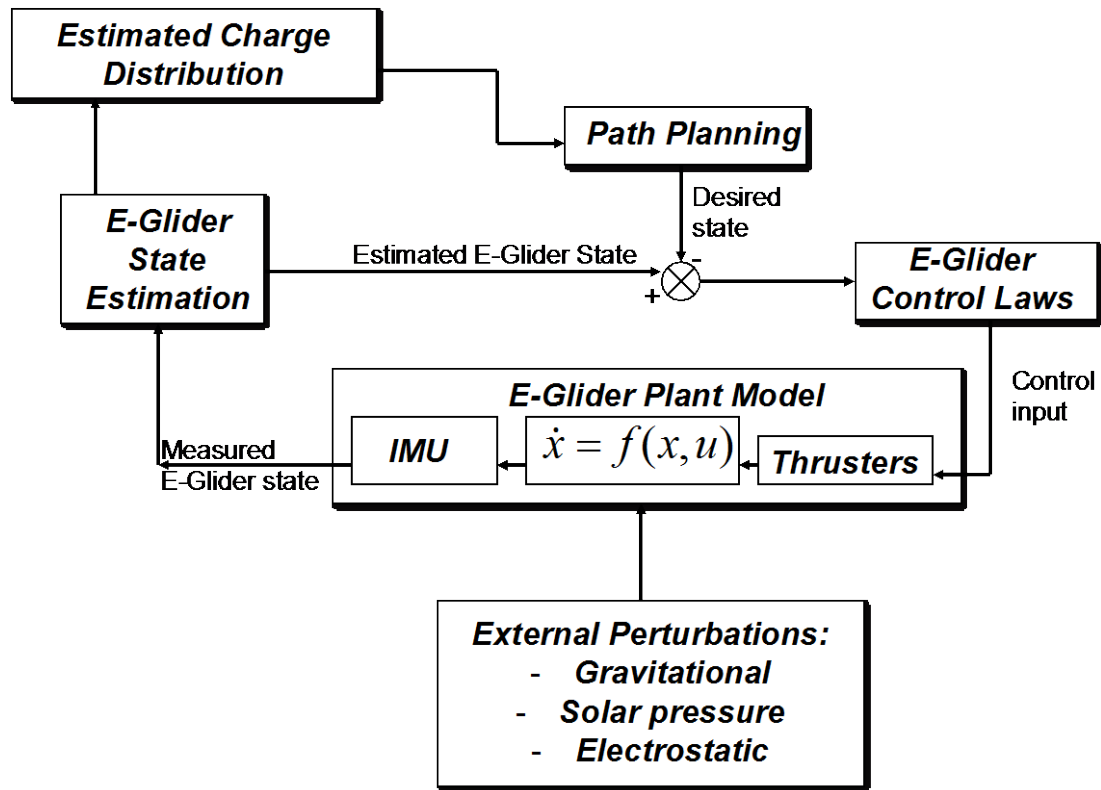
Figure 30. *Block diagram of E-Glider autonomy.*
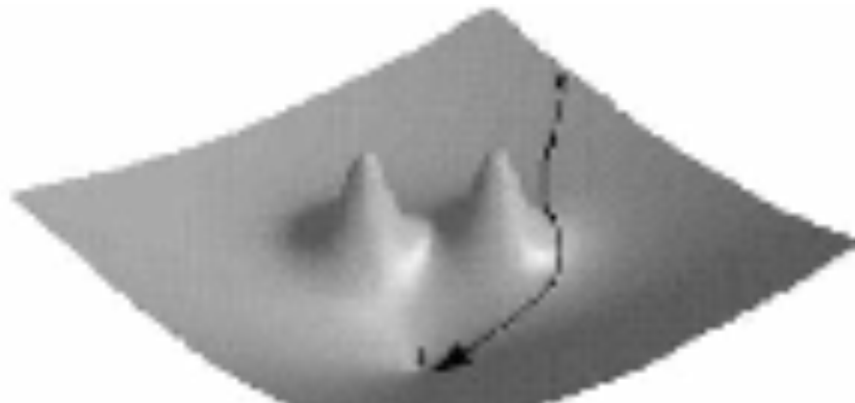
Figure 31. *Navigating a potential field distribution.*
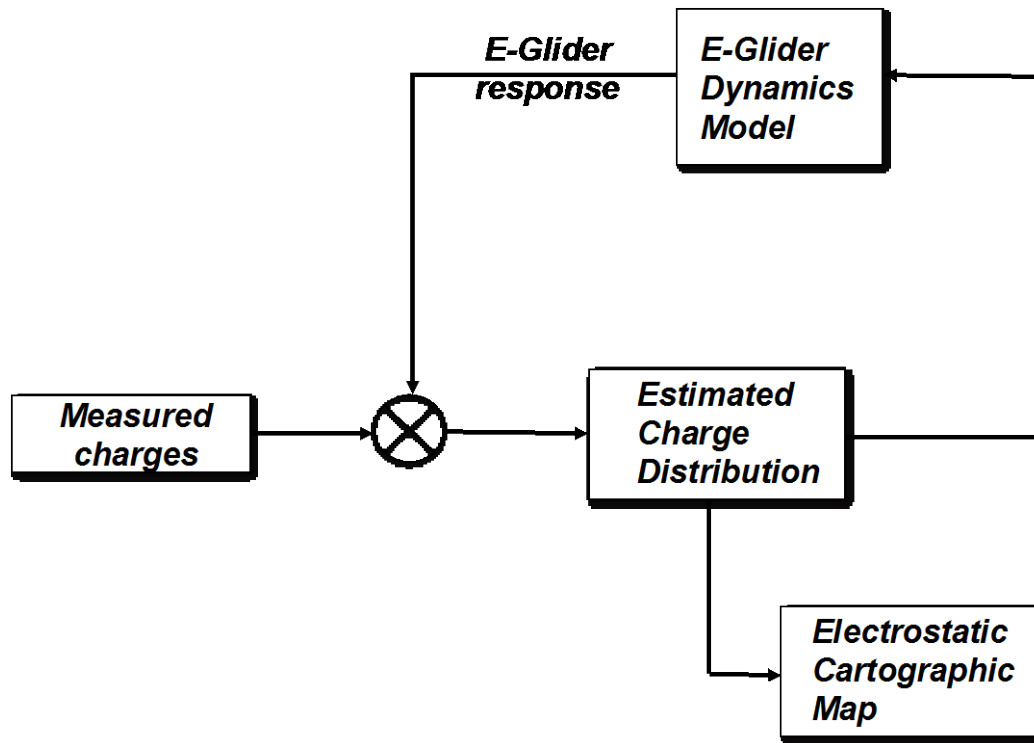
Figure 32. *E-Glider scheme for electrostatic cartographic map generation..*

11. Testing Approaches

Figure 33 shows the results of test of electrostatic inflation, from [Stiles2010, Stiles2011, Stiles2012]. The test setup consists of an aluminized Mylar ribbed sandwich structure resting on a conducting surface, which is connected to a high voltage power source. In this 1-g test environment, the normal force of the object upon which it rests always balances the forces on the lower plate. The other plate is subjected to the Coulomb force to inflate, the compressive force of gravity, and tension in the ribs to hold the structure together. The structure used in the test shown in Figure 33 consists of two 12x15 cm plates of 75 gauge aluminized Mylar. Three ribs of the aluminized Mylar connect the two plates. Charge was applied to the conducting sphere on which the sandwich structure rested. In the sandwich structure inflation experiment, inflation occurred between 7 and 13 kV. Figure 33 shows snapshots of the charging experiment. The duration of the inflation shown between the first

and last frames of Figure 33 is approximately 5 seconds. This experiment clearly shows how a collapsed sandwich membrane structure can inflated with kilo-Volt levels of potential. It should be noted here that the rib structures were simply glued to the outer membrane plates. This results in some bending stiffness of the ribs that is not accounted for in the earlier models. Despite these challenges, the experiments indicate that such self-supporting membrane structures can repeatably and reliably be electrostatically inflated in a laboratory environment. Higher fidelity modeling of such lightweight structures is very challenging due to the strong nonlinear coupling between charge distribution and membrane shape. Adding the plasma space environment complicates the matter even further. Such experimental results are critical to explore experimentally appropriate material properties, construction methods, packing methods, and charging behaviors that lead to desirable membrane motions. Further, such testing would be used for validation and verification purposes to be developed higher fidelity modeling of charged membrane structures. Figure 18 shows the inflation of a gossamer ribbon structure, an example of a structure with large open surface segments. This ribbon structure was initially compacted to height of approximately 2 cm, then inflated to a height of 25 cm. This experiment shows the potential of high deployed to stowed volume ratios with the electrostatic inflation concept. Notice in this photo series that the structure has obtained the fully inflated shape at 5 kV, yet gravity is preventing the structure from standing upright. As the voltage increases to 9 kV, the electrostatic repulsion between the ribbon structure and the conducting surface to which it is attached cause the entire structure to become upright as well as inflated to the desired shape.
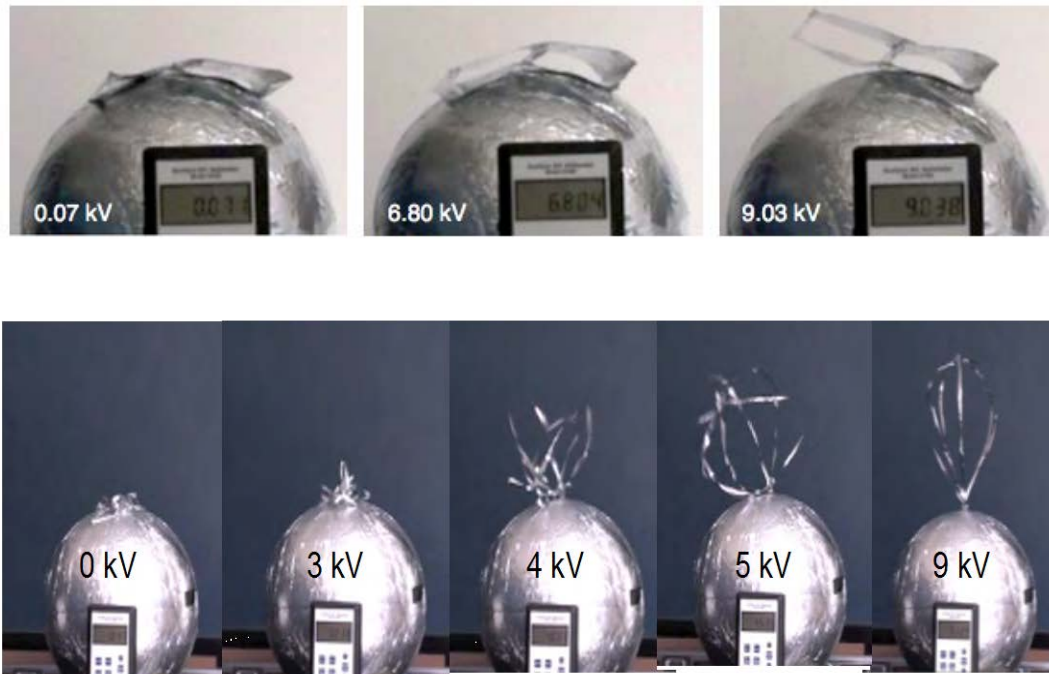
Figure 33. *Test of electrostatic inflation [Stiles2010].*

The large vacuum bell jar at JPL[5] is a possible experimental facility to conduct larger scale tests. This facility (Figure 34) has an inside diameter of 72.13 inches, is 78.00 inches high at the center, and is made of 1.250 inches thick acrylic plastic that is both RF and optically transparent. The entire facility is enclosed in an RF shielded room, including a control room and a 15 ft x 15 ft RF anechoic chamber around the bell jar. The vacuum system operates from normal atmospheric pressure to 2×10^{-5} torr at room temperature, with local chilling possible using LN2 and/or local heating possible using a heat-plate inside the bell jar. It includes a 52,000 liter per second oil diffusion pump, liquid nitrogen chilled chevron baffle cold trap, mechanical pumps, blower and high vacuum valves. The facility has supported the testing of spacecraft antenna system hardware since 1968. It has also supported the German HELIOS project and other NASA and non-NASA programs. Power monitoring and data logging is computer automated. The system is certified for flight hardware tests.

---

[5] http://mesa.jpl.nasa.gov/Vaccuum_Breakdown_Facility/
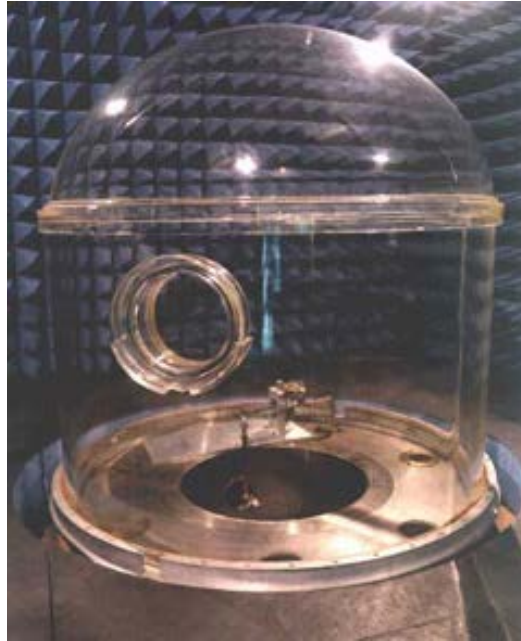
Figure 34. *Vacuum bell jar at JPL.*

12. Levitation studies

In this section, we discuss the simulation studies that were done to determine the levitation capability of the EGlider, and its orbital mechanics in proximity of the surface of an asteroid. A sensitivity study has been conducted to investigate the sensitivity of the trajectory to various environmental parameters, such as ambient electric field, Debye length, and charge.

12.1 Preliminary simulation studies

Restrictive assumptions have been used for the current models being used for simulation. The goal is to investigate how prototypical hoop structures could be considered for levitation. First, the bodies are modeled as rigid bodies under spherical gravity and spherical distribution of charge. Second, no intervening plasma electric field is included. Third, the charge of the body is set to be equal the charge of the hoop. The latter is a very strong assumption and decouples these results from the direct asteroid application. However, they do provide insight the E fields behave about hoops. The hoop is aligned so that it is normal to the body. In the case of the hoop, the analytical expression of the potential that can be found in [MacMillan1958] was used, and it is:

$$V = \frac{2\kappa^2 M}{\pi} \int_0^{\frac{\pi}{2}} \frac{d\omega}{\sqrt{\rho_1^2 cos^2\omega + \rho_2^2 sin^2\omega}}$$

(45)

where κ^2 is the gravitational constant, M is the mass of the glider, ρ_1 and ρ_2 are the distances from the opposite edges to the body, and ω is the angle between the line between points 1 and 2 and any test point along the hoop. When the hoop is aligned to be normal to the body at a distance of ρ_a, the potential simplifies to:

$$V_a = \frac{\kappa^2 M}{\rho_a}$$

(46)

and the force is then given by:

$$F = -\frac{\kappa^2 M_{hoop} M_{body}}{\rho_a^2}$$

(47)

A similar approach can be used to find the electrostatic potential and forces by replacing the gravitational constant and masses with Coulomb's constant and charges.We find that, for a 1 cm tall, 1 m diameter, 500 μm thick hoop, the equilibrium charge is ~ 22 μC. With an additional payload mass of 10 kg, a 20 m diameter hoop that begins at 10 m above the surface needs a little less than 55 μC of charge to hover. These calculations are important, since once we know the charge required to levitate, we can compute the power needed to deliver that charge. Figure 35 shows the total force on the hoop and the equilibrium value of forces required for levitation. Figure 36 shows the trajectory of the levitated hoop as a function of charge, and Figure 37 shows the same trajectories as a function of initial altitude. Figure 38 shows the total force on the levitated hoop as function of charge, size, and distance from surface. These plots are the result of a sensitivity study that was conducted to gain insight into the influence of various parameters affecting the behavior of the E-Glider in the relevant environment at an airless body.
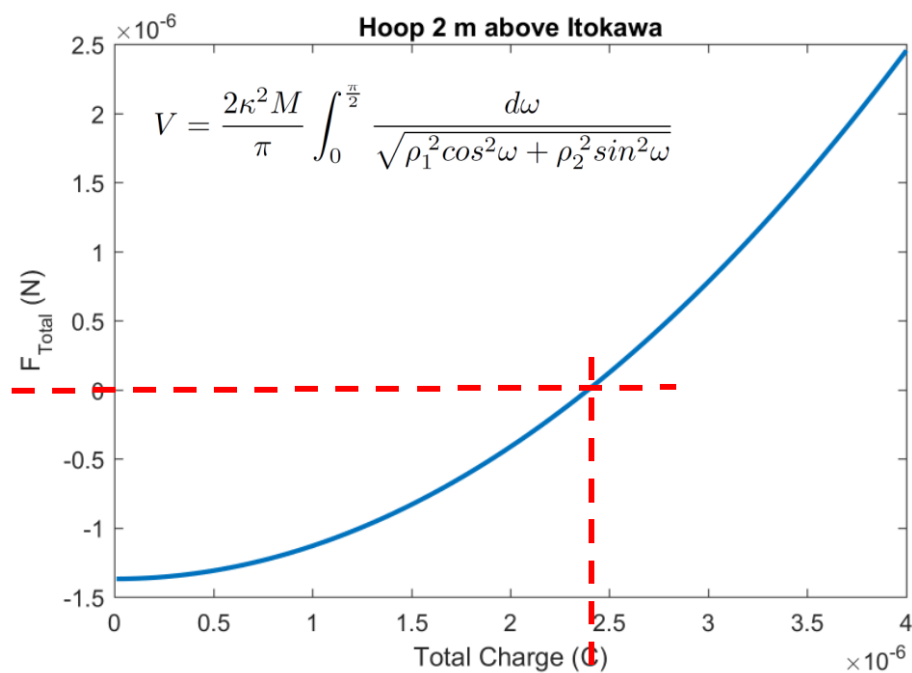
Figure 35. *Total force on hoop and equilibrium value for levitation.*
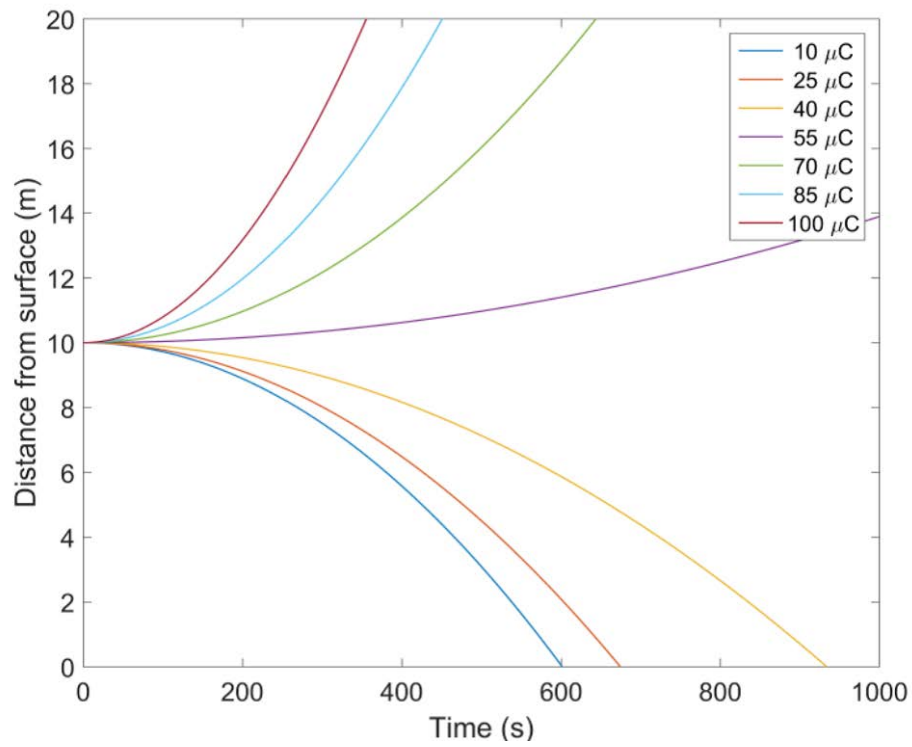
Figure 36. *Trajectory of levitated hoop as function of charge.*
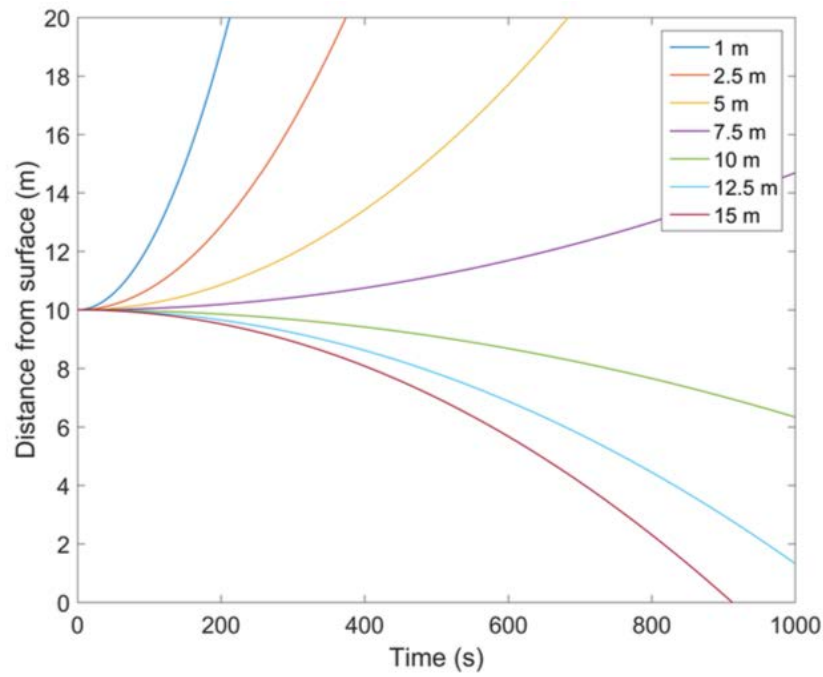
Figure 37. *Simulation results for levitated hoop.*
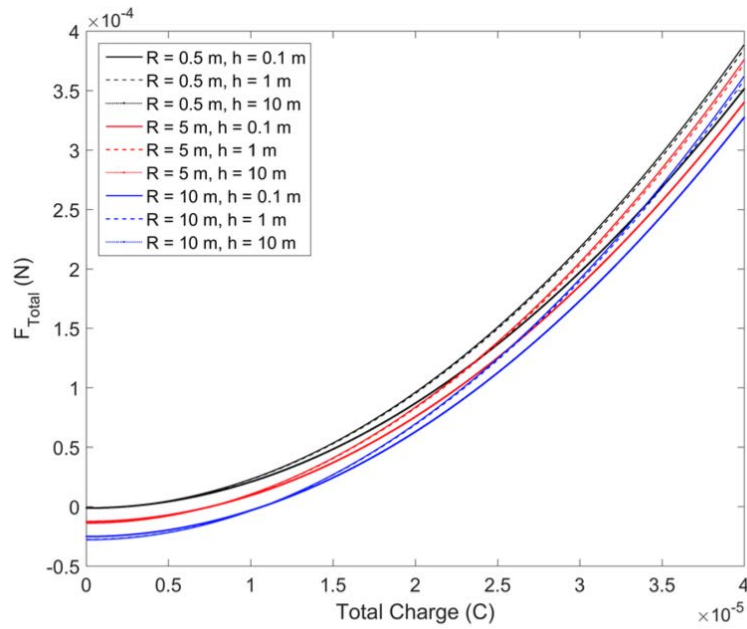
Figure 38. *Total force on levitated hoop as function of charge, size, and distance from surface.*
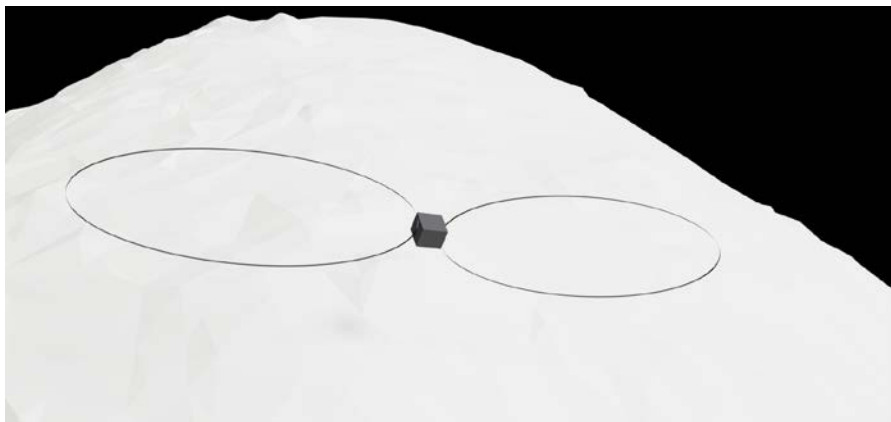
Figure 39. *Implementation of E-Glider CAD model.*
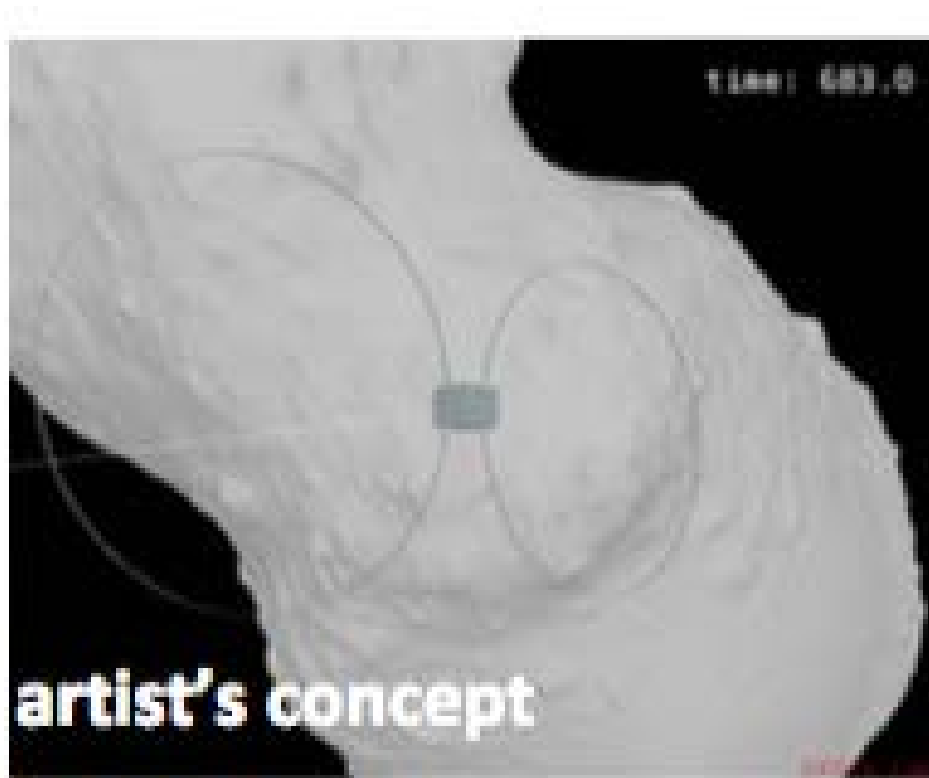
Figure 40. *Implementation of E-Glider model in JPL's DSENDS simulator.*

Figure 39 shows a CAD model of the E-Glider in flight. JPL has developed the Dynamics Simulator for Entry, Descent and Landing (DSENDS) [DSENDS2002] as a high-fidelity spacecraft simulator for Entry, Descent, and Landing (EDL) on planetary and small astronomical bodies. It is an extension of a core set of software tools (Darts/Dshell) that is capable of modeling the dynamics of complex multi-body systems with flexible nodes. The core tool set is in use for multiple interplanetary and science-craft missions (Cassini, Galileo, SIM, and Starlight). DSENDS has been heavily used by Mars Lander missions to test precision landing and hazard avoidance functions for those missions. High-fidelity, physics-based engineering simulations of a spacecraft interacting with its environment are crucial in the analysis, development, test, validation, and operation of space flight missions. JPL's simulation framework (DSENDS) was developed for the simulation of spacecraft ascent, orbit, deep-space flight, rendezvous, proximity operations, atmospheric Entry, Descent and Landing (EDL), and planetary surface mobility. The DSENDS simulator incorporates physics-based models for articulated multi-body systems with flexible modes, aerodynamics, environments such as the atmosphere and planetary topography, spacecraft devices, and on-

board flight guidance, navigation and control. The simulator allows the user to set up multi-spacecraft and mission configurations using elements from a modular library of components and determine the system trajectory and related quantities of interest. Simulation parameters may be selected from a dispersed set to determine variations in trajectories for either Monte-Carlo or parametric analysis. The gravitational model of the asteroid is obtained from a polyhedral model. Figure 39 and Figure 40 show snapshots of the DSENDS simulation of the E-Glider in flight around Itokawa. Figure 41 and Figure 42 show snapshots of the simulation of the trajectory of the E-Glider contacting the surface of the asteroid, and in Figure 43 the rebounds at the surface are clearly visible from the simulation results. While these are only preliminary results, future work will include an extension of these models including the effect of radiation pressure and electrostatic interactions, with autonomy. This interesting trajectory was explored in more detail, and the results are summarized in the next section.


**Figure 41.** *Implementation of E-Glider model in JPL's DSENDS simulator.*
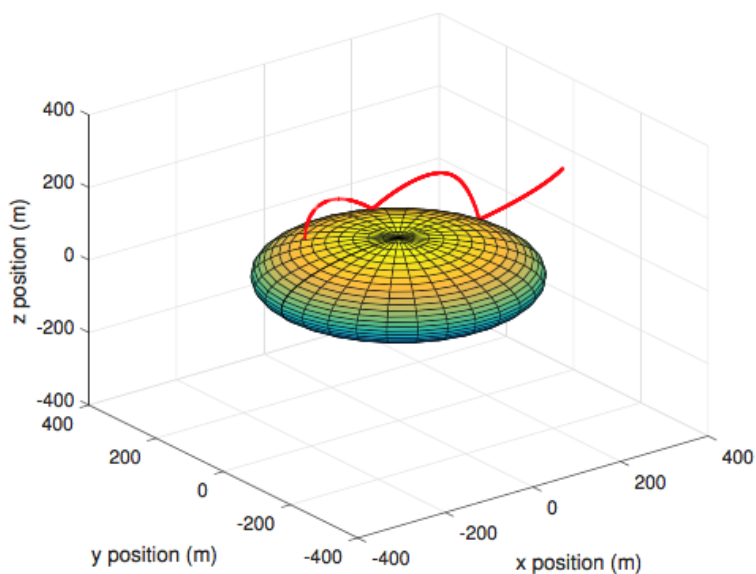
**Figure 42.** *Trajectory of point mass during drop on Itokawa surface.*
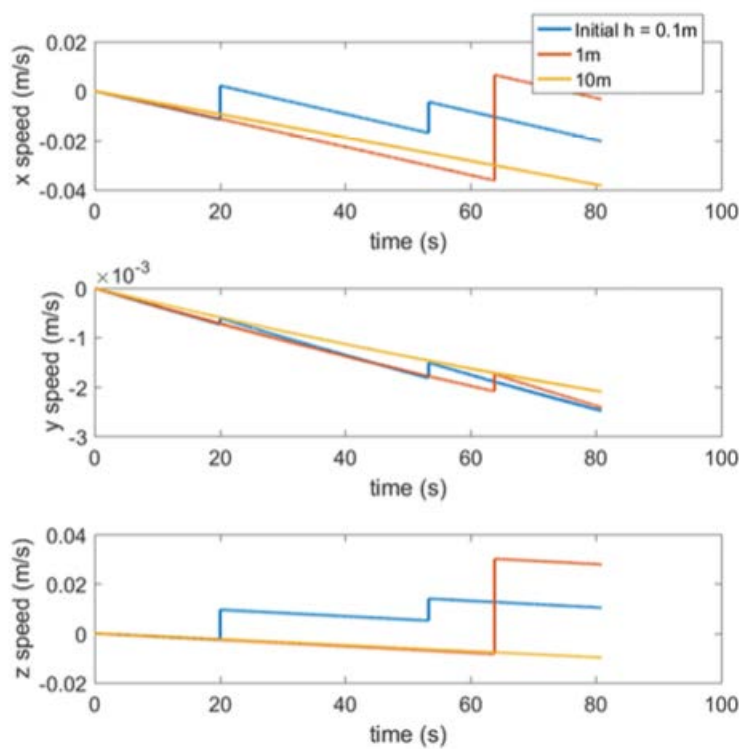
Figure 43. *Trajectory of point mass during drop on Itokawa surface.*

12.2 Parametric Analysis of E-Glider Trajectory in Proximity to Surface

In this section, a parametric analysis is performed to have a deeper insight into the electrostatic environment considered in the simulation. It is still not very clear, during the simulation, what are the parameters the trajectory is more sensitive to. In order to have a better understanding of what are the values of the main electric parameters affecting the dynamics, a parametric analysis is accomplished. It is done by keeping the same initial conditions as in the previous simulations in terms of mass of the spacecraft (m=1 kg), altitude (h=200 m) and speed (V=0 m/s), and changing the values related to the electric field, such as the E-field on the surface of the small body E_0, the electric charge of the spacecraft q_b and the Debye length λ_d. Moreover, the impact is considered to be not perfectly elastic with a restitution coefficient of 0.83. The values of the three parameters chosen for the parametric analysis are E_0 = [1 10 100 1000] V/m, q_b = [1 10 100 1000] μC, λ_d= [0.1 1 10 100] m. These values show that the parametric analysis performed is composed by 4^3=64 different cases. For sake of simplicity only the most interesting and possibly realistic cases will be reported, focusing mainly on the trajectory the spacecraft is subjected to and on the time history of the states, i.e. position, velocity and acceleration along the three axis, with the latter showing both its gravitational and electrostatic components. These results are shown in Figures 44 to Figure 70. First the trajectory is shown in the asteroid body frame, then the components of the position and acceleration vector of the E-glider with respect to the origin of the rotating asteroid frame are shown. During the simulation, the maximum number of bounces on the surface of Itokawa is set to 10 and the maximum simulation time is 100000 s, that is slightly more than one day (86400 s). After evaluating all the cases, the ones with E_0=1000 V/m are not studied in depth since most of these cases show the point mass going out of the area of interest around the small body, without bouncing even once with the ground. Clearly the electric field on the surface of the small body is too big for such a small spacecraft of 1 kg. Other cases where q_b =1000 μC and λ_d= 100 m are not considered.
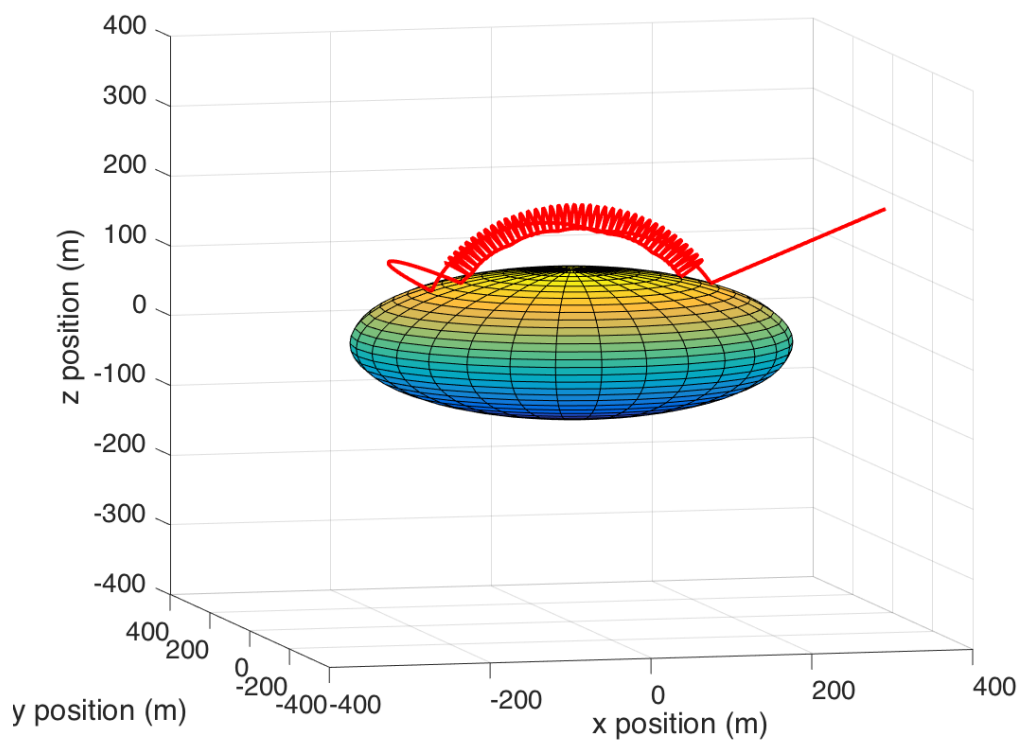
Figure 44. *Trajectory of point mass during drop on Itokawa surface, $E_0 = 10$ V/m; $q_b = 1\ \mu C$; $\lambda_d = 0.1\ m$*
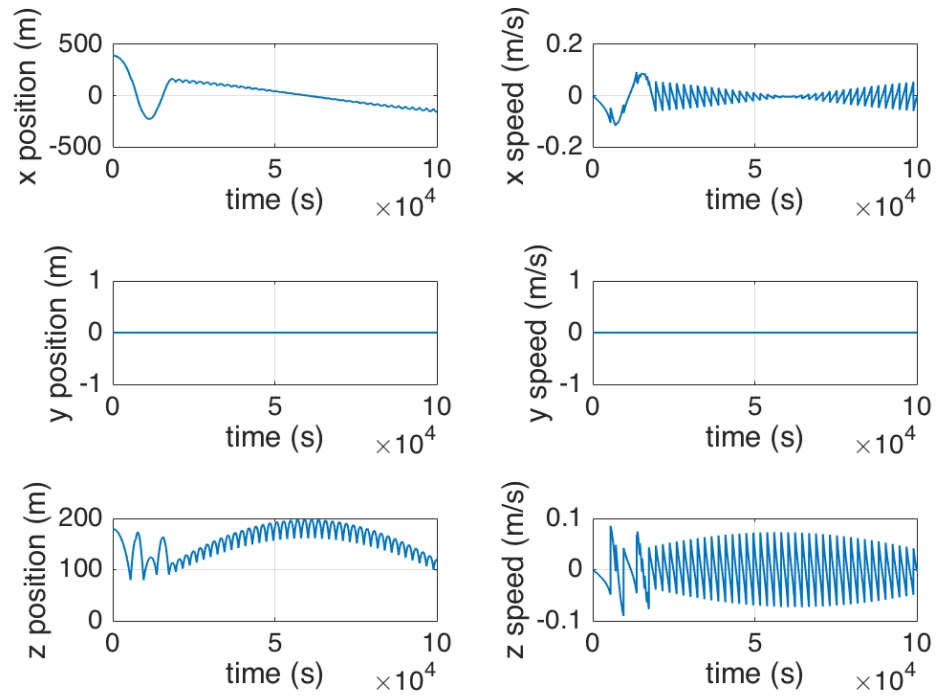
Figure 45 *Trajectory of point mass during drop on Itokawa surface, $E_0 = 10 \ V/m$; $q_b = 1 \ \mu C$; $\lambda_d = 0.1 \ m$*
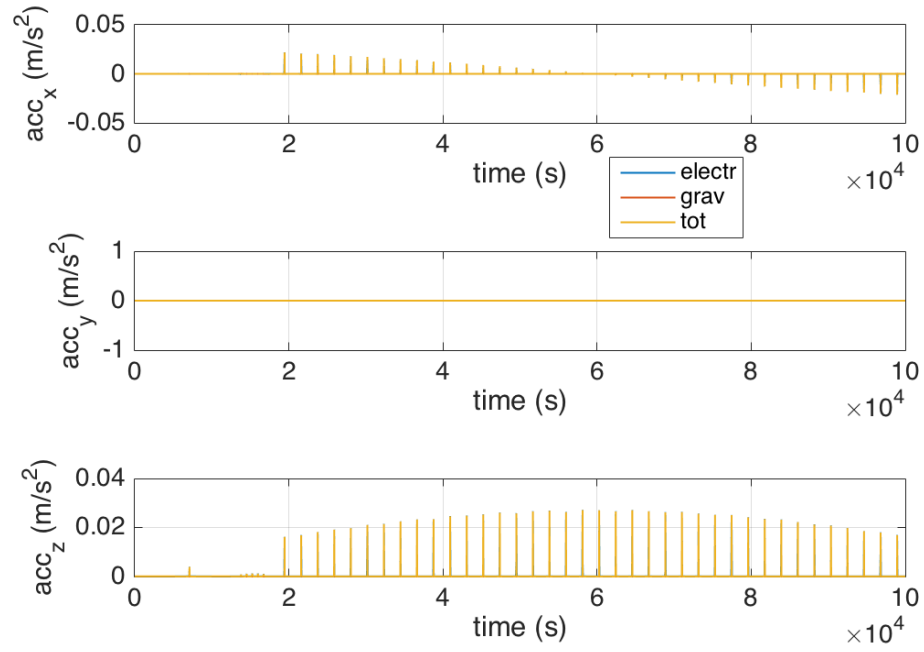
Figure 46. *Trajectory of point mass during drop on Itokawa surface, $E_0 = 10 \, V/m$; $q_b = 1 \, \mu C$; $\lambda_d = 0.1 \, m$*
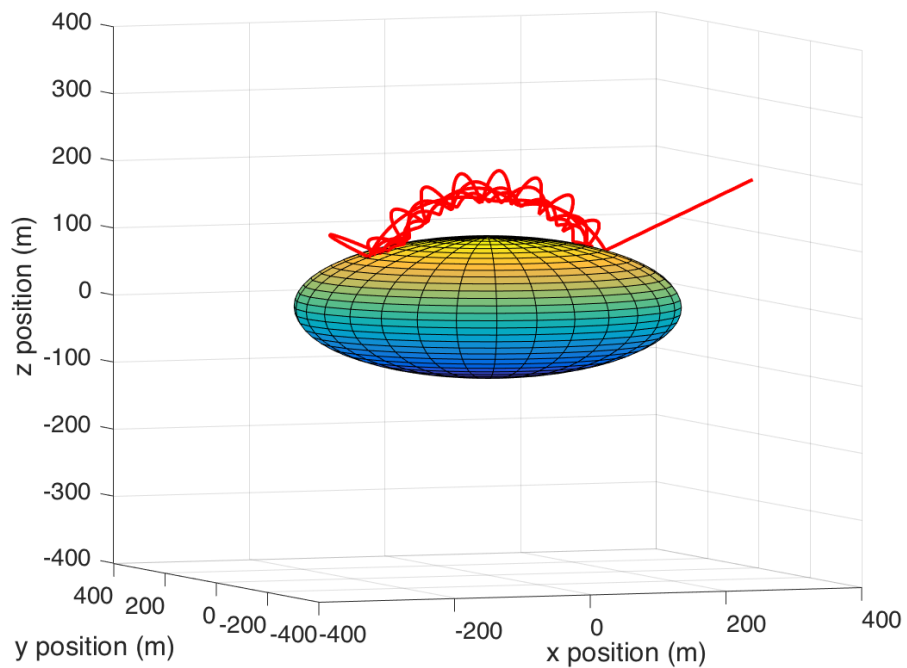
Figure 47. *Trajectory of point mass during drop on Itokawa surface, $E_0 = 10\ V/m; q_b = 1\ \mu C; \lambda_d = 1\ m$*
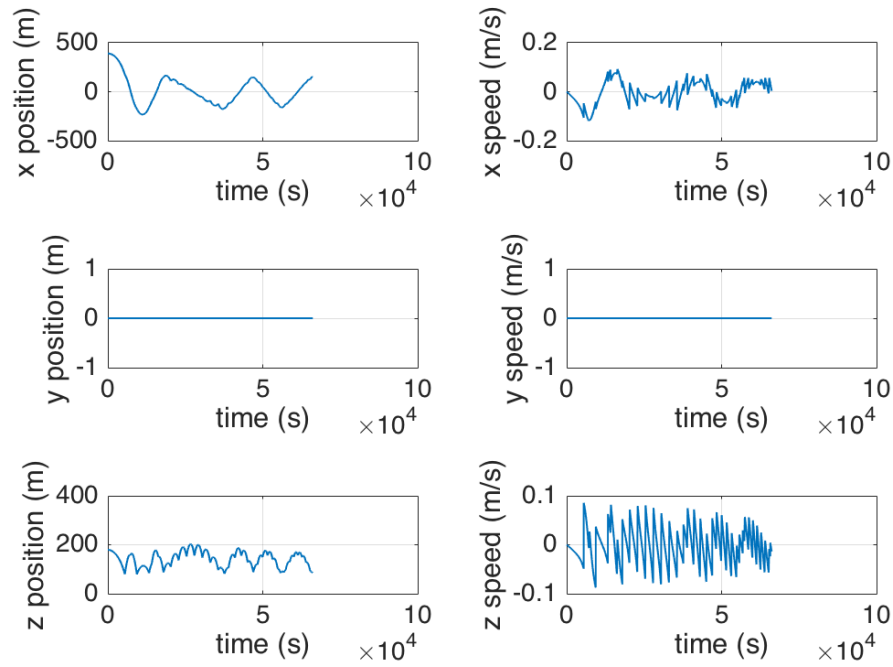
Figure 48. *Trajectory of point mass during drop on Itokawa surface, $E_0 = 10$ V/m; $q_b = 1$ μC; $\lambda_d = 1$ m*
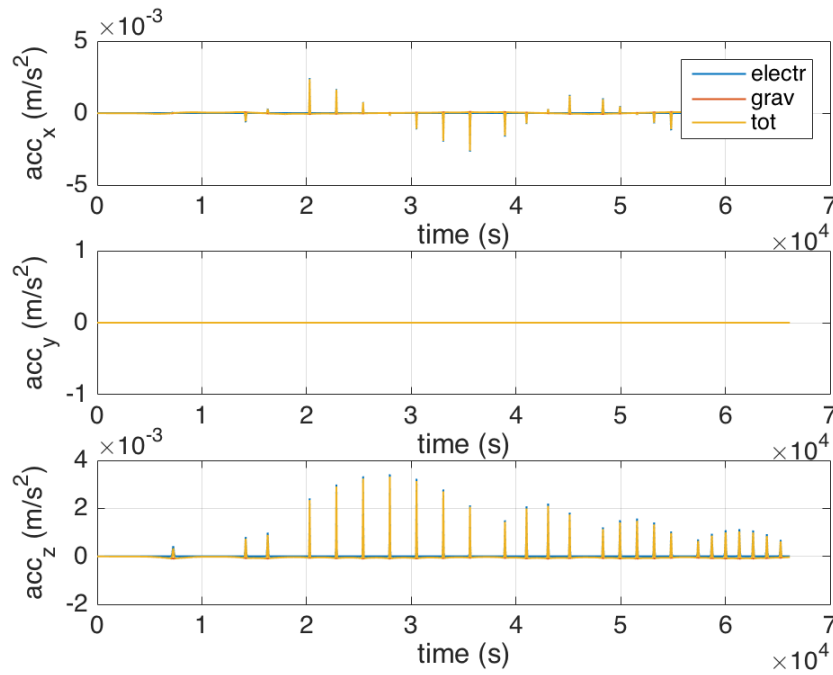
Figure 49. *Trajectory of point mass during drop on Itokawa surface, $E_0 = 10$ V/m; $q_b = 1$ μC; $\lambda_d = 1$ m*
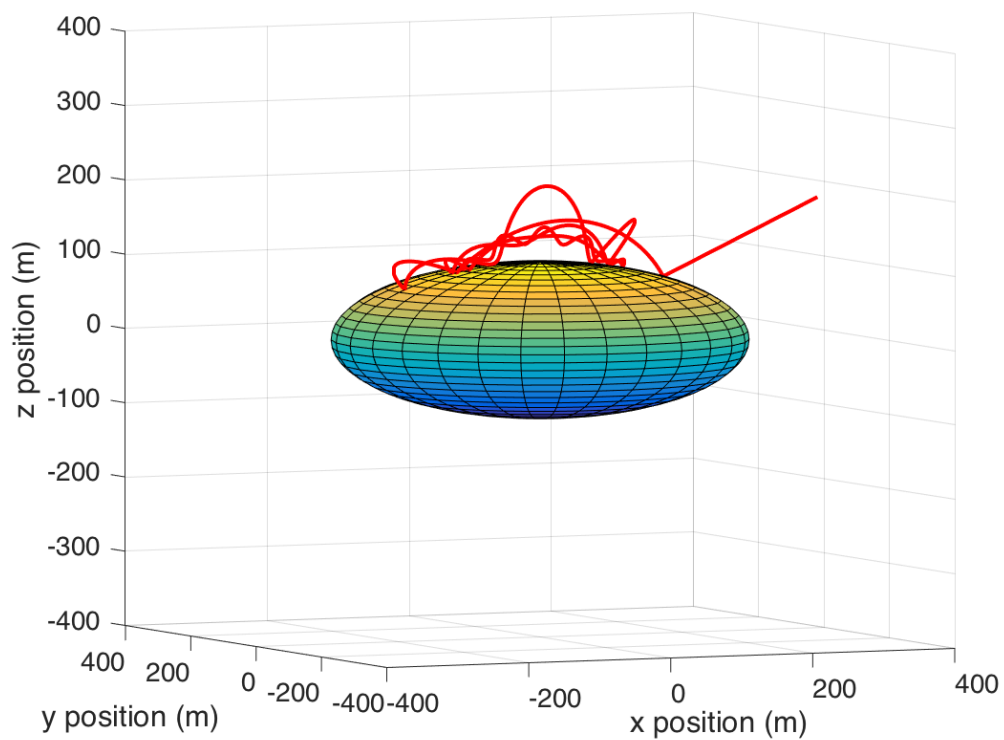
Figure 50. *Trajectory of point mass during drop on Itokawa surface $E_0 = 10$ V/m; $q_b = 1$ μC; $\lambda_d = 10$ m*
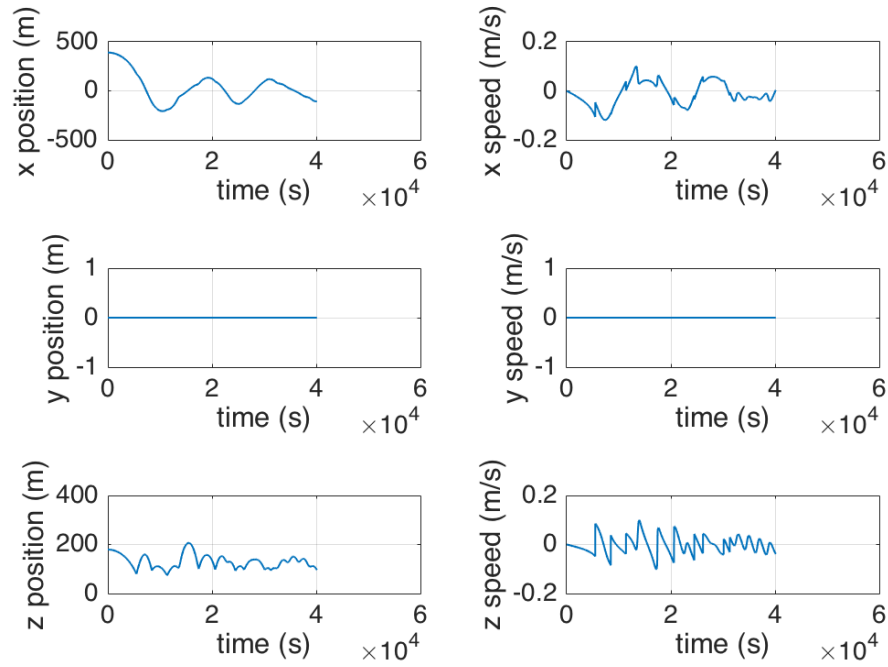
Figure 51. *Trajectory of point mass during drop on Itokawa surface* $eE_0 = 10\ V/m;\ q_b = 1\ \mu C;\ \lambda_d = 10\ m$
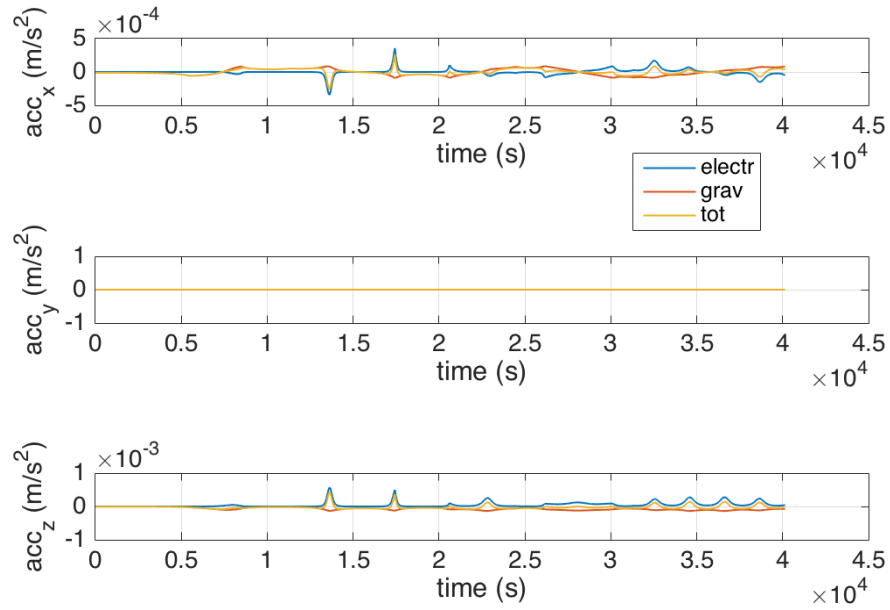
Figure 52. *Trajectory of point mass during drop on Itokawa surface* $E_0 = 10\ V/m;\ q_b = 1\ \mu C;\ \lambda_d = 10\ m$

$$E_0 = 10\ \text{V/m};\ q_b = 10\ \mu C;\ \lambda_d = 0.1\ m$$
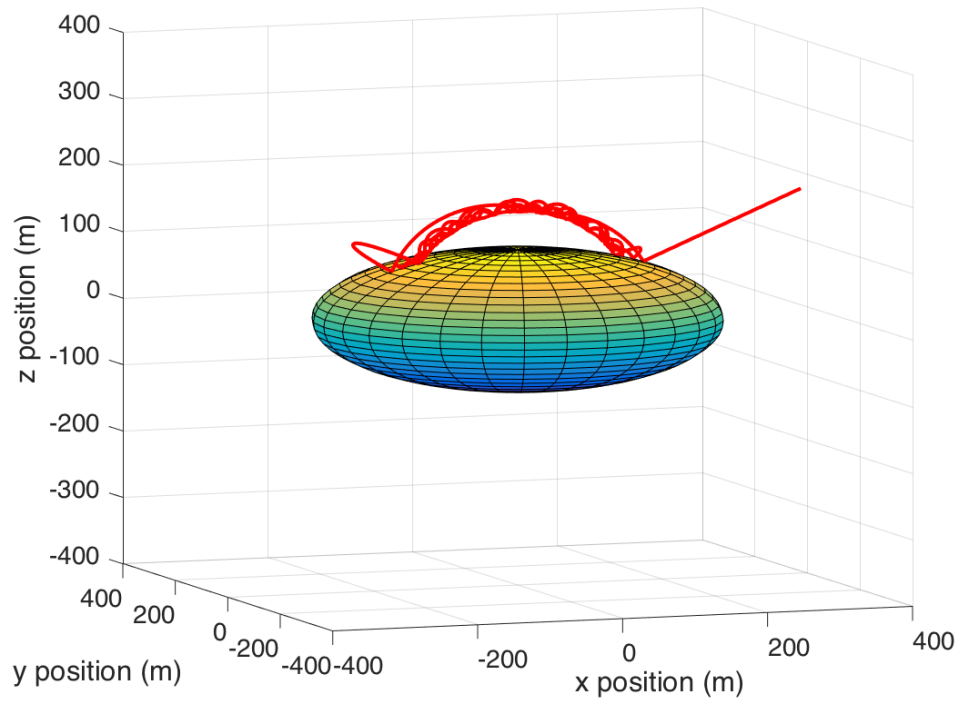
Figure 53. *Trajectory of point mass during drop on Itokawa surface $E_0 = 10\ V/m; q_b = 10\ \mu C; \lambda_d = 0.1\ m$*
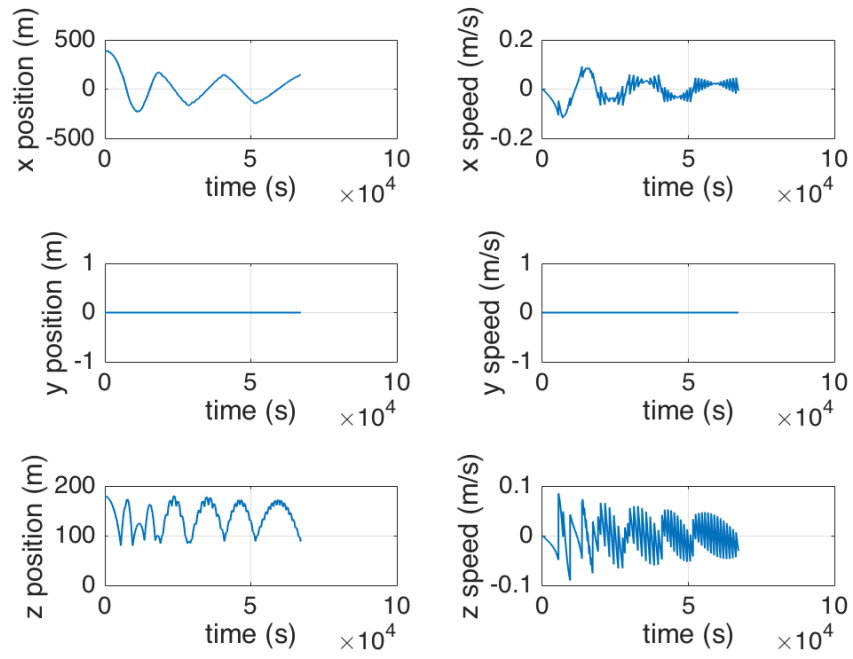
Figure 54. *Trajectory of point mass during drop on Itokawa surface* $E_0 = 10$ *V/m;* $q_b = 10$ *μC;* $\lambda_d = 0.1$ *m*
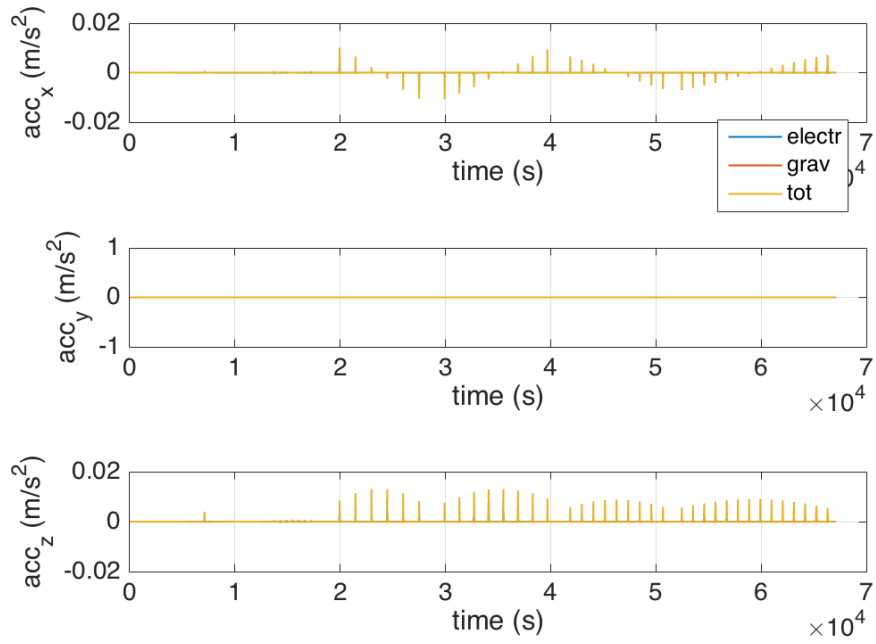
Figure 55. *Trajectory of point mass during drop on Itokawa surface $E_0 = 10$ V/m; $q_b = 10$ μC; $\lambda_d = 0.1$ m*

$$E_0 = 10 \text{ V/m}; q_b = 10 \ \mu C; \lambda_d = 1 \ m$$
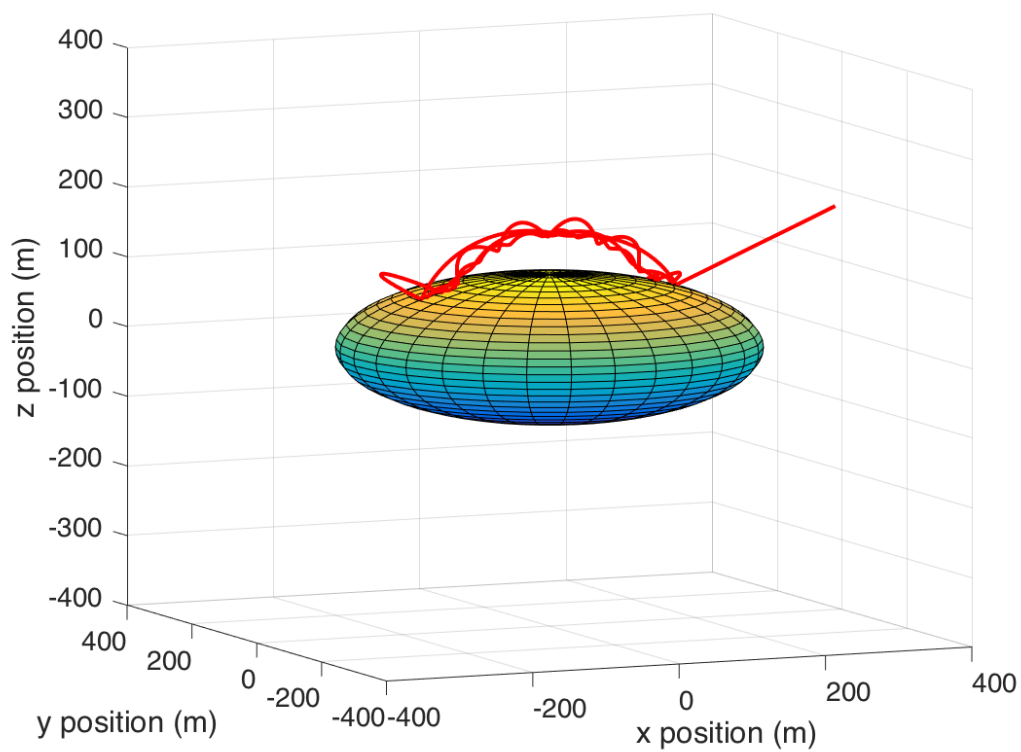
Figure 56. *Trajectory of point mass during drop on Itokawa surface $E_0 = 10 \; V/m; q_b = 10 \; \mu C; \lambda_d = 1 \; m$*
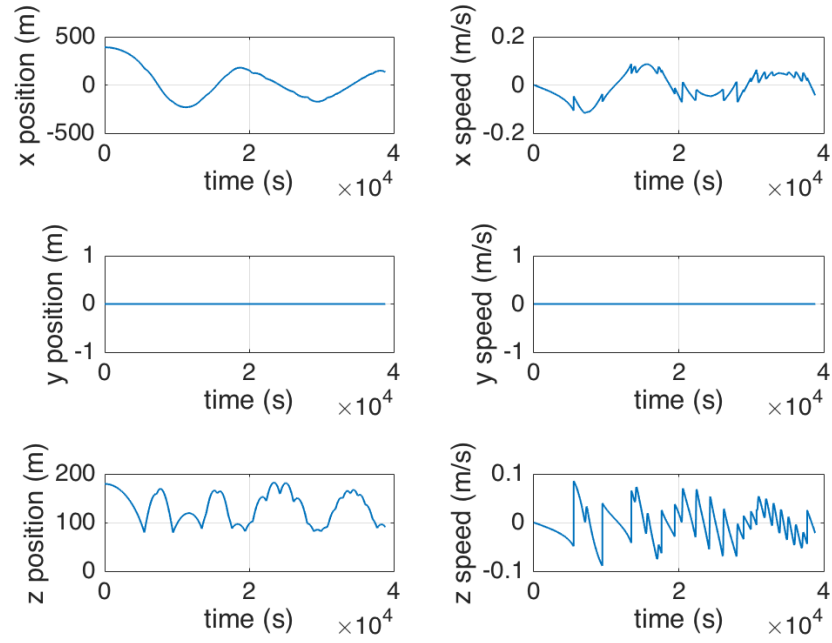
Figure 57. *Trajectory of point mass during drop on Itokawa surface $E_0 = 10$ V/m; $q_b = 10$ μC; $\lambda_d = 1$ m*
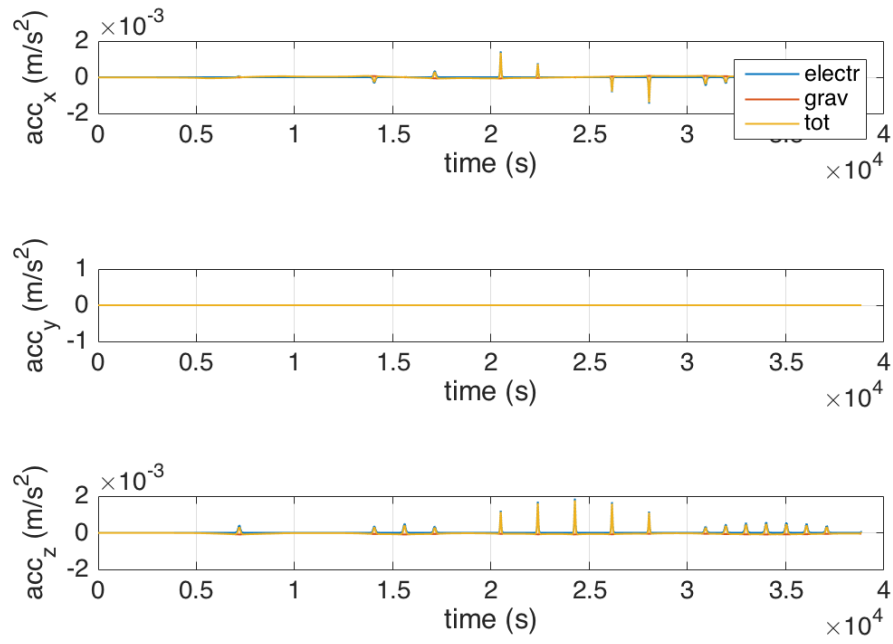
Figure 58. *Trajectory of point mass during drop on Itokawa surface* $E_0 = 10$ *V/m;* $q_b = 10$ μC; $\lambda_d = 1$ m
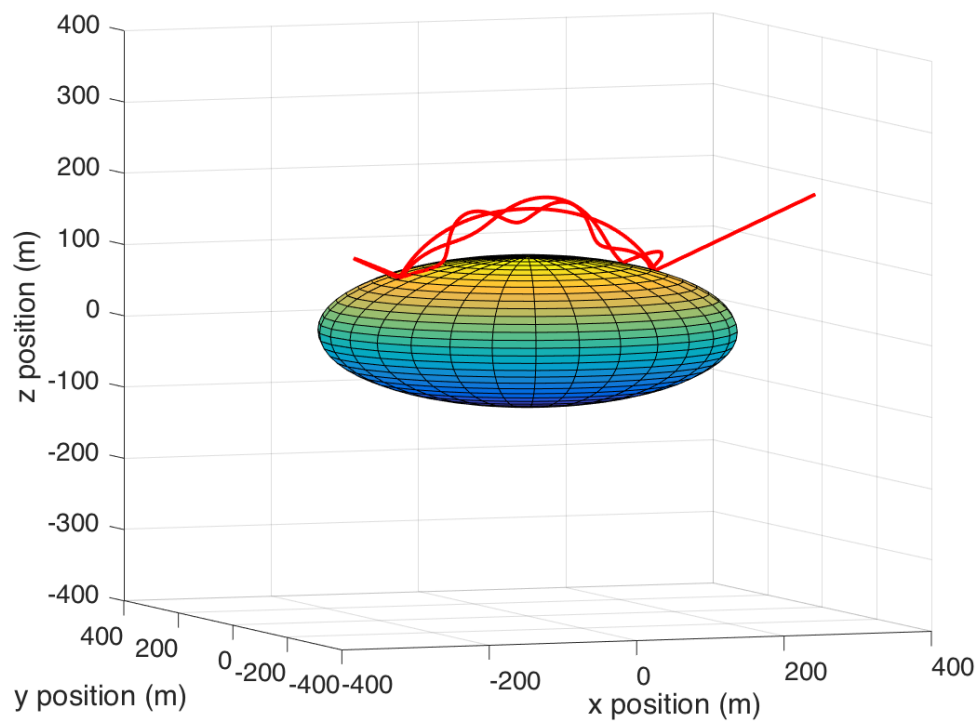
Figure 59 *Trajectory of point mass during drop on Itokawa surface* $E_0 = 10\ V/m; q_b = 10\ \mu C; \lambda_d = 10\ m$
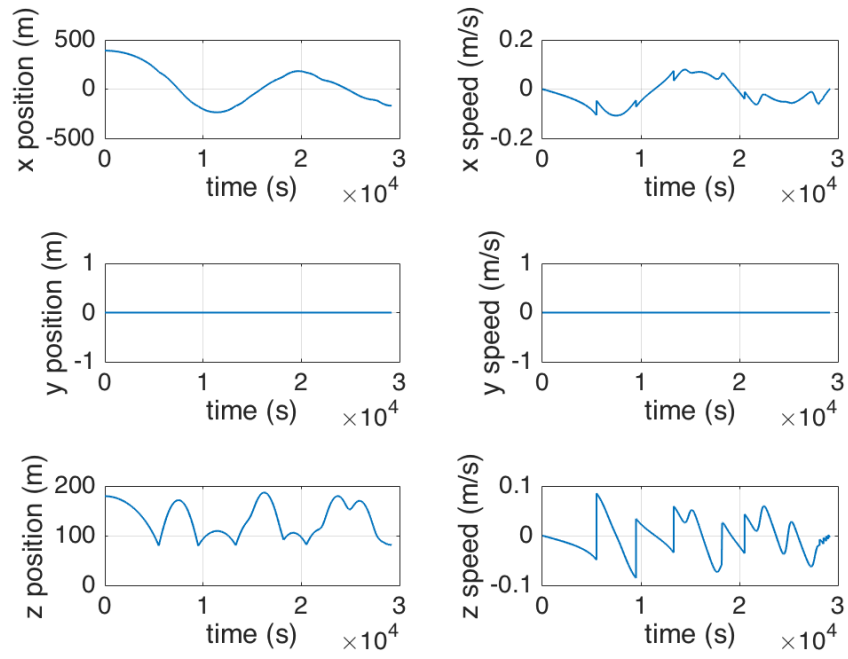
Figure 60. *Trajectory of point mass during drop on Itokawa surface $E_0 = 10$ V/m; $q_b = 10$ μC; $\lambda_d = 10$ m*
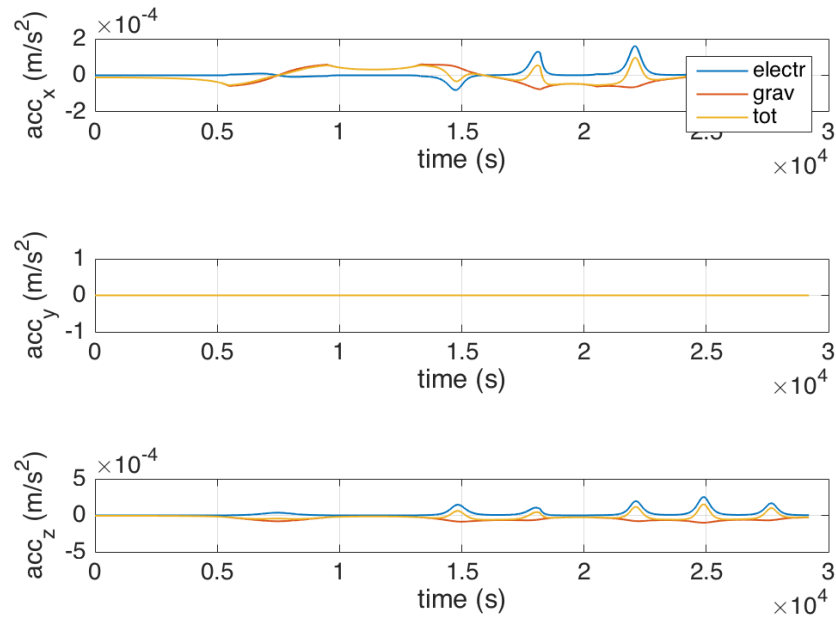
Figure 61. *Trajectory of point mass during drop on Itokawa surface $E_0 = 10\ V/m;\ q_b = 10\ \mu C;\ \lambda_d = 10\ m$*
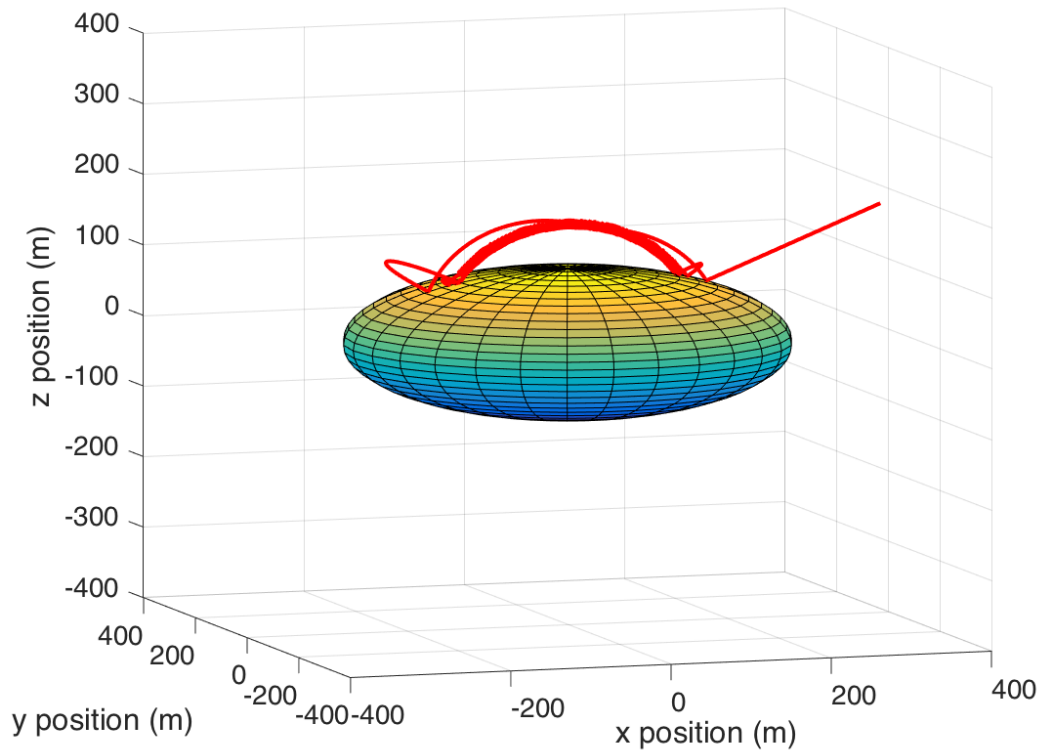
Figure 62. *Trajectory of point mass during drop on Itokawa surface* $E_0 = 10\ V/m; q_b = 100\ \mu C; \lambda_d = 0.1\ m$
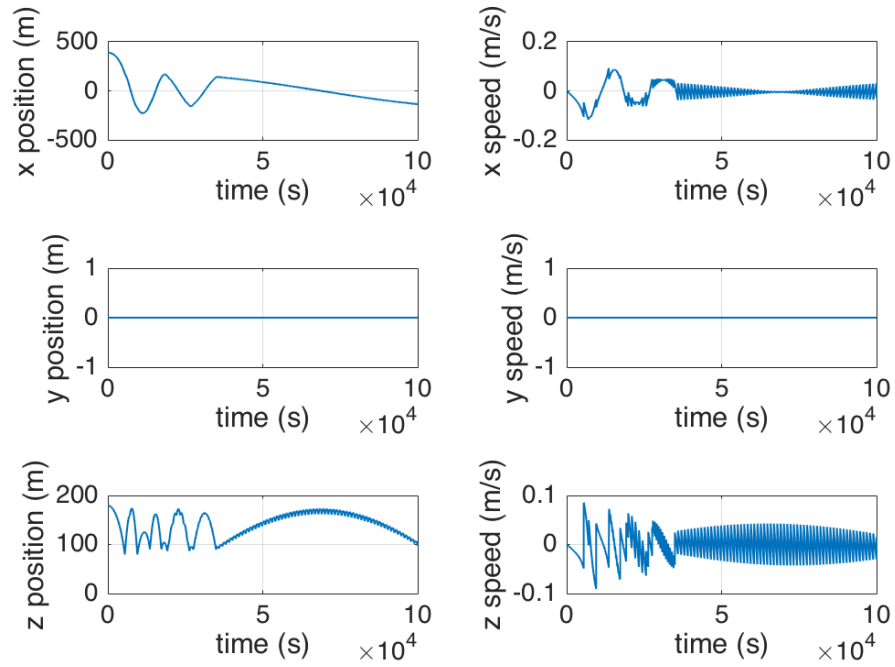
Figure 63. *Trajectory of point mass during drop on Itokawa surface $E_0 = 10$ V/m; $q_b = 100$ μC; $\lambda_d = 0.1$ m*
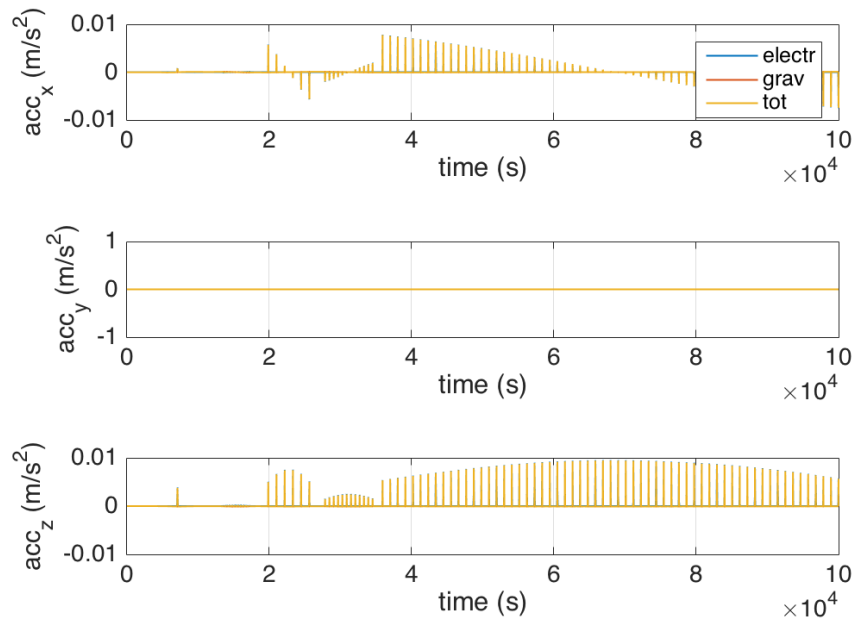
Figure 64. *Trajectory of point mass during drop on Itokawa surface* $E_0 = 10\ V/m;\ q_b = 100\ \mu C;\ \lambda_d = 0.1\ m$
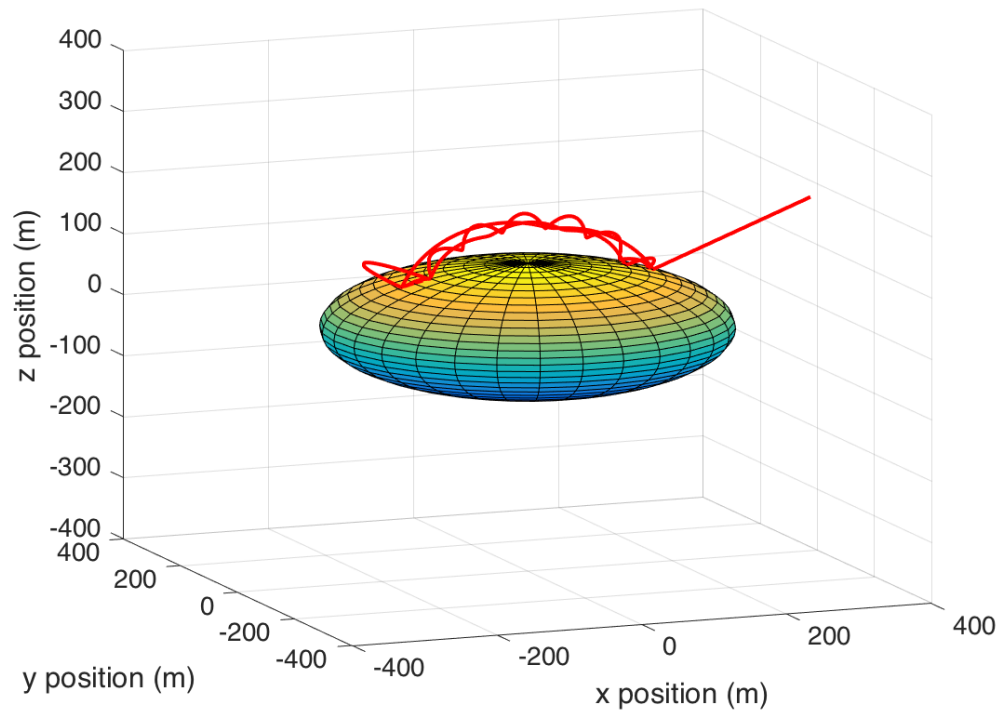
Figure 65. *Trajectory of point mass during drop on Itokawa surface $E_0 = 10 \ V/m; q_b = 100 \ \mu C; \lambda_d = 1 \ m$*
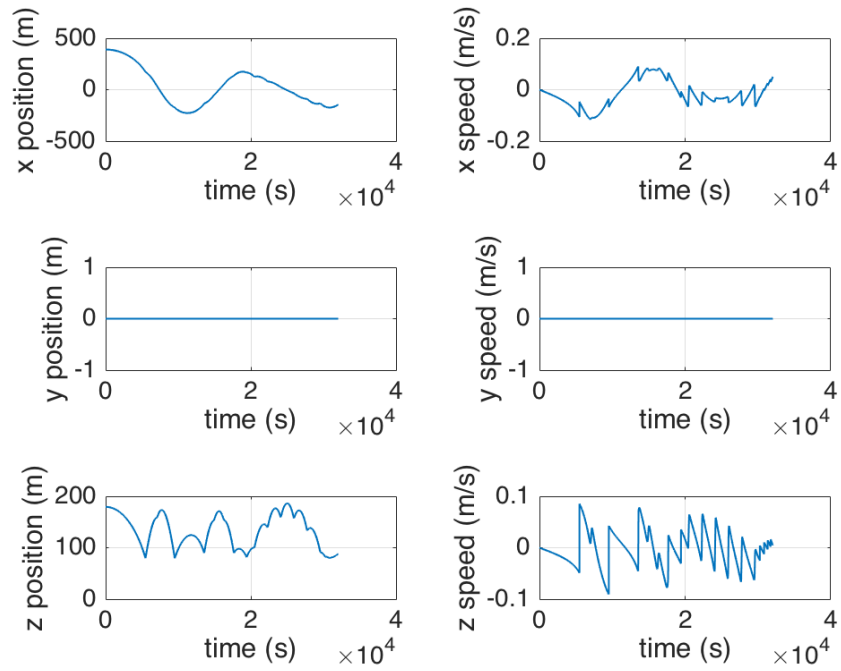
Figure 66. *Trajectory of point mass during drop on Itokawa surface* $E_0 = 10 \ V/m; \ q_b = 100 \ \mu C; \ \lambda_d = 1 \ m$
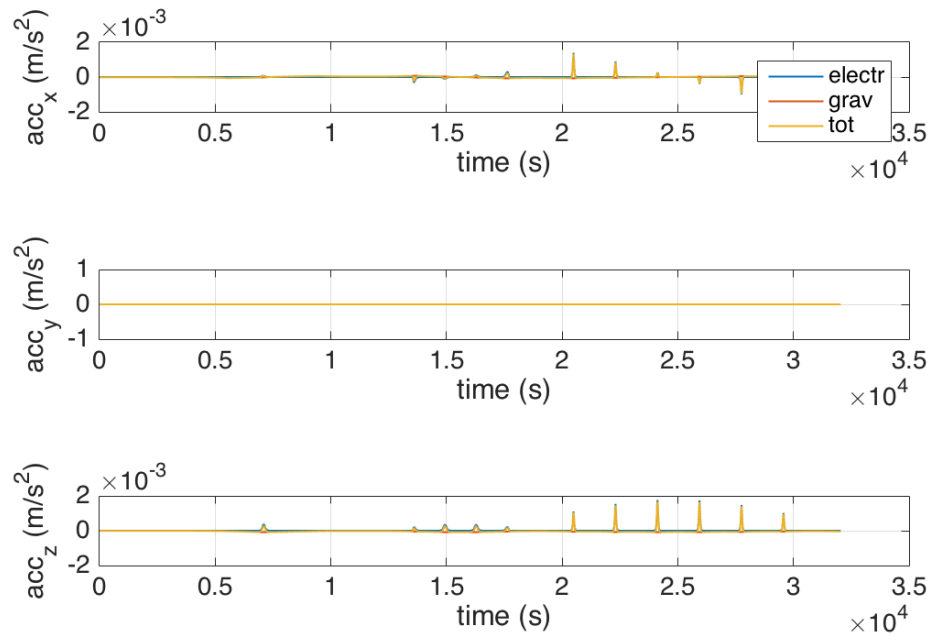
Figure 67. *Trajectory of point mass during drop on Itokawa surface $E_0 = 10$ V/m; $q_b = 100$ μC; $\lambda_d = 1$ m*
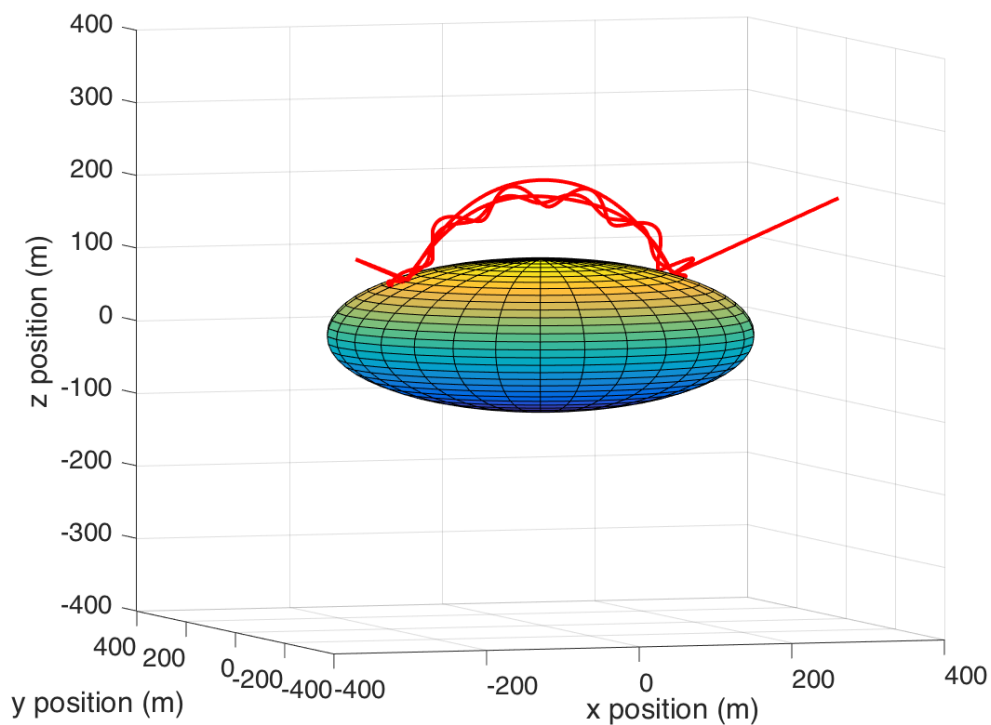
Figure 68. *Trajectory of point mass during drop on Itokawa surface $E_0 = 10\ V/m; q_b = 100\ \mu C; \lambda_d = 10\ m$*
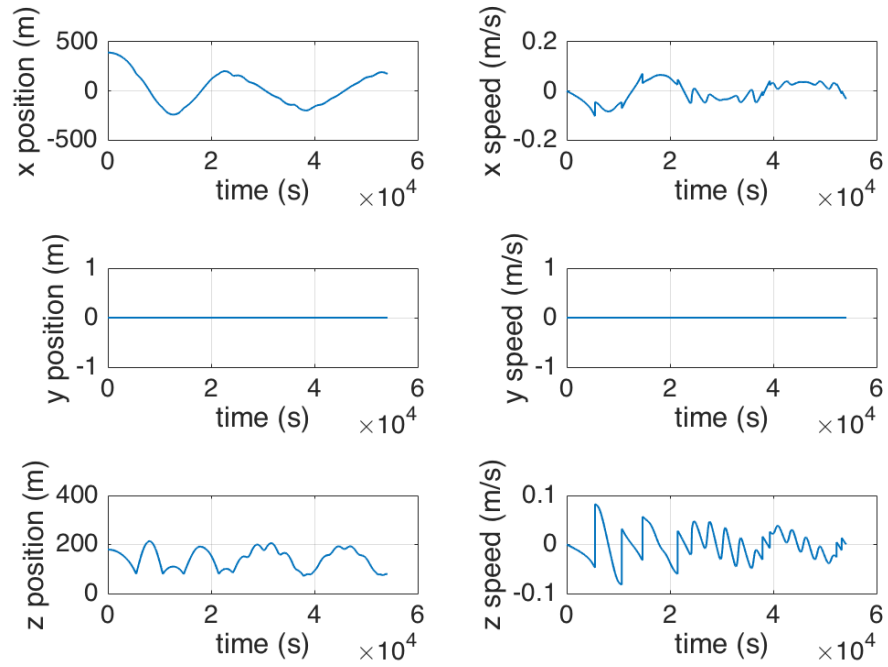
Figure 69. *Trajectory of point mass during drop on Itokawa surface $E_0 = 10$ V/m; $q_b = 100$ μC; $\lambda_d = 10$ m*
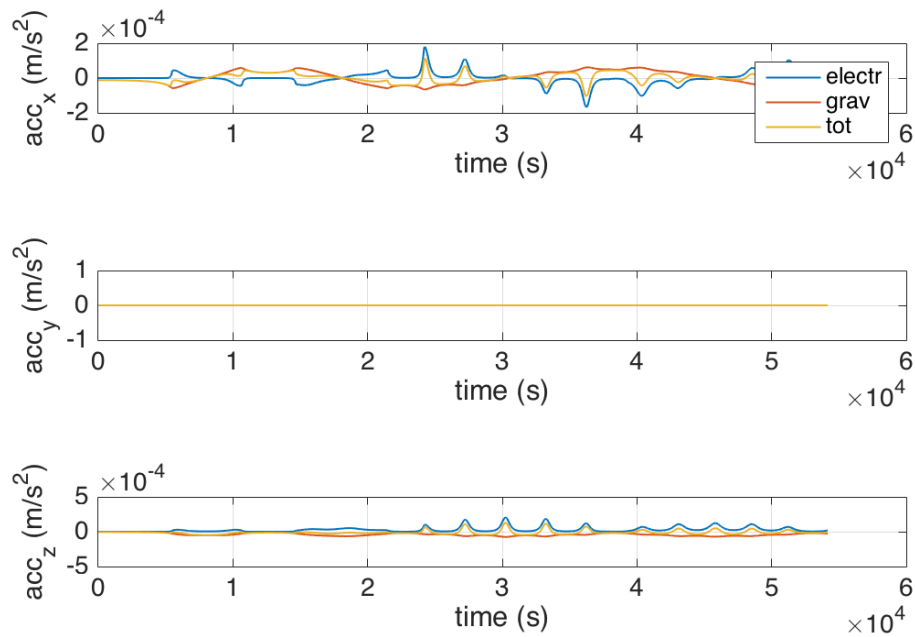
Figure 70. *Trajectory of point mass during drop on Itokawa surface $E_0 = 10 \ V/m; \ q_b = 100 \ \mu C; \ \lambda_d = 10 \ m$*

13. Electrostatic Hovering

This section proposes electrostatic hovering method for an E-Glider to maintain its relative position with respect to an asteroid. The basic strategy of electrostatic hovering is to create artificial equilibrium points by inducing electrostatic force with a constant charge. In order to identify the possible equilibrium points, it is essential to understand the potential field around an asteroid. Although the dynamics around asteroids is highly non-linear and can only be solved numerically, zero-velocity curves are known to be a powerful analytical tool in the comprehensive investigations of the motion of a spacecraft. In this research, the conventional analysis method with zero-velocity curves is extended for an E-Glider system by incorporating the effect of electrostatic potential.

13.1 Zero-Velocity Curves

Equations of motion presented in Eq. (21) can be rewritten by using the effective potential U as follows:

$$\ddot{x} - 2n\dot{y} = -\frac{\partial U}{\partial x}$$
$$\ddot{y} + 2n\dot{x} = -\frac{\partial U}{\partial y}$$
$$\ddot{z} = -\frac{\partial U}{\partial z}$$

(48)

Here, U is a function of the position vector $\boldsymbol{r}$ and given by the equation below.

$$U(\boldsymbol{r}) = -\frac{\mu}{r} - \frac{n^2}{2}(3x^2 - z^2) + \frac{Q}{m}\phi(\boldsymbol{r}) - a_{SRP} \cdot x$$

(49)

The first, second, third, and fourth terms on the right hand side correspond to the potential of the gravitational force, the centrifugal force, the electrostatic force, and the SRP force, respectively. Then, the following equation can be derived from Eq. (48):

$$\dot{x}\ddot{x} + \dot{y}\ddot{y} + \dot{z}\ddot{z} = -\left(\frac{\partial U}{\partial x}\dot{x} + \frac{\partial U}{\partial y}\dot{y} + \frac{\partial U}{\partial z}\dot{z}\right) = -\dot{U}$$

(50)

By integrating this equation, the integration constant can be defined as

$$C_J \equiv \frac{v^2}{2} + U(\boldsymbol{r}) = \text{const.}$$

(51)

where v denotes the velocity of a spacecraft. The constant variable C_J is referred to as the Jacobi integral, in the classical three-body problems. Given the fact that $v^2 \geq 0$ always holds true, the motion of a spacecraft must satisfy the following inequality:

$$U(\boldsymbol{r}) \leq C_j$$

(52)

For a given constant value of C_J, Eq. (52) provides a constraint on the position of a spacecraft, which bounds regions that are accessible to a spacecraft. The boundaries between regions of allowable and forbidden motion are defined by the equality in Eq. (52) and they are called zero-velocity curves in the planar case [Scheeres2012, Koon2011].

As shown in Eq. (49), the effective potential U is dependent on the charge Q, and therefore, the potential field around an asteroid is dominated by the charge value. In order to comprehend the transition of the potential field, zero-velocity curves for several different charge levels are computed in the x-y plane as shown in Figures 71 and 72. In each figure, zero-velocity curves with different C_J values are displayed as a contour map. Figure 71(a) corresponds to the case where the spacecraft does not possess any charge. This figure illustrates that the motion in the proximity of the asteroid is dominated by the gravitational potential, while, in the region far from the asteroid, SRP blows the spacecraft away toward the anti-sun direction (the positive direction of the x axis) [Scheeres2012, Giancotti2014]. Figure 71 (b)-(c) show positively charged cases, and Figure 71(d)-(g) show negatively charged cases. The complex potential fields appear in these figures due to the interaction between the gravitational, SRP, and electrostatic potential. Importantly, when the spacecraft is positively charged, the electrostatic force acts as a repulsive force on the dayside near the surface, increasing the effective potential, and the electrostatic force acts as an attractive force on the nightside, decreasing the effective potential; by contrast, when the spacecraft possesses a negative charge, electrostatic force acts in the opposite manner. This difference stems from the characteristic of the electrostatic field formed around an asteroid investigated in the previous section.

This analysis approach with zero-velocity curves provides an insight into the possible motion of an E-Glider, and it enables to establish the strategy to control the potential field via charge level for a desired motion. It is important to reiterate that the eclipse effect of SRP force and the wake effect of electrostatic force are not considered in the current model, which might affect the potential structure in the nightside region behind the asteroid.
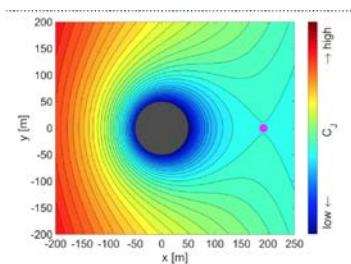
(a) $Q = 0\ \mu C$
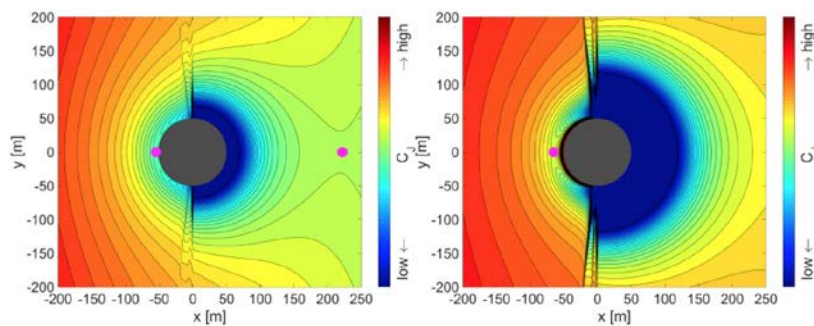
(b) $Q = +80\ \mu C$ (c) $Q = +1000\ \mu C$
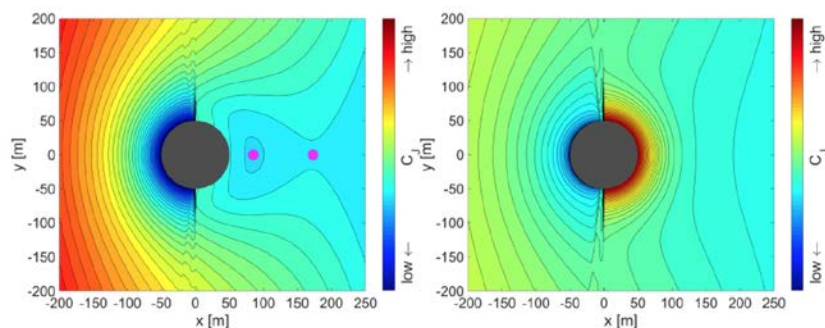
(d) $Q = -25\ \mu C$ (e) $Q = -100\ \mu C$

(f) $Q = -1000 \, \mu C$ (g) $Q = -2000 \, \mu C$
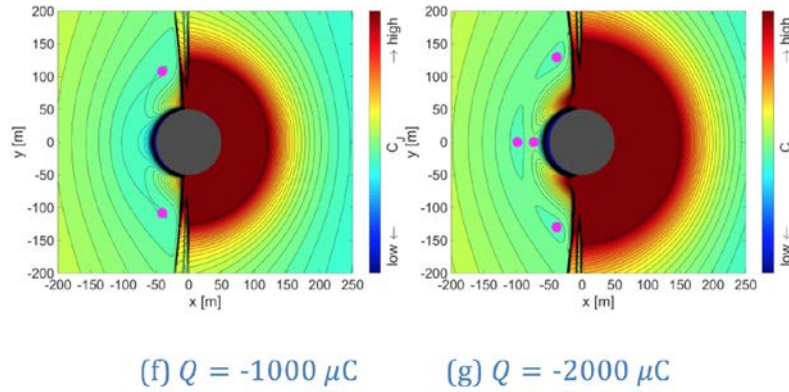
Figure 71. Zero-velocity curves for different spacecraft charge levels

13.2 Equilibrium Points

Equilibrium point solutions are obtained by substituting $\dot{r} = \ddot{r} = 0$ into Eq. (21), and expressed as follows:

$$\frac{\partial U}{\partial x} = \frac{\partial U}{\partial y} = \frac{\partial U}{\partial z} = 0$$

(53)

This equation can only be solved numerically due to the lack of an analytical expression of the electrostatic potential. Figure 72 contains the locations of equilibrium points, which are represented as magenta points, in the x-y plane for different charge values. These figures demonstrate a unique characteristic of an E-Glider system that the number and positions of equilibrium points differ depending on the charge of the spacecraft. It is also illustrated that these equilibrium points are located at the points where the gradients of contours are zero.

As for the natural motion case without charging, which is illustrated Figure 71(a), an equilibrium point in the proximity of an asteroid exists only on the nightside. This is because SRP constantly acts in the anti-sun direction, such that the dayside equilibrium point (the L1 point) moves farther from an asteroid, while the nightside equilibrium point (the L2 point) moves closer to an asteroid. In contrast to the natural motion, dayside equilibrium points are present in some cases when the spacecraft possesses a charge, as shown in Figure 71(b), (c), (f), and (g). These dayside equilibrium points are useful for an E-Glider mission concepts,

because electrostatic hovering on the dayside is advantageous for optical observation and solar power generation compared with hovering on the nightside.
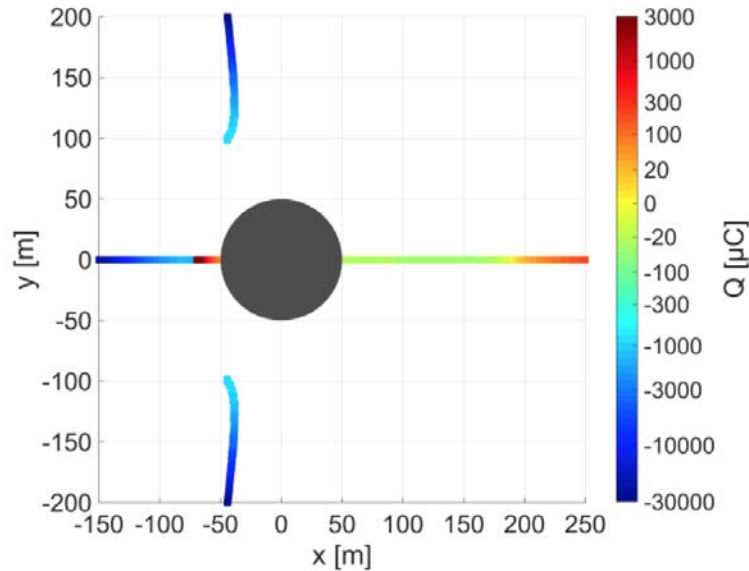
Figure 72. Transition of equilibrium points in the x-y plane.

Figure 73 illustrates the transitions of equilibrium points with variations in the value of charge Q. Each plot shows the location of an equilibrium point, and its color represents the corresponding charge level. It can be observed that the equilibrium points can be categorized into two types: collinear equilibrium points with $y = 0$ and non-collinear equilibrium points with $y \neq 0$. Unlike the Lagrangian points (three collinear and two triangular points) existing in the circular restricted three-body problem, these artificial equilibrium points are created in the vicinity of a target asteroid and therefore useful for hovering operation in a mission. Moreover, the location of an equilibrium point for electrostatic hovering can be controlled via the charge of the spacecraft. Here, non-collinear equilibrium points appear only when the spacecraft possesses a large negative charge ($Q \leq -810 \ \mu C$) in this system.

The relationship between the position of an equilibrium point and the required charge can be observed in detail in Figure 73. This figure is plotted for collinear equilibrium points and provides their altitudes and charges. Here, the altitude along the x axis, $h_x \equiv \text{sign}(x) \cdot (|x| - R)$, is defined such that it can represent both the dayside ($h_x < 0$) and the darkside ($h_x > 0$) regions by allowing a negative value. This figure indicates that a single charge

values can correspond to several equilibrium points at different altitudes, which is also shown in Figure 73. The black point in the figure corresponds to the natural equilibrium point, and it moves to both higher and lower altitude in accordance with the sign of the charge. Another unique feature is that the charge value diverges to the positive and negative infinite at $h_x \simeq -20$ m. This is because the electrostatic potential has non-monotonic profile and possesses minimum potential where the electrostatic field is zero, as shown in Figure 73. According to this analysis, the minimum amount of charge to levitate the spacecraft on the dayside is $Q \simeq 12\ \mu C$, which is consistent with previous research [Quadrelli2017].
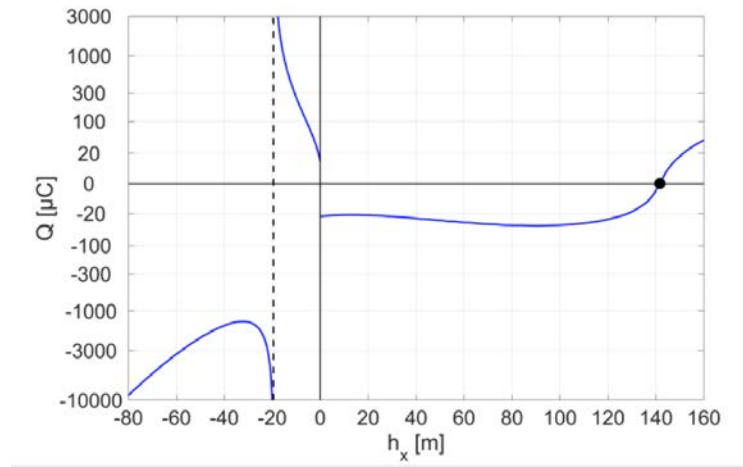
Figure 73. Altitude and required charge of a collinear equilibrium point

13.3 *Power Required for Electrostatic Hovering*

In the analysis above, we found that electrostatic hovering above an asteroid could potentially be achieved by creating artificial equilibrium points with electrostatic force. This section investigates the feasibility of electrostatic hovering from the perspective of power requirement. Analyses are performed for the collinear equilibrium point solutions obtained in the previous subsection. Figure 74(a) shows the magnitude of voltage required for electrostatic hovering at the corresponding altitude. The power supply voltage is calculated from the required charge based on Eq. (43). This result indicates that dayside hovering requires at least 100 kV levels of charge. Although such high-voltage charging itself might not cause any risk to a spacecraft, it can cause electrostatic discharge, which might be harmful

to spacecraft sub-systems. Therefore, provisions should be taken to prevent electrostatic discharge itself or instrument damage due to it, as discussed in previous research [Schaub2003, King2002b]. Section 9 already discussed various options for differentially charging surfaces of the EGlider in a way that precludes damaging the vehicle.

Figure 74(b) illustrates the power required to hover the spacecraft at an equilibrium point. It is indicated that hovering on the dayside near the surface requires the power of as much as 100 kW, while hovering on the nightside requires only about 15 W, in spite of almost the same charge levels (Figure 74b). This difference primarily stems from two reasons. First, the mass of an electron is much smaller than that of an ion, and thus, electrons are much mobile in a plasma. This results in a large negative current flux, requiring much power to maintain a positive charge. Second, a dense photoelectron layer near the surface is present around the sub-solar region, as shown in Figure 74. This environment also involves large negative current for a positively charged spacecraft. These results imply that electrostatic hovering with a negative charge is more feasible than that with a positive charge from the perspective of power requirement.

(a) Voltage   (b) Power
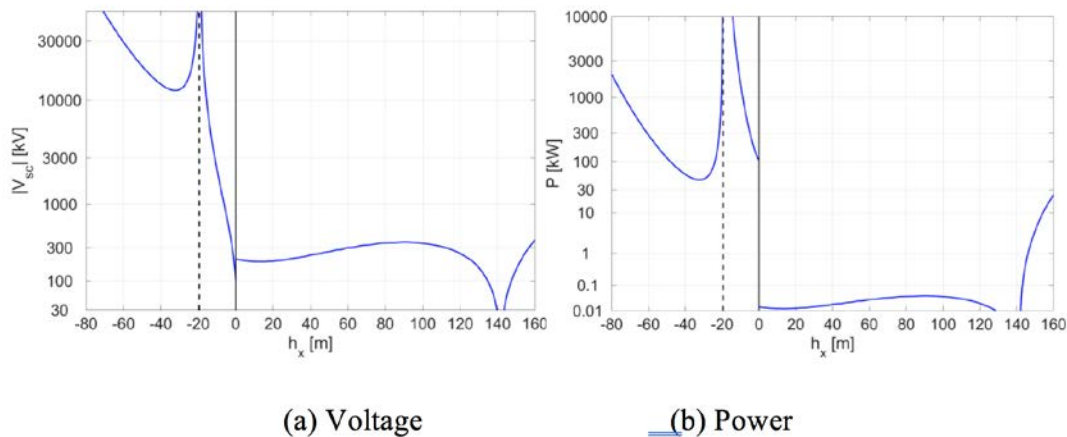
Figure 74. Required voltage/power for electrostatic hovering at a collinear equilibrium point

14.   Electrostatic Orbiting

It has been revealed that dayside equilibrium points can be created by inducing electrostatic force; however, electrostatic hovering at such an equilibrium point will consume

large amount of power. For this reason, this section proposes the electrostatic orbiting method as an alternative strategy for an E-Glider operation and identifies a new class of periodic orbits around asteroids called *electrostatic periodic orbits*.
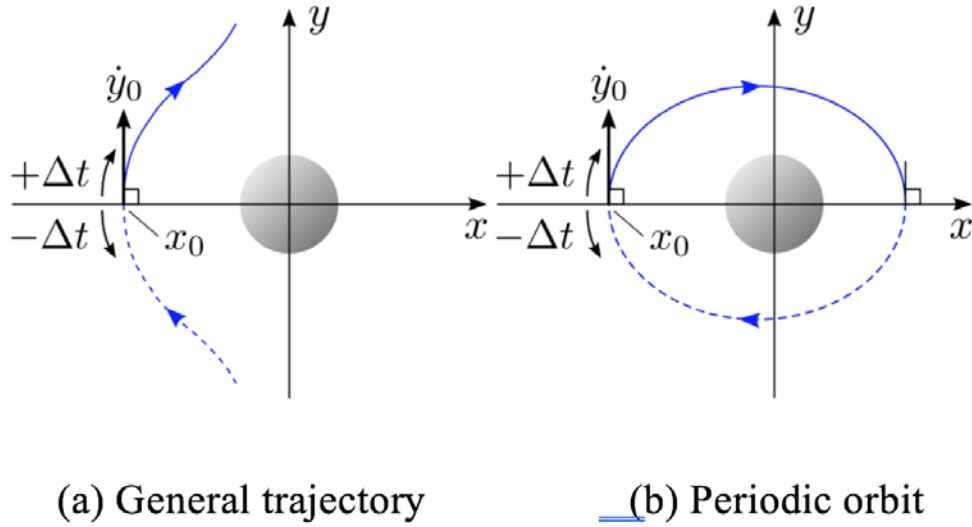
Figure 75. Orbit design methodology of electrostatic periodic orbits

14.1 Orbit Design Methodology

Electrostatic periodic orbits are designed by using the symmetry inherent in the equations of motion, Eq. (21) which can be expressed as follows [Broschart2011, Henon1969]:

$$(t, x, y, z) \rightarrow (-t, x, -y, z)$$

(54)

If the set of variables on the left-hand side of Eq. (54) satisfies Eq. (21), then that on the right-hand side also satisfies the equation. This symmetry is known to hold for the circular restricted three-body problems subject to SRP, and it holds true for an E-Glider system as well because the electrostatic potential is assumed to have symmetry about the x axis. Because of the symmetry, if an initial position on the x-z plane is given as $\boldsymbol{r} = [x_0, 0, z_0]^{\mathrm{T}}$ and an initial velocity perpendicular to this plane is given as $\dot{\boldsymbol{r}} = [0, \dot{y}_0, 0]^{\mathrm{T}}$, then the spacecraft trajectories obtained through forward and backward propagation are

symmetrical to each other about the x-z plane (Figure 75a). Thus, when a spacecraft perpendicularly intersects the x-z plane again, a periodic orbit solution is obtained as a closed continuous trajectory (Figure 75b).

Then, a set of initial conditions, with three degrees of freedom, are expressed as $(x_0, z_0, \dot{y}_0)$. On the other hand, terminal constraints, $\dot{x} = \dot{z} = 0$, must be satisfied when a trajectory intersects the x-z plane after half a period. Consequently, an electrostatic periodic orbit solution, which is obtained by numerical computation, has one degree of freedom. To systematically analyze the solution space, an initial altitude h_0 and an initial phase ψ_0, which are alternative parameters for describing the initial position in place of x_0 and z_0, are introduced as follows:

$$h_0 = \sqrt{x_0^2 + z_0^2} - R$$
$$\psi_0 = \tan^{-1}\left(-\frac{z_0}{x_0}\right)$$

(55)

Note that $\psi_0 = 0$ and 90 deg correspond to the sub-solar point and the terminator point, respectively. Among the three initial variables $(h_0, \psi_0, \dot{y}_0)$, an initial altitude h_0 is designated as a free parameter to search periodic orbit solutions.

14.2 Electrostatic Periodic Orbits

Figure 76 provides an example of a natural periodic orbit (i.e. $Q = 0$), which is commonly referred to as a terminator orbit, and Figure 77 provides examples of electrostatic periodic orbits for two different charge levels. These orbits are obtained with $h_0 = 15$ m. Note that these figures are expressed in the Hill coordinate, and thus, the negative direction of the x axis corresponds to the sun direction. According to the definition of the coordinate system, these orbits can also be classified as sun-synchronous orbits that do not experience eclipse. Here, the periods of the orbits shown in Figure (76), Figure 77(a), Figure 77(b) are $T = 3.5, 4.9,$ and 7.3 hr, respectively.

Figure 76 shows that the orbital plane is displaced from the terminator plane in the anti-sun direction due to the effect of SRP. This observation indicates that this natural periodic orbit is located on the nightside of the asteroid; thus, it is not suitable for optical observations. This is the primary drawback of terminator orbits around asteroids. By contrast, as shown in Figure 77, electrostatic periodic orbits are located on the dayside. Therefore, these orbits

offer significant advantage for optical observations. Moreover, as mentioned above, these orbits are sun-synchronous and achieve constant illumination from the sun, which is advantageous for solar power generation and thermal design. Broadly speaking, when the magnitude of a charge increases, an orbit achieves larger displacement from the terminator plane in the sun direction, as depicted in Figure 77(a) and (b). Another important fact is that these orbits are accomplished by inducing negative charging and thus require only small amount of power, as will be pointed out in a later section.
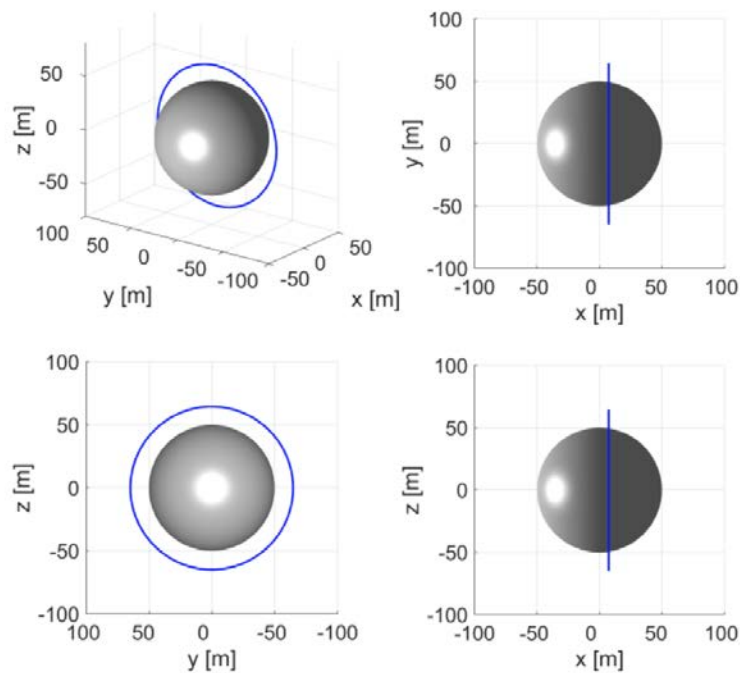
Figure 76. Natural periodic orbit.

(a) $Q = -10 \ \mu C$ (b) $Q = -250 \ \mu C$
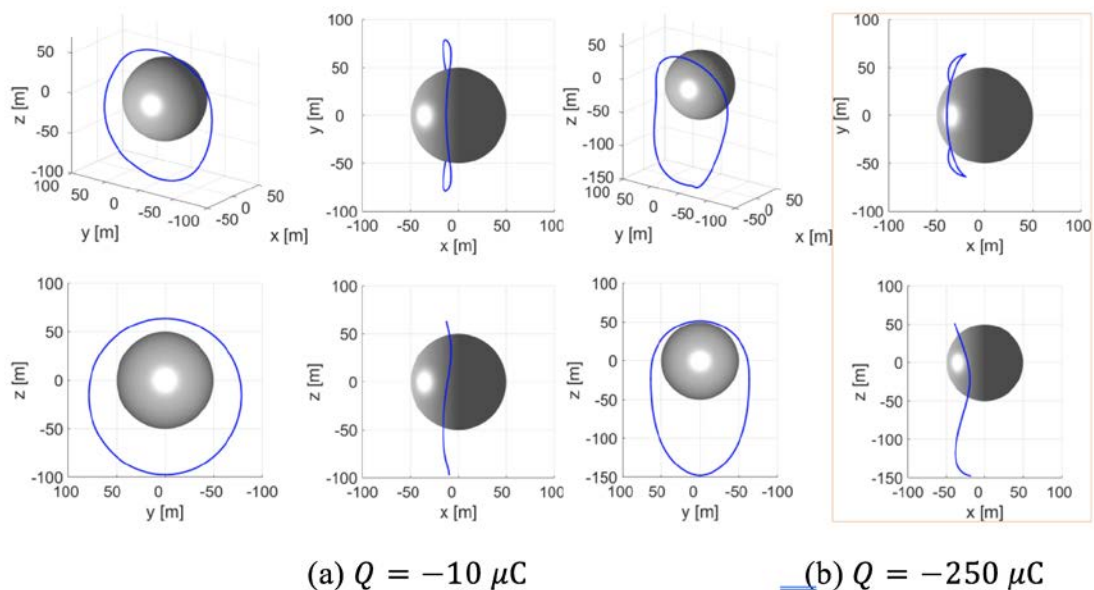
Figure 77. Electrostatic periodic orbits.
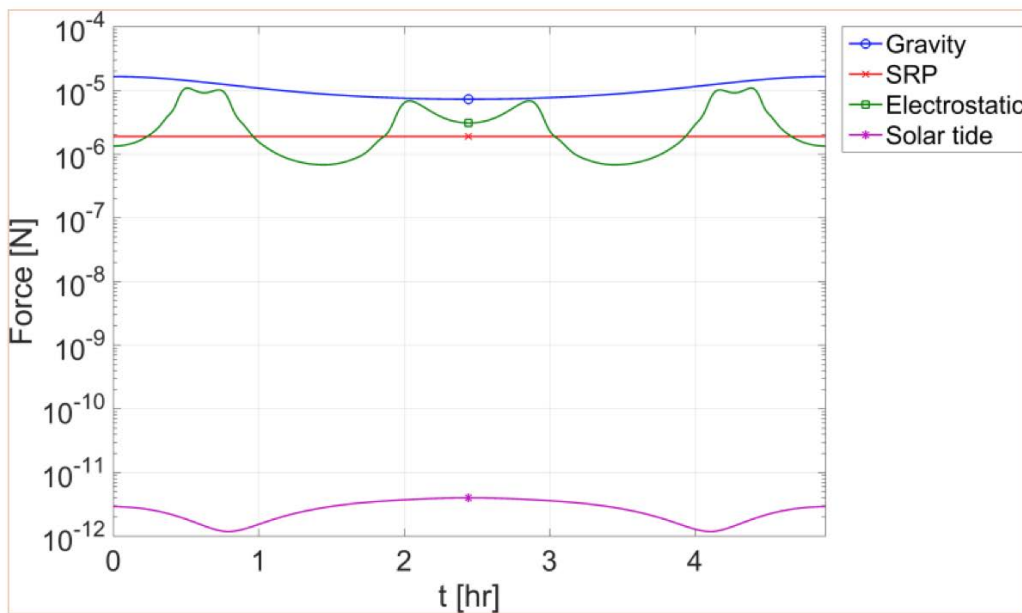
Figure 78. Forces acting on spacecraft during one orbital period.

Figure 78 illustrates the history of the magnitudes of forces acting on a spacecraft during one orbital period in the orbit provided in Figure 77(a). The magnitude of the electrostatic force was computed as 1-10 μN in this simulation. While the electrostatic force is weaker than the gravitational force, it has the same order of magnitude with that of the SRP force. This result indicates that electrostatic orbiting can be achieved without fully compensating for the gravitational force, leading to energy-efficient operation compared with electrostatic hovering.

14.3 Evolution of Periodic Orbit Solutions

Shape transitions of electrostatic periodic orbits are depicted in Figure (79). These orbits are computed for different charge values, $-200\ \mu C \leq Q \leq -3\ \mu C$, and a constant initial altitude, $h_0 = 15$ m, by applying numerical continuation method [Seydel2010]. The vertical axis represents an initial phase ψ_0 obtained as a result of the numerical calculation. This figure shows intriguing structures of both the entire solution space and orbital shapes themselves. The orbit that is expressed as the diamond marker at $Q = 0$ corresponds to the natural periodic orbit, which is also shown in Figure 76 and it has an initial phase larger than 90 deg. By contrast, all of the electrostatic periodic orbit solutions depicted in this figure are obtained with initial phases smaller than 90 deg. It can be inferred from this result that these electrostatic periodic orbits are placed on the dayside, unlike natural terminator orbits. Interestingly, bifurcation appears in the region with comparatively small magnitude of charge, and it involves several different orbit solutions with exactly the same charge value. As already mentioned, an orbit with larger magnitude of a charge appears to have larger displacement from the terminator plane.

Figure 79 illustrates electrostatic periodic orbits computed for different initial altitudes, $10\ \text{m} \leq h_0 \leq 80\ \text{m}$, and a constant charge, $Q = -50\ \mu C$. The vertical axis represents an initial velocity $\dot{y}_0$ obtained as a result of the numerical calculation. As observed from the figure, a higher initial altitude does not necessarily results in a larger periodic orbit. Moreover, the orbits on the left side and the right side are almost symmetric each other about the x-z plane. This result implies that the size of an electrostatic periodic orbit is limited by the charge level, because electrostatic force cannot exert influence on the motion of a spacecraft at a high altitude.

It is to be noted that Figure 79 and Figure 80 merely show examples of electrostatic periodic orbit families, but not the entire orbit solutions. It is probable that there exist other

orbit families that are not presented in this study, because multiple equilibrium points are present in this system.
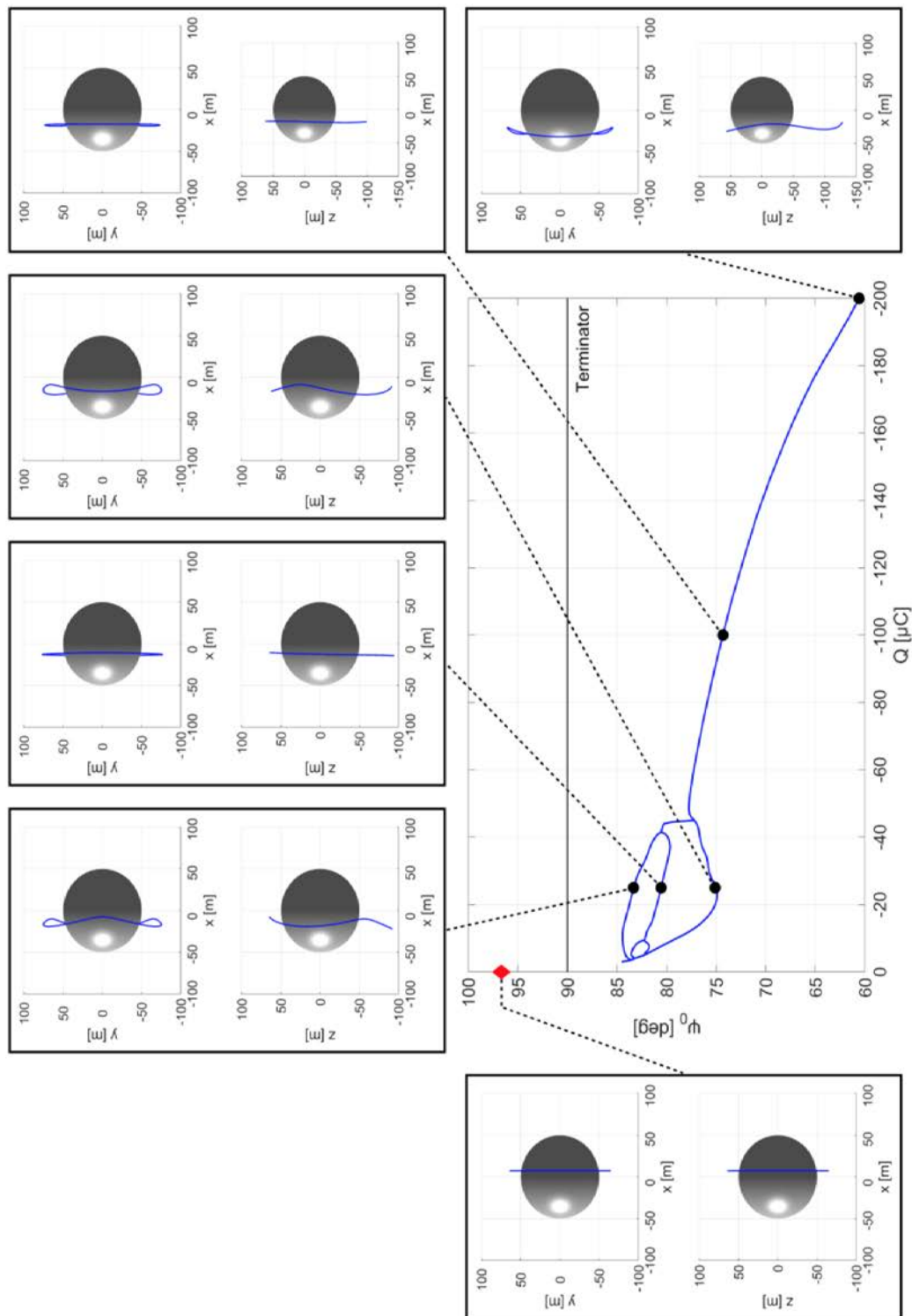
Figure 79. Electrostatic periodic orbit solutions for different charge levels
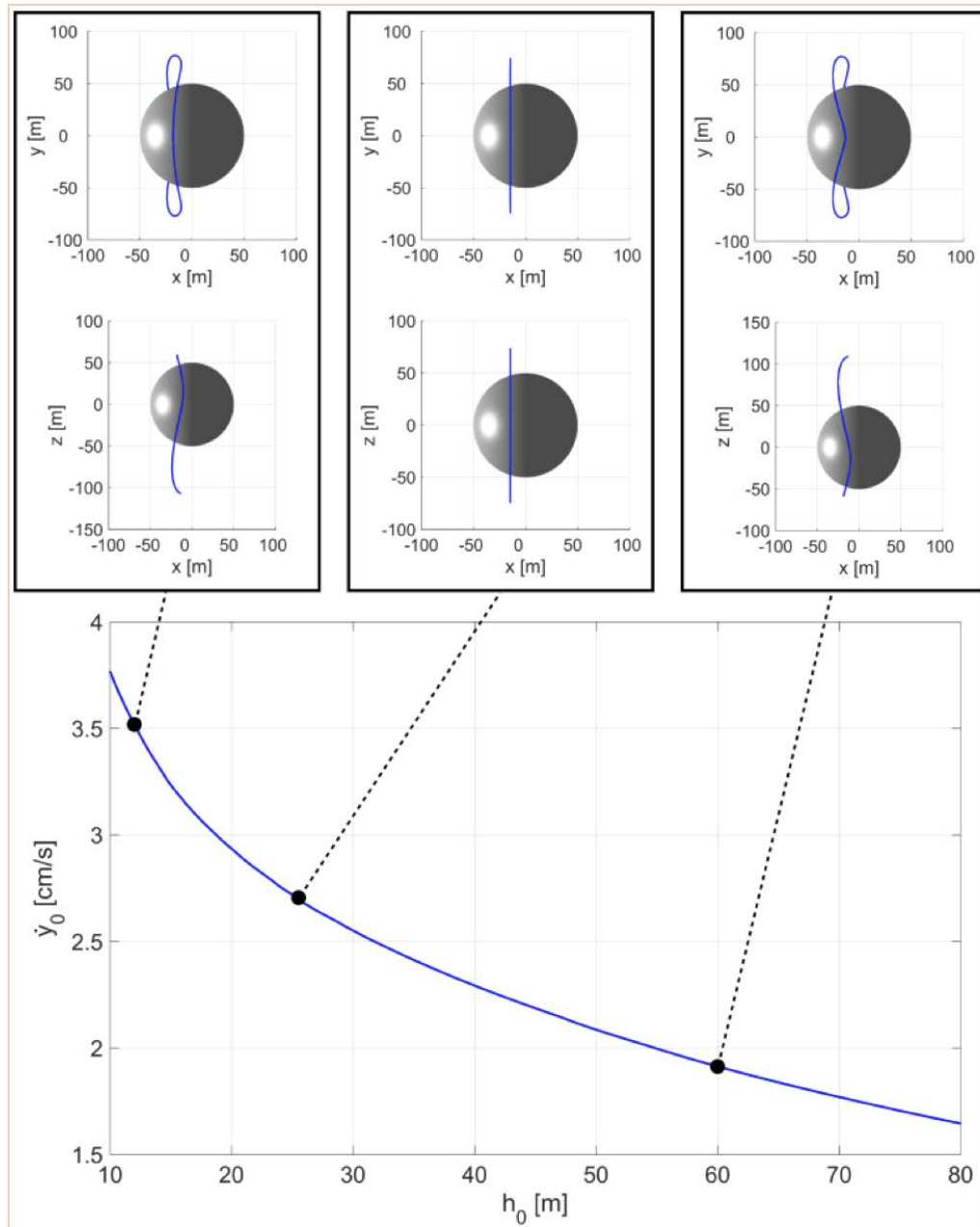
Figure 80. Electrostatic periodic orbit solutions for different initial distances

14.4 Power Required for Electrostatic Orbiting

The power requirement for electrostatic orbiting is analyzed in this subsection. Figure 81 shows the power history of the orbit provided in Figure 77(a) during one orbital period. Even though the charge Q is given as a constant, the required power varies because the current flux from an ambient plasma depends on the position of a spacecraft with respect to an asteroid. The broken line in the figure represents the average power defined by the following equation:

$$P_{ave} = \frac{1}{T}\int_0^T P(t)dt$$

(56)

The average power required for this electrostatic periodic orbit is calculated as 2.56 W, and it appears to be feasible for missions.

Figure 82 shows the voltage and power required to achieve electrostatic periodic orbit solutions provided in Eq. (36). Figure 82(a) is simply obtained from the relationship between the charge and the voltage given by Eq. (31), and Figure 82(b) plots the average power of each single periodic orbit. Interestingly, even though the solution space structure of electrostatic periodic orbits is complex and involves bifurcation, the power diagram exhibits a simple profile as shown Figure 82(b). According to this analysis, example values of the required voltage and power are: $|V_{sc}| = 89.9$ kV and $P_{ave} = 2.56$ W for the orbit with $Q = -10\ \mu C$; and $|V_{sc}| = 449$ kV and $P_{ave} = 63.8$ W for the orbit with $Q = -50\ \mu C$.

Comparing Figure 82(a) and Figure 82(b), electrostatic orbiting requires considerably lower energy than does electrostatic hovering on the dayside. Although an E-Glider must be inserted into an orbit either by itself or a mother spacecraft, after the insertion, it can be orbiting around an asteroid without requiring any fuel. The required voltage and power largely depend on the design of an E-Glider, and thus, the further investigations must be carried out to optimize the entire system design of the E-Glider. In addition, as mentioned in Subsection 13.3, the spacecraft must be designed to have the capability of handling high voltage.
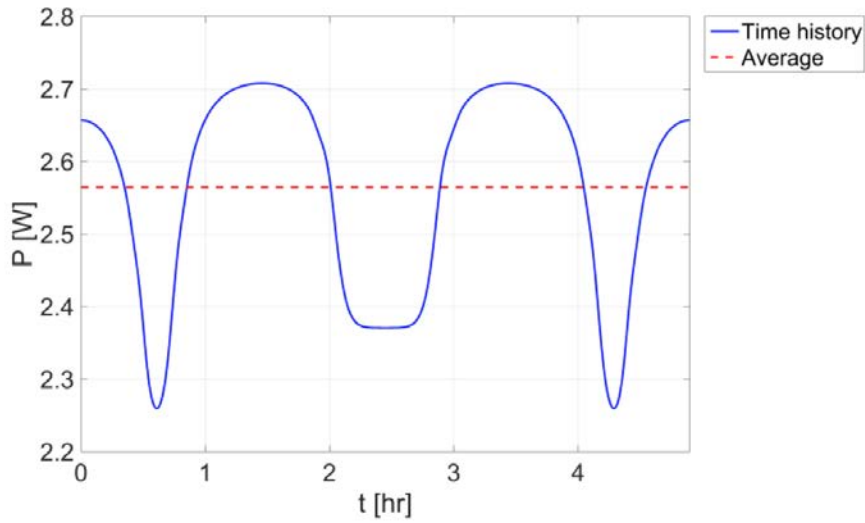
Figure 81. Power consumption during one orbital period.
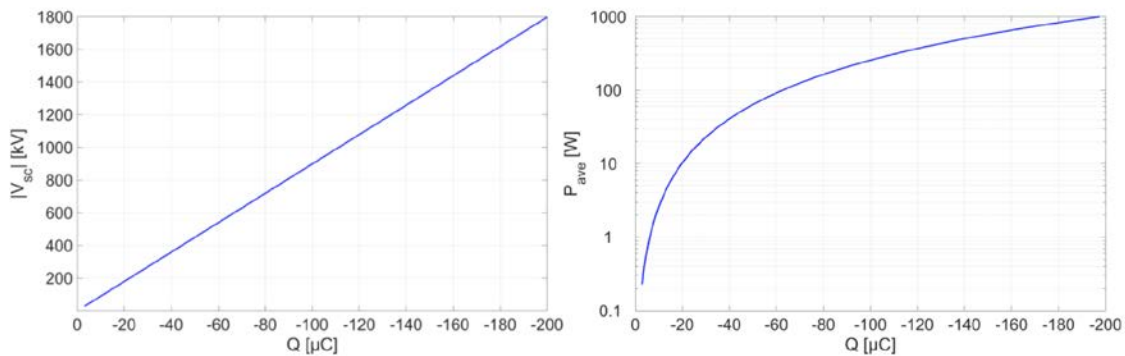
Figure 82. Required voltage/power for electrostatic orbiting.

14.5 Specific Impulse of an E-Glider System

As previously mentioned, electrostatic hovering and orbiting requires current emission from an E-Glider to maintain its charge level in a plasma environment. Because the current emission involves a decrease in spacecraft mass, the specific impulse of an E-Glider system can be defined in the same manner as conventional thruster systems [Schaub2003, King2002b].

Assuming that an ion current is emitted from the spacecraft for negative charging, the mass flow rate is given by the following equation:

$$\dot{m} = m_i \times \frac{|I_{sc}|}{e}$$

(57)

where e is the elementary charge; m_i is the mass of an ion; and I_{sc} is the emission current. By using this mass flow rate, the specific impulse is calculated as follows from its definition:

$$I_{SP} = \frac{|\mathbf{F}_E|}{\dot{m} g_0}$$

(58)

where $g_0 \simeq 9.8$ m/s^2 is the standard gravitational acceleration.

Figure 83 illustrates the specific impulse of the E-Glider orbiting around the asteroid. Since the electrostatic force and the emission current depend on the position of a spacecraft, the specific impulse is expressed as a time-dependent function. Then, the time average of the specific impulse is given by

$$\bar{I}_{sp} = \frac{1}{T} \int_0^T I_{sp}(t) dt$$

(59)

Consequently, the average specific impulse of the E-Glider system for the electrostatic orbiting is calculated as $\bar{I}_{sp} = 1.2 \times 10^6$ s. Note that the value of a specific impulse largely depends on the required charge and current to achieve a specific electrostatic periodic orbit.

Table 6 lists the specific impulse values of the E-Glider system calculated above and those of cold gas, chemical (bipropellant), and ion thrusters [SMAD2005]. It is evident that the specific impulse of the E-Glider system is considerably higher than those of the conventional thruster systems. Therefore, the proposed electrostatic propulsion method is much more fuel efficient, and would be useful for asteroid exploration mission concepts.
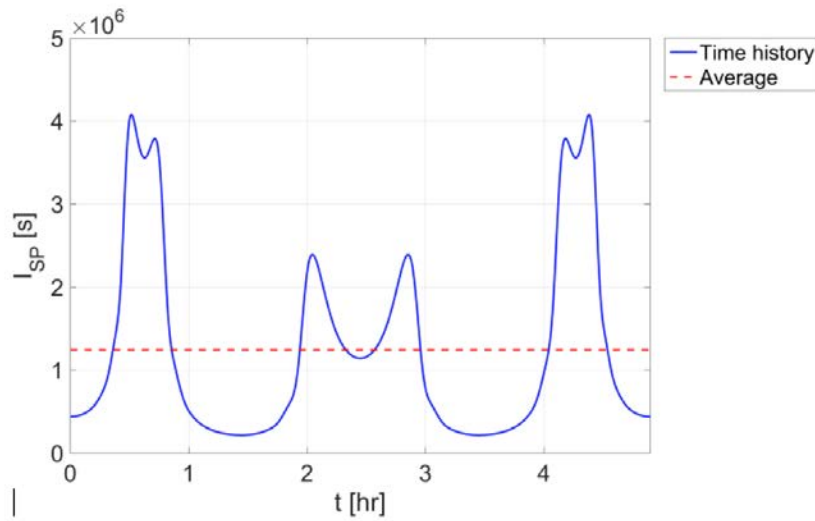
Figure 83. Specific impulse during one orbital period.

Table 6. Comparison between the E-Glider system and conventional thrusters [SMAD2005]

Type	Typical I_{sp} value [s]
Cold gas thruster	50
Chemical thruster	300
Ion thruster	2000-6000
E-Glider system	1×10^6

15.   Effects of Shape Irregularity

Analysis results that have been presented in previous sections are based on the spherical asteroid model. However, asteroids have irregular shapes in general, and the motion of a spacecraft around such an asteroid can be strongly perturbed due to its irregular gravitational field. Moreover, considering an E-Glider system, irregularly shaped asteroids form irregular electrostatic fields around them, posing an additional perturbation on the spacecraft. This section evaluates the effects of these perturbations on the spacecraft dynamics.

15.1 Asteroid Model

The asteroid is modelled as a homogeneous triaxial ellipsoid with semi-major axes R_a, R_b, and R_c ($R_a \geq R_b \geq R_c$). The mean radius of the asteroid is given as $R = 50$ m, which satisfies $R^3 = R_a R_b R_c$, and the axis ratio is taken as a variable in later subsections. The asteroid is rotating uniformly about the shortest axis with the rotation period of $T_{rot} = 8$ hr, and the rotation axis is assumed to be perpendicular to the ecliptic plane. Then, the asteroid body-fixed coordinate can be defined as shown in Figure 84. Here, a left superscript "H" represents the Hill coordinate system and "B" represents the asteroid body-fixed frame. The $^H z$ axis and $^B z$ is identical because of the assumption regarding the rotation axis. Henceforth, the position of a spacecraft is expressed in terms of the Hill coordinate as $^H r = [x, y, z]^T$ and in terms of the asteroid body-fixed frame as $^B r = [x_B, y_B, z_B]^T$.
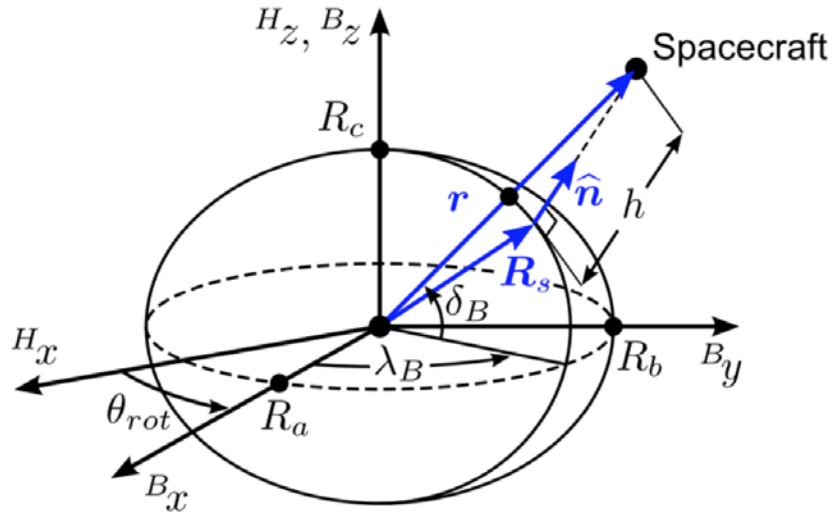
Figure 84. Reference frames around an ellipsoidal asteroid.

Let $^H C_B$ denote the rotational transformation matrix from the asteroid body-fixed coordinate to the Hill coordinate system. Then, the coordinate transformation for an arbitrary state vector u is expressed as $^H u = {}^H C_B {}^B u$, where $^H C_B$ is given by the equation below.

$$^H C_B = \begin{bmatrix} \cos\theta_{rot} & -\sin\theta_{rot} & 0 \\ \sin\theta_{rot} & \cos\theta_{rot} & 0 \\ 0 & 0 & 1 \end{bmatrix}$$

(60)

Here, θ_{rot} is the rotation phase of an asteroid and given as a function of time by the following equation:

$$\theta_{rot} = \frac{2\pi}{T_{rot}} t$$

(61)

15.2 Irregular Gravitational Field

The gravitational potential of an asteroid is calculated based on an triaxial ellipsoid model. The gravitational coefficients C_{mn} of its spherical harmonics expansion up to the fourth order are defined by the following equations [Scheeres2012]:

$$C_{20} = \frac{1}{10R_a^2}\{2R_c^2 - (R_a^2 + R_b^2)\}$$
$$C_{22} = \frac{1}{20R_a^2}(R_a^2 - R_b^2)$$
$$C_{40} = \frac{15}{7}(C_{20}^2 + 2C_{22}^2)$$
$$C_{42} = \frac{5}{7}C_{20}C_{22}$$
$$C_{44} = \frac{5}{28}C_{22}^2$$

(62)

Using these coefficients, the gravitational potential is given by the equation below.

$$U_G = \frac{\mu}{r}\left[1 + \left(\frac{R}{r}\right)^2 \left\{\frac{1}{2}C_{20}(3\sin^2\delta_B - 1) + 3C_{22}\cos^2\delta_B \cos 2\lambda_B\right\} \right.$$
$$+ \left(\frac{R}{r}\right)^4 \left\{\frac{1}{8}C_{40}(35\sin^4\delta_B - 30\sin^2\delta_B + 3)\right.$$
$$\left.\left. + \frac{15}{2}C_{42}\cos^2\delta_B (7\sin^2\delta_B - 1)\cos 2\lambda_B + 105C_{44}\cos^4\delta_B \cos 4\lambda_B \right\}\right]$$

(63)

where δ_B and λ_B denote the latitude and longitude, respectively, defined in terms of the asteroid body-fixed frame. The relation between (δ_B, λ_B) and the position of a spacecraft can be expressed as follows:

$$\delta_B = \sin^{-1}\left(\frac{z_B}{r}\right)$$
$$\lambda_B = \tan^{-1}\left(\frac{y_B}{x_B}\right)$$

(64)

Then, substitution of Eq. (63) into Eq. (22) yields the gravitational acceleration from an ellipsoidal asteroid.

15.3 Irregular Electrostatic Field

Electrostatic potential around an asteroid is obtained from Eq. (36) as a function of the altitude h and the solar incident angle θ. In the case of a spherical asteroid, there exists an explicit relationship between (h, θ) and the position vector $\boldsymbol{r}$, as presented in Eq. (31). On the other hand, in the case of an ellipsoidal asteroid, there is no such explicit expression because the position vector and the normal vector to the surface are not parallel. Therefore, this subsection derives the implicit relationship (h, θ) and the position vector $\boldsymbol{r}$ to compute the electrostatic potential around an ellipsoid.

An arbitrary position on the surface of the ellipsoid is defined as

$$^B\boldsymbol{R}_s = [x_s, y_s, z_s]^T$$

(65)

Then, these position variables satisfy the equation below.

$$f(x_s, y_s, z_s) = \frac{x_s^2}{R_a^2} + \frac{y_s^2}{R_b^2} + \frac{z_s^2}{R_c^2} - 1 = 0$$

(66)

The normal vector with respect the surface of the ellipsoid at (x_s, y_s, z_s) can be derived as follows:

$$^B\boldsymbol{n} = \left[\frac{\partial f}{\partial x_s}, \frac{\partial f}{\partial y_s}, \frac{\partial f}{\partial z_s}\right]^T = \left[\frac{2x_s}{R_a^2}, \frac{2y_s}{R_b^2}, \frac{2z_s}{R_c^2}\right]^T, \qquad ^B\widehat{\boldsymbol{n}} = \frac{^B\boldsymbol{n}}{|^B\boldsymbol{n}|}$$

(67)

where $\widehat{\boldsymbol{n}}$ represents a unit normal vector. The position vector can be expressed by the following equation:

$$^B\boldsymbol{r} = {}^B\boldsymbol{R}_s + h \cdot {}^B\widehat{\boldsymbol{n}}$$

(68)

Coordinate transformation from the asteroid body-fixed coordinate to the Hill coordinate yields the equations below.

$$^{H}\boldsymbol{r} = {}^{H}\boldsymbol{C}_B{}^{B}\boldsymbol{r}, \qquad {}^{H}\widehat{\boldsymbol{n}} = {}^{H}\boldsymbol{C}_B{}^{B}\widehat{\boldsymbol{n}}$$

(69)

Finally, the solar incident angle can be calculated as

$$\theta = \cos^{-1}\left(-{}^{H}\widehat{\boldsymbol{n}} \cdot {}^{H}\widehat{\boldsymbol{d}}\right)$$

(70)

where ${}^{H}\widehat{\boldsymbol{d}} = [1, 0, 0]^{\mathrm{T}}$. Based on these equations, h and θ can be calculated implicitly, which can be expressed as follows:

$$h = f_1(t, x, y, z)$$
$$\theta = f_2(t, x, y, z)$$

(71)

Note that these implicit functions are time dependent because the coordinate transformation ${}^{H}\boldsymbol{C}_B$ is a function of the asteroid rotation phase θ_{rot}. Once h and θ are obtained from Eq. (71), the electrostatic potential around an ellipsoidal asteroid can be computed based on Eq. (49). The calculation process described above is presented in Figure 85.
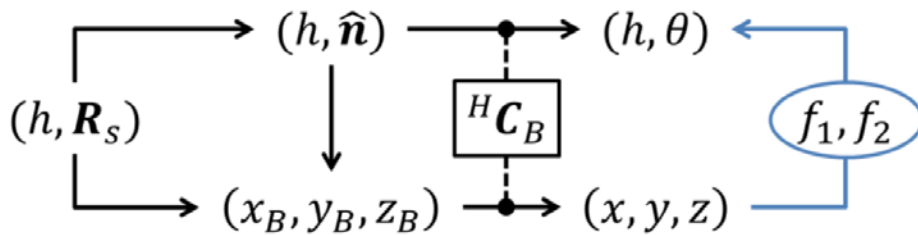
Figure 85. Calculation process of the altitude and the solar incident angle for an ellipsoid

(a) $\theta_{rot} = 0$ deg   (b) $\theta_{rot} = 30$ deg

(a) $\theta_{rot} = 60$ deg   (b) $\theta_{rot} = 180$ deg
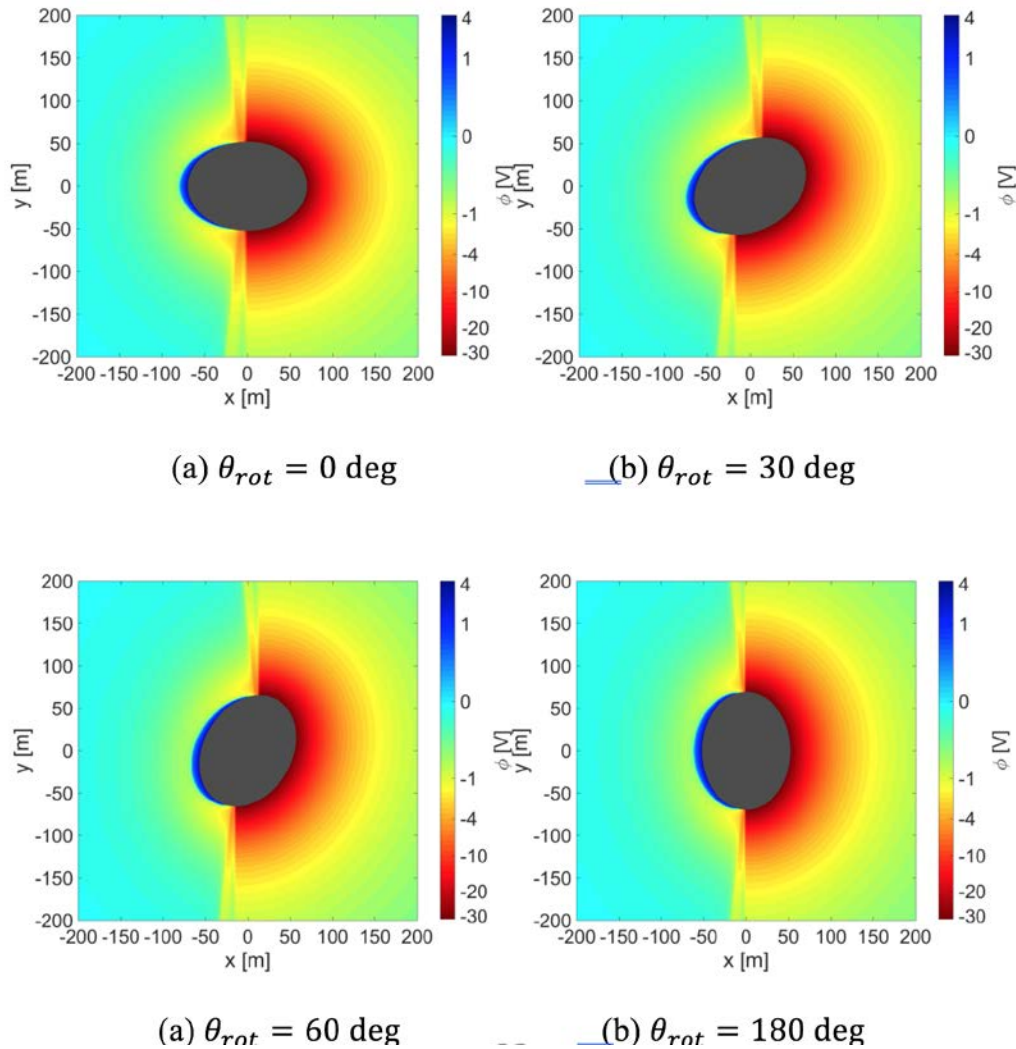
Figure 86. Electrostatic potential around the ellipsoidal asteroid

Figure 86 provides simulation results of the electrostatic potential around an asteroid modelled as a triaxial ellipsoid with an axis ratio of $R_a : R_b : R_c = 2.0 : 1.5 : 1$. The electrostatic potentials were calculated for four different rotation angles. These figures demonstrate that a time-varying irregular electrostatic field has been successfully simulated based on the proposed method. It appears that the structure of the electrostatic potential changes dynamically in accordance with the rotation phase of the asteroid. Moreover, this analysis method is performed by mapping an electrostatic potential from a spherical coordinate to an ellipsoidal coordinate based on the geometrical relationship between them; therefore, it can

emulate the time-varying behavior with relatively low computational cost compared with the classical particle-in-cell method [Han2016, Yu2016].

15.4 *Orbital Motion around an Irregularly Shaped Asteroid*

Figure 87 provides the simulation results of the orbital motion of an E-Glider around an ellipsoidal asteroid. The initial position and velocity used in these simulations is that of the periodic orbit solution around a spherical asteroid which is depicted in Figure 87(a). The equation of motion is the same as the one used for a spherical asteroid, but the gravitational potential U_G and the electrostatic potential ϕ are replaced by the model incorporating the irregular-shape effects, as discussed in Subsection 15.2 and 15.3. Note that the directions of asteroids illustrated in Figure 87 merely show the initial states of them, and the asteroids are rotating with respect to the Hill coordinate.

Figure 87(a) shows the case for an asteroid with a relatively small oblateness, such as Bennu and Ryugu (1999 JU3) [Nolan2013, Bellerose2010]. Although the simulated orbit is perturbed from the reference orbit, the position of the spacecraft after one period is close to the initial position. This result demonstrates that electrostatic orbits obtained in Section 14 can serve as good approximations around a nearly spherical asteroid. On the other hand, the simulation result for an asteroid with a highly irregular shape, such as Itokawa, is depicted in Figure 87(b). It is evident that the spacecraft escapes from the asteroid and is pushed away in the anti-sun direction by the SRP.

In conclusion, it has been demonstrated that the motion around an irregularly shaped asteroid is perturbed because of the irregular gravitational and electrostatic field effects, and the perturbations might cause escape or collision in the worst case scenario. This problem can be solved with two different approaches. The first one is to re-design a reference orbit by taking into account the effects of the shape irregularity. The other approach would be the implementation of feed-back control of the electrostatic force. The magnitude of forces acting on the spacecraft orbiting around the ellipsoidal asteroid is presented in Figure 88 which corresponds to the simulation provided Figure 87(a). Here, the labels "J2" and "J4" represent the higher-order gravitational forces due to the $J_2(=-C_{20})$ and $J_4(=-C_{40})$ terms, respectively. As observed from this figure, the electrostatic force is stronger than the higher-order gravity and the SRP force. This result implies the perturbations can potentially be compensated by applying the feed-back control of electrostatic force via the spacecraft charge.
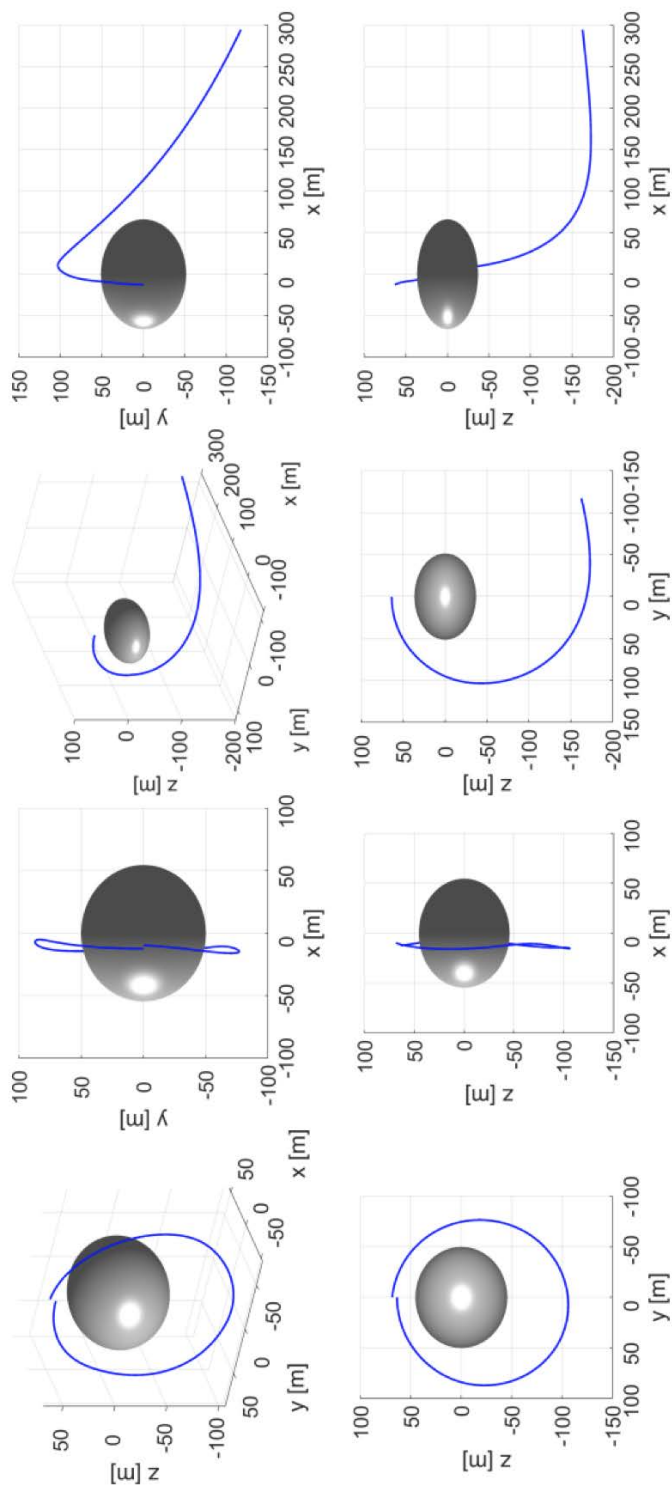
(a) $R_a : R_b : R_c = 1.2 : 1.1 : 1$

(b) $R_a : R_b : R_c = 1.8 : 1.4 : 1$

Figure 87. Orbital motion around an irregularly shaped asteroid
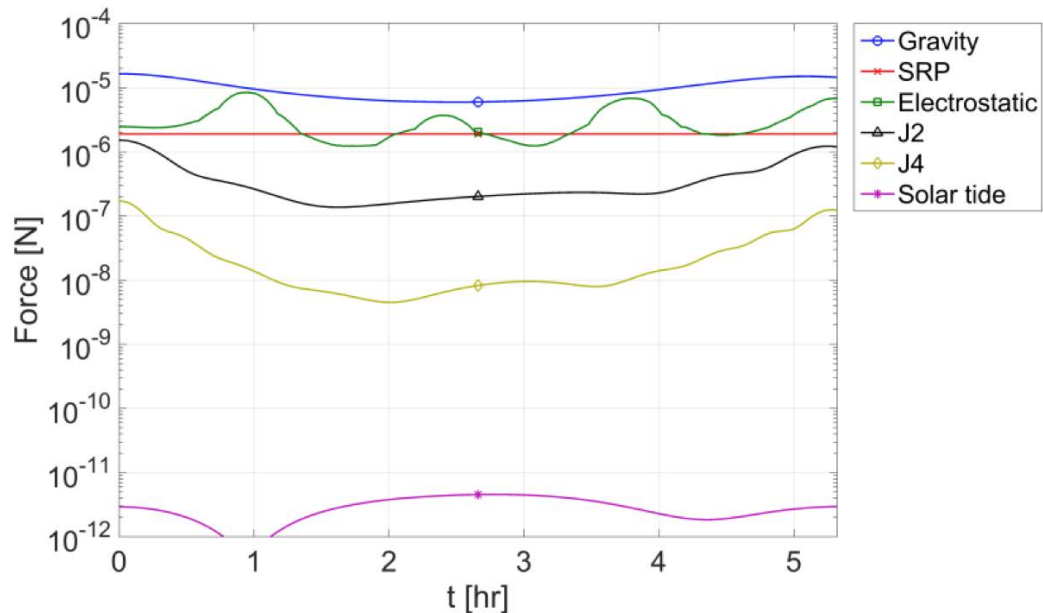
Figure 88. The forces acting on the spacecraft orbiting around the irregularly shaped asteroid

15.   Phase I Findings

Phase I engaged the team expertise to identify the technology tent poles in favor of breadth with a minimum of analytical effort, which instead was left for detailed development in Phase II. The objectives of the Phase I Study were to: a) show that it is actually feasible and determine the mass and optimum form factor of the E-glider; b) lay the ground for the technique of electrostatic cartography; c) develop electrostatic flight mechanics; d) answer key questions such as: is there a sufficient electric field to use for propulsion? How to handle its uncertainty? How big is the payload that can be lifted? How large are the wings? How are the wings deployed? and d) define the elements of a small testbed for experiments to be done in Phase II. The work plan included the following steps: 1) analyze the known environmental conditions of the electrostatics of the levitated dust on airless bodies; 2) develop science-driven mission concepts for the E-Glider, focusing on robotic missions to small bodies, with a mission scenario involving an electrostatic glider maneuvering above the surface of a

reference asteroid such as Itokawa; 3) this would also results in determining requirements for this system: candidate methodologies for E-Glider deployment and retrieval, energy required for reconfiguration, relaying data back to a rover or to an orbiter, etc. 4) as part of the preliminary engineering assessment, perform calculations for electrostatic system shape and material properties to provide the above, analyze means to actuate the wings for environmental survivability and methodologies for thermal control, determine E-glider vehicle configurations, and specific methods for energy harvesting, mobility, communication, survivability, and science instruments.

The Phase I findings are the following:

- The resulting rough estimates of levitated masses are shown in Figure 8 assuming an effective Debye length of 2.5 meters. If the asteroid surface E-fields are low around 5V/m, it would take about 19kV to levitate 1kg of mass. In contrasts, considering the terminator regions shown in Figure 3 with 50V/m of E-fields, the 1kg mass can be levitated using only 2kV.

- Figure 9 illustrates that there are optimal wing sizes that provide the largest payload mass for a given E-Glider potential.

- The resulting trade-space for power analyses is illustrated in Figure 11. Due to the high density and the photo-electron sheath and associate small Debye length, significant power is required to levitate even a few kilo-grams. The power requirement are in the kilo-Watt range to maintain a constant charge level.

- We assumed that the E-Glider never lands, but ejects a number of charged probes, which are the ones to touch the surface of the small body for science data collection and surface locomotion. This was discussed in Section 8. A preliminary probe design using inflated dielectric elastomeric material, already under advanced development in other laboratories, has been proposed.

- The ejected probes are expected to deform their spherical shape by differentially charging the dielectric elastomer in the walls. Upon volumetric deformation, this deformed shape should conform to the surface of the airless body, in a predominantly micro-gravity environment, and "roll" on the surface by internal means. The probe will be comprised of several DEA panels that can be individually actuated. The internal structure of the probe will be inflated pneumatically to a positive pressure to establish the shape of the probe. DE activation will control bulging of the individual

DE panels, allowing the probe to roll with directional control. Since the surface of small bodies is expected to be highly charged, the polarity of the external DEA panels can be controlled to attract (via opposite charge) or repel (via like charges) the surface of the body. This concept will be further explored in Phase II.

- A sensitivity analysis of the trajectory of the delivered probes is discussed in section 12.1. This analysis was done considering values of electric field of $E_0 = $ [1 10 100 1000] V/m, system charge of $q_b = $ [1 10 100 1000] μC, and local plasma Debye length of $\lambda_d = $ [0.1 1 10 100] m. This analysis indicates that the number of bounces, the direction of flight, and the height of the rebound are highly dependent on the field parameters, and need to be taken into consideration for the design of the trajectory of an object in close proximity to the surface. Future work in Phase II will further analyze this behavior in light of the vehicle geometry, attitude, and varying charge distribution.

- The approach for autonomous navigation is based on distributed sensing and actuation. Through an array of Langmuir probes, which measure the spatial distribution of the charges surrounding the vehicle, an "electrostatic map" is thus generated. Once the electric potential has been mapped, the E-glider is able to use this "electrostatic topographic map" for path planning and navigation. Further articulation at the root of the lateral strands or inflated membrane wings, would generate a component of lift depending on the articulation angle, hence a selective maneuvering capability which, to all effects, would lead to electrostatic (rather than aerodynamic) flight. We have proposed a methodology to estimate the charge distribution around the vehicle, and use it for navigation.

- Two distinct types of operations have been presented, namely electrostatic hovering and electrostatic orbiting. It has been demonstrated that both of these methods allow the dayside operation without requiring any fuel. Therefore, the electrostatic flight around asteroid offers significant advantages against conventional methods based on the natural dynamics, from the perspective of mass budget, optical observation, solar power generation, and thermal design.

- By inducing the electrostatic force, several different artificial equilibrium points around an asteroid can be created, including the dayside equilibrium that cannot be observed in the natural dynamics. The electrostatic hovering can be achieved by placing a spacecraft at these artificial equilibrium points, and it could potentially be

an option for the proximity operation around asteroids. However, the power analyses showed that the electrostatic hovering on the dayside requires at least 10 kW level of power, based on our current model.

- A new class of periodic orbits, called electrostatic periodic orbits, was successfully designed. These orbits exist on the dayside of an asteroid, requiring only few watts of power for some cases.

- The specific impulse of the E-Glider was found to be extremely higher than conventional propulsion systems. From these observations, the electrostatic orbiting strategy appears to be promising for asteroid mission concepts.

- We demonstrated that an electrostatic periodic orbit solution can serve as a good approximation for an asteroid with a relatively small oblateness. Although an asteroid with a highly irregular shape perturbs the orbital motion significantly, possible approaches to this problem were also proposed, including the feed-back control of the spacecraft charge.

- Testing approaches are discussed in Section 11. They include inflation tests of the wings of the E-Glider in a variety of configurations, experiments on the actuation needed to articulate them at the root, and tests of coupled translation and attitude changes when the wings are structurally changed. Some of these tests will be conducted in a vacuum environment, such as the JPL vacuum bell jar, or the vacuum chamber in the USC plasma lab.

- Simulation studies are also discussed in Section 12. JPL has developed the Dynamics Simulator for Entry, Descent and Landing (DSENDS) [DSENDS2002] as a high-fidelity spacecraft simulator for Entry, Descent, and Landing (EDL) on planetary and small astronomical bodies. We used this simulator and its advanced visualization capabilities to develop advanced simulations of the trajectory of the E-Glider in very complex gravity fields such as the microgravity environment around Itokawa. These simulations will be further developed in Phase II, with the addition of the electrostatic coupling effects, such as those described in Section 15, which will provide an excellent platform to test E-Glider mission operations in a realistic environment.

16.   Next Steps

Figure 89 gives an overview of the tasks covered in Phase I and those planned for Phase II. In Phase I we started to spec the testbed that will be developed in Phase II. At this time, we have identified an approach to electrostatic navigation, identified a preliminary electrostatic charge required for levitation of the vehicle, and defined the approach to differentially charge the surfaces so that electro-maneuvering can be achieved. The next steps (in Phase II) will include small scale ground tests in vacuum chamber, high-fidelity plasma particle-in-cell simulation of vehicle flying immersed in dusty plasma around asteroid, and large scale physics-based flight mechanics simulation including more accurate details of the vehicle shape.   Ultimately, we would like to demonstrate the E-Glider performance in flight with cubesat on the Moon's surface. Consequently, in Phase II, we will explore the possibility of generating physical simulations with approximate models of the E-glider, including their energy harvesting, mobility, and comm., mechanisms, and elaborate the mission concepts developed in Phase I into detailed scenarios and requirements.

Task	Phase I	Phase II
Concept definition for Small Body application	✔	
Electrostatic dust environment characterization	✔	✖
Autonomy/Maneuverability assessment	✖	✖
Electromechanical actuation assessment	✖	
Determination of key miniaturization requirements for science instruments	✔	
System trades	✖	✖
Preliminary assessment of simulation needs	✔	
Demonstration of flight system performance in simulation		✖
PIC plasma simulations in charged environment		✖
Proposed experimental efforts	✖	
Identify technology gaps for selected architectures, roadmap	✖	
E-Glider prototype		✖

Figure 89. Phase I and Phase II plans.

17.   Publications and Patents

This final report will be made available as a NIAC report in the public domain. In addition, the paper *Active Electrostatic Flight for Airless Bodies*, will be presented at the IEEE Aerospace Conference, Big Sky, MT, March 2017, and we are planning to submit two journal papers based on the work described in Sections 6, and 7, and Sections 13, 14, and 15. We also submitted two NASA Tech briefs: *Electrostatic glider for planetary exploration* (NTR 50039), and *Electrostatic cartography and estimation for autonomous navigation in a sea of charges* (JPL NTR 50259).

18.   Conclusions

Exploration of comets, asteroids, moons and planetary bodies is limited by mobility on those bodies. The E-Glider concept directly addresses the "All Access Mobility" Challenge, one of the NASA's Space Technology Grand Challenges, specifically aimed at enabling robotic operations and mobility, in the most extreme environments of our solar system. In our work to date, we have: a) started to gain insight into physics of electrostatic levitation in plasma environment; b) explored analytical solutions and investigated critical parameters for levitation under restrictive assumptions; c) designed 3D CAD model of E-Glider; d) implemented an E-Glider simulation in DSENDS to investigate dynamics in non-spherical micro-gravity; e)   identified what type of science investigations E-glider could perform; f) introduced an approach for autonomy.   Future work will include: further developing the simulation model, refining the E-Glider system design, improving the levitation model with plasma physics, continuing the analytical studies to gain insight in the engineering behavior, developing approaches for path-planning and navigation, and conceiving plans to build and test a prototype at a later phase of the project.

We have proposed the E-Glider as a novel flight mechanism around asteroids, utilizing the electrostatic field around them. Two distinct types of operations have been presented, namely electrostatic hovering and electrostatic orbiting. It has been demonstrated that both of these methods allow the dayside operation without requiring any fuel. Therefore, the electrostatic flight around asteroid offers significant advantages against conventional methods based on the natural dynamics, from the perspective of mass budget, optical observation, solar power generation, and thermal design.

By inducing the electrostatic force, several different artificial equilibrium points around an asteroid can be created, including the dayside equilibrium that cannot be observed in the natural dynamics. The electrostatic hovering can be achieved by placing a spacecraft at these artificial equilibrium points, and it could potentially be an option for the proximity operation around asteroids. However, the power analyses showed that the electrostatic hovering on the dayside requires at least 10 kW level of power, based on our current model.

For this reason, the electrostatic orbiting method was also discussed as an alternative strategy for an E-Glider operation. A new class of periodic orbits, called electrostatic periodic orbits, was successfully designed. These orbits exist on the dayside of an asteroid, requiring only few watts of power for some cases. Moreover, the specific impulse of the E-Glider was

found to be extremely higher than conventional propulsion systems. From these observations, the electrostatic orbiting strategy appears to be promising for asteroid mission concepts.

Finally, the effects of shape irregularity of an asteroid, including the irregular gravitational field and the irregular electrostatic field, have been formulated and evaluated. As a result, it has been demonstrated that an electrostatic periodic orbit solution can serve as a good approximation for an asteroid with a relatively small oblateness. Although an asteroid with a highly irregular shape perturbs the orbital motion significantly, possible approaches to this problem were also proposed, including the feed-back control of the spacecraft charge.

Consequently, we have clarified that the electrostatic flight method using an E-Glider can be useful for asteroid missions and exhibits intriguing and valuable dynamic characteristics.

In summary, the E-Glider will: a) open new avenues for low-cost, persistent, reconnaissance of airless bodies without interacting with the surface for locomotion, leading to effective prospecting of mineral-rich asteroids before reaching the surface to collect samples; b) provide a framework for the effective use of the coupling between the naturally existing electrostatic environment and gossamer extended surfaces as a novel mechanism for locomotion and exploration in airless bodies; c) enable new sampling techniques for in-situ spatial and temporal sensing of the environment around airless bodies, and d) lead to new concepts for robotic exploration of planets, natural satellites, and other bodies by taking advantage of existing natural plasma and charge distributions. There are other aerospace benefits: we'll have invented a new area of spacecraft technology, namely electrostatic flight technology, which will allow NASA to circumnavigate, map, and reconnoiter airless bodies at low cost, and to do unconventional in-situ science without necessarily landing on surface. E-Glider may also lead to new forms of transportation on the Earth.

Other potential spinoffs include an extended maglev vehicle, new types of electric vehicles for Earth, and the possibility of reducing the cost for launch, with benefits for future sample return mission concepts. E-Glider is also inspired on the ballooning spider, hence there is a biomorphic component. The ground test levitation experiments that will be done in Phase II will undoubtedly shed light on the intriguing physics of spider silk and motion in the presence of the Earth's static atmospheric electric field.

19.   References

[Abell2012] Abell, P. A.: Analysis of Strategic Knowledge Gaps associated with potential Hu-man missions to the Martian system, Report to the Small Bodies Assessment Group. 2012.

[Aplin2011] Aplin, et al.: Asteroid electrostatic instrumentation and modeling, Journal of Phys-ics: Conference Series 301 (2011) 012008, doi:10.1088/1742-6596/301/1/012008.

[Artusi2011] M. Artusi, M. Potz, J. Aristiźabal, C. Menon, S. Cocuzza, and S. Debei, "Electroactive elastomeric actuators for the implementation of a deformable spherical rover," IEEE/ASME Trans. Mechatronics, vol. 16, no. 1, pp. 50–57, 2011.

[Bellerose2010] J. Bellerose and H. Yano, "Dynamics of Asteroid 1999 JU3: Target of the Hayabusa Follow-on Mission," Transactions of JSASS Aerospace Technology Japan, Vol. 8, No. ists27, p. Tk_23–Tk_28, 2010.

[Broschart2005] S. B. Broschart and D. J. Scheeres, "Control of Hovering Spacecraft Near Small Bodies: Application to Asteroid 25143 Itokawa," Journal of Guidance, Control, and Dynamics, Vol. 28, No. 2, pp. 343–354, 2005.

[Broschart2010] S. B. Broschart, D. J. Scheeres, and B. F. Villac, "New Families of Multi-Revolution Terminator Orbits near Small Bodies," Advances in the Astronautical Sciences, Vol. 135, No. 3, pp. 1685–1702, 2010.

[Broschart2013] S. B. Broschart, G. Lantoine, and D. J. Grebow, "Characteristics of Quasi-Terminator Orbits near Primitive Bodies," 23rd AAS/AIAA Spaceflight Mechanics Meeting, Kauai, HI, AAS Paper 13-335, 2013.

[Chow2016] P. Chow, J. Hughes and H. Schaub, "Automated Sphere Geometry Optimization For The Volume Multi-Sphere Method," AAS Spaceflight Mechanics Meeting, Napa Valley, California, February 14–18, 2016. Paper No. 16-472.

[Carpi2005] Carpi, F., et al., "Electroactive Polymers: New Materials for Spacecraft Structures," European Conference on Spacecraft Structures, Materials & Mechanical Testing 2005, Noordwijk, The Netherlands, May 10 - 12, 2005.

[Carpi2007]   F. Carpi, A. Tralli, D. De Rossi, and P. Gaudenzi, "Martian jumping rover equipped with electroactive polymer actuators: A preliminary study," IEEE Trans. Aerosp. Electron. Syst., vol. 43, no. 1, pp. 79–92, 2007.

[Castillo2012] Castillo-Rogez, J.C. and J.I. Lunine, "Astrobiology: The Next Frontier," Part IV, Chapter 10, Small Habitable Worlds, Ed. by Chris Impey, Cambridge University Press, 2012.

[Colwell2005] J. E. Colwell, A. A. S. Gulbis, M. Horányi, and S. Robertson, "Dust transport in photoelectron layers and the formation of dust ponds on Eros," Icarus, Vol. 175, No. 1, pp. 159–169, 2005.

[Davis2004] V. A. Davis, M. J. Mandell, B. M. Gardner, I. G. Mikellides, L. F. Neergaard, D. L. Cooke, and J. Minow, "Validation of NASCAP-2k Spacecraft-Environment Interactions Calculations," presented at 8th Spacecraft Charging Technology Conference, Huntsville, Alabama, in NASA Technical Reports Server, 2004.

[Decadal2011] Committee on the Planetary Science Decadal Survey, National Research Council of the National Academies, Vision and Voyages for Planetary Science in the Decade 2013–2022, National Academies Press, Washington, DC, 2011. The National Academies Press, 400 pp., http://www.nap.edu/catalog.php?record_id=13117

[DeRossi2004] D. De Rossi, F. Carpi, G. Jeronimidis, P. Gaudenzi, A. Tralli, V. Zolesi, and M. Ayre, "Electro-active polymers for actuation and sensing in space applications," Int. Astronaut. Fed. - 55th Int. Astronaut. Congr. 2004, vol. 3, no. October 2016, pp. 1991–2001, 2004.

[DSENDS2002] Balaram, J., Austin, R., Banerjee, P., Bentley, T., Henriquez, D., Martin, B., McMahon, E., Sohl, G.: "DSENDS - A High-Fidelity Dynamics and Spacecraft Simulator for Entry, Descent and Surface Landing," IEEE 2002 Aerospace Conf., Big Sky, Montana, March 9-16, 2002.

[Dubowsky2006] S. Dubowsky, J. Plante, and P. Boston, "Low cost micro exploration robots for search and rescue in rough terrain," … Safety, Secur. Rescue …, 2006.

[Dubowsky2005] S. Dubowsky, K. Iagnemma, S. Liberatore, D. M. Lambeth, J. S. Plante, and P. J. Boston, "A concept mission: Microbots for large-scale planetary surface and subsurface exploration," AIP Conf. Proc., vol. 746, no. 2005, pp. 1449–1458, 2005.

[Fujiwara2006] A. Fujiwara et al., "The Rubble-Pile Asteroid Itokawa as Observed by Hayabusa," Science, Vol. 312, No. 5778, pp. 1330–1334, 2006.

[Garrett2004] Garrett, H., Minow, J.: Charged particle effects on solar sails - an overview, Solar Sail Technology and Applications Conference, Greenbelt, Maryland, September 28 - 29, 2004.

[Giancotti2014a] M. Giancotti, S. Campagnola, Y. Tsuda, and J. Kawaguchi, "Families of Periodic Orbits in Hill's Problem with Solar Radiation Pressure: Application to Hayabusa 2," Celestial Mechanics and Dynamical Astronomy, Vol. 120, No. 3, pp. 269–286, 2014.

[Giancotti2014b] M. Giancotti, "Stable Orbits in the Proximity of an Asteroid: Solutions for the Hayabusa 2 Mission," Ph.D. Dissertation, Department of Astronautics, Electrical and Energetics Engineering, Univ. of Rome "La Sapienza," Rome, 2014.

[Goertz1989] Goertz, C.K., 1989. Dusty plasmas in the Solar System. Rev. Geophys. 27 (2), 271–292.

[Gorham2013] Gorham, P.: Ballooning Spiders: The Case for Electrostatic Flight, eprint arXiv:1309.4731

[Han2015] Daoru Han, "PARTICLE-IN-CELL SIMULATIONS OF PLASMA INTERACTIONS WITH ASTEROIDAL AND LUNAR SURFACES," PhD Dissertation, University of Southern California, August, 2015.

[Han2016] D. Han, J. Wang, and X. He, "A Nonhomogeneous Immersed-Finite-Element Particle-in-Cell Method for Modeling Dielectric Surface Charging in Plasmas," IEEE Transactions on Plasma Science, Vol. 44, No. 8, pp. 1326–1332, 2016.

[Harzell2011] Hartzell, C.M., and Scheeres, D.J.: The Role of Cohesive Forces in Particle Launching on the Moon and Asteroids, Planetary and Space Sciences, vol. 59, 2011, pp. 1758-1768.

[Harzell2013] Hartzell, C.H., and Scheeres, D.J.: Dynamics of Levitating Dust Particles Near Asteroids and the Moon, Journal of Geophysical Research: Planets, vol. 118, 2013, pp. 116-125.

[Harzell2008] C. M. Hartzell , "The Dynamics of Near-Surface Dust on Airless Bodies," Ph.D. Dissertation, Department of Aerospace Engineering Sciences, University of Colorado Boulder, Boulder, CO, 2008.

[Havnes1987] O. Havnes, C. K. Goertz, G. E. Morfill, E. Grün, and W. Ip, "Dust Charges, Cloud Potential, and Instabilities in a Dust Cloud Embedded in a Plasma," Journal of Geophysical Research, Vol. 92, No. A3, pp. 2281–2287, 1987.

[Henon1969] M. Hénon, "Numerical Exploration of the Restricted Problem. V. Hill's Case: Periodic Orbits and Their Stability," Astronomy and Astrophysics, Vol. 1, No. 1, pp. 223–238, 1969.

[Hirata2012] N. Hirata and H. Miyamoto, "Dust Levitation as a Major Resurfacing Process on the Surface of a Saturnian Icy Satellite, Atlas," Icarus, Vol. 220, No. 1, pp. 106–113, 2012.

[Ip1986] Ip, W.H., 1986. Electrostatic charging and dust transport at Mercury's surface. Geophys. Res. Lett. 13, 1133–1136.

[Jeong2008] H. Jeong, "Kinetic Simulations of Spacecraft Charging and Plasma Interactions in the Solar Wind," Ph.D. Dissertation, Department of Aerospace Engineering, Virginia Polytechnic Institute and State University, Blacksburg, VA, 2008.

[Johnson2007] Johnson, A., et al: A General Approach to Terrain Relative Navigation for Planetary Landing, AIAA paper 2007-2854, AIAA Infotech@Aerospace 2007 Conference and Exhib-it, 7 - 10 May 2007, Rohnert Park, California

[King2002a] L. B. King, G. G. Parker, S. Deshmukh, and J. Chong, "A Study of Inter-Spacecraft Coulomb Forces and Implications for Formation Flying," 38th AIAA/ASME/SAE/ASEE Joint Propulsion Conference and Exhibit, Indianapolis, IN, AIAA Paper 2002-3671, 2002.

[King2002b] L. B. King, G. G. Parker, S. Deshmukh, and J. Chong, "Spacecraft Formation-flying using Inter-vehicle Coulomb Forces," NASA/NIAC Technical Report, 2002.

[Kobrick2014] Kobrick et al, : Overview of Instruments for Investigating Dust Interactions on Small Solar System Bodies by Landers and Rovers, ICES-2014-257, 2014.

[Kominato2006] T. Kominato, M. Matsuoka, M. Uo, and J. Kawaguchi, "Optical Hybrid Navigation and Station Keeping around Itokawa," AIAA/AAS Astrodynamics Specialist Conference and Exhibit, Keystone, CO, AIAA Paper 2006-6535, 2006.

[Koon2011] W. S. Koon, M. W. Lo, J. E. Marsden, and S. D. Ross, Dynamical Systems, the Three-Body Problem and Space Mission Design, Marsden Books, 2011.

[Kryszczyńska2007] A. Kryszczyńska, A. La Spina, P. Paolicchi, A. W. Harris, S. Breiter, and P. Pravec, "New findings on asteroid spin-vector distributions," Icarus, Vol. 192, No. 1, pp. 223–237, 2007.

[Koren1991] Y. Koren, J. Borenstein, "Potential Field Methods and Their Inherent Limitations for Mobile Robot Navigation," Proceedings of the 1991 IEEE International Conference on Robotics and Automation, Sacramento, California – April 1991.

[Lee1996] Lee, P., Dust Levitation as Asteroids, Icarus, 124, 181-194 (1996)

[Lochmatter2007] Lochmatter, P.: Development of a shell-like electroactive polymer (EAP) actuator, ETH PhD Thesis, 2007.

[MacMillan1958] MacMillan, W.D., Theory of the Potential, Dover, 1958.

[Mandell2006] M. J. Mandell, V. A. Davis, B. M. Gardner, I. G. Mikellides, D. L. Cooke, and J. Minor, "NASCAP-2k—An Overview," Transactions on Plasma Science, vol. 34, no. 5, pp. 2084–2093, 2006.

[Mendis1981] Mendis, D.A., Hill, J.R., Houpis, H.L.F., Whipple Jr., E.C., 1981. On the electrostatic charging of the cometary nucleus. Astrophys. J. 249, 787–797.

[Menon2009] C. Menon, F. Carpi, and D. De Rossi, "Concept design of novel bio-inspired distributed actuators for space applications," Acta Astronaut., vol. 65, no. 5–6, pp. 825–833, 2009.

[Miyamoto2007] Miyamoto, H., H. Yano, D.J. Scheeres, et al., Science, 316, 1011-1014 (2007).

[Nitter1998] T. Nitter, O. Havnes, and F. Melandsø, "Levitation and dynamics of charged dust in the photoelectron sheath above surfaces in space," Journal of Geophysical Research, Vol. 103, No. A4, pp. 6605–6620, 1998.

[Nolan2013] M. C. Nolan et al., "Shape model and surface properties of the OSIRIS-REx target Asteroid (101955) Bennu from radar and lightcurve observations," Icarus, Vol. 226, No. 1, pp. 629–640, 2013.

[Ono2016] G. Ono et al., "Generalized Attitude Model for Momentum-Biased Solar Sail Spacecraft," Journal of Guidance Control and Dynamics, Vol. 39, No. 7, pp. 1491–1500, 2016.

[Parness2011] Parness, A., "Anchoring Foot Mechanisms for Sampling and Mobility in Micro-gravity," presented at the IEEE International Conference on Robotics and Automation, Shanghai, China, May 2011.

[Pelrine1998] R. E. Pelrine, R. D. Kornbluh, and J. P. Joseph, "Electrostriction of polymer dielectrics with compliant electrodes as a means of actuation," Sensors Actuators A Phys., vol. 64, no. 1, pp. 77–85, 1998.

[Pfau2001] S. Pfau and M. Tichy, Low Temperature Plasma Physics: Fundamental Aspects and Applications. Wiley, Berlin, June 2001.

[Plante2007] J.-S. Plante, L. M. Devita, and S. Dubowsky, "A road to practical dielectric elastomer actuators based robotics and mechatronics: discrete actuation," Proc. SPIE 6524,

Smart Struct. Mater. 2007 Electroact. Polym. Actuators Devices, vol. 6524, pp. 652406-652406–15, 2007.

[Poppe2011] A. R. Poppe , "Modeling, Theor etical and Obser vational Studies of the Lunar Photoelectron Sheath," Ph.D. Dissertation, Department of Physics, University of Colorado Boulder, Boulder, CO, 2011.

[Potz2010] M. Potz, M. Artusi, M. Soleimani, C. Menon, S. Cocuzza, and S. Debei, "Rolling dielectric elastomer actuator with bulged cylindrical shape," Smart Mater. Struct., vol. 19, no. 12, p. 127001, 2010.

[Quadrelli2012] Quadrelli, B.M., H. Mazhar, and D. Negrut, "Modeling and Simulation of An-choring Processes for Small Body Exploration," presented at the AIAA SPACE 2012 Conference & Exposition, 2012.

[Quadrelli2013] Quadrelli et al.: Guidance, Navigation, and Control Technology Assess-ment for Future Planetary Science Missions: Part III. Surface Guidance, Navigation, and Control (GN&C), Report No. JPL D-78106, April 2013.

[Quadrelli2004a] Quadrelli, B.M., Kowalchuck, S., and Chang, J.: Dynamics and Control of a Herd of Sondes Guided by a Blimp on Titan, presented at the 14th AAS/AIAA Space Flight Mechanics Meeting, Maui, Hawaii, February 8-12 2004.

[Quadrelli2004b] Quadrelli M.B., Zimmermann, W., Chau, S.: System Architecture for a Guided Herd of Robots for Surface/Sub-Surface Exploration of Titan, presented at the 2004 IEEE Aerospace Conference, Big Sky, MT.

[Quadrelli2017] M. B. Quadrelli, H. Garrett, J. Castillo, A. Stoica, M. Ono, D. Lusso, and H. Schaub, "Active Electrostatic Flight For Airless Bodies," IEEE Aerospace Conference, Big Sky, MT, 2017. (scheduled)

[Reif1999] J. H. Reif, H. Wang, "Social Potential Fields: A Distributed Behavioral Control for Autonomous Robots," Robotics and Autonomous Systems 27 (1999) 171-194.

[Renno2008] Renno, Kok: Electrical Activity and Dust Lifting on Earth, Mars, and Beyond, Space Sci Rev (2008) 137: 419–434 DOI 10.1007/s11214-008-9377-5

[Schaub2003] H. Schaub, G. G. Parker, and L. B. King, "Challenges and Prospects of Coulomb Spacecraft Formations," AAS John L. Junkins Astrodynamics Symposium, College Station, TX, AAS Paper 03-278, 2003.

[Schaub2014] Schaub, H. and Sternovsky, Z., "Active Space Debris Charging for Contactless Electrostatic Disposal Maneuvers," Advances in Space Research, Vol. 43, No. 1, 2014, pp. 110–118, doi:10.1016/j.asr.2013.10.003.

[Scheeres1994] D. J. Scheeres, "Satellite Dynamics about Asteroids," Advances in the Astronautical Sciences, Vol. 87, No. 1. pp. 275–292, 1994.

[Scheeres1999] D. J. Scheeres, "Satellite Dynamics about Small Bodies: Averaged Solar Radiation Pressure Effects," Journal of the Astronautical Sciences, Vol. 47, No. 1, pp. 25–46, 1999.

[Scheeres1998] D. J. Scheeres, S. J. Ostro, R. S. Hudson, E. M. Dejong, and S. Suzuki, "Dynamics of Orbits Close to Asteroid 4179 Toutatis," Icarus, Vol. 132, No. 1, pp. 53–79, 1998.

[Scheeres2007] D. J. Scheeres, "Orbit mechanics about small asteroids," 20th International Symposium on Space Flight Dynamics, Annapolis, ME, Paper ISSFD 2007/21-2, 2007.

[Scheeres2002] D. Scheeres and F. Marzari, "Spacecraft Dynamics in the Vicinity of a Comet," Journal of the Astronautical Sciences, Vol. 50, No. 1, 2002.

[Scheeres2012] D. J. Scheeres, Orbital Motion in Strongly Perturbed Environments, Springer-Verlag, Berlin, 2012.

[Seubert2014] Seubert, R.C., Stiles, L.A., and Schaub, H., "Effective Coulomb Force Modeling For Spacecraft In Earth Orbit Plasmas," Advances in Space Research, Vol. 54, No. 2, 2014, pp. 209–220. doi:10.1016/j.asr.2014.04.005

[Seydel2010] R. Seydel, Practical Bifurcation and Stability Analysis, Springer-Verlag, New York, 2010.

[SMAD2005] W. J. Larson, J. R. Wertz, Space Mission Analysis and Design (Third Edition), Microcosm Press, El Segundo, 2005.

[Stiles2010] Stiles, L., et al., "Electrostatic Inflation of Membrane Space Structures," AAS/AIAA Astrodynamics Specialist Conference, Toronto, Canada, Aug. 2–5, 2010. Paper No. AIAA-10–8134.

[Stiles2011] Stiles and Schaub, "Voltage Requirements for Electrostatic Inflation of Gossamer Space Structures," 12th AIAA Gossamer Systems Forum, Denver, Colorado, April 4–7, 2011.

[Stiles2012] Stiles, Seubert and Schaub, "Effective Coulomb Force Modeling in a Space Environment," AAS Spaceflight Mechanics Meeting, Charleston, January 29 – February 2, 2012.

[Seeni2010] Seeni, A., B. Schafer, and G. Hirzinger, Robot Mobility Systems for Planetary Sur-face Exploration – State-of-the-Art and Future Outlook: A Literature Survey, Ed. by A.T. Arif, Aerospace Technology Advancements, January 2010.

[Stubbs2005] Stubbs et al: A Dynamic Fountain Model for Lunar Dust, LPI, 2005.

[US2013] US Patent 8,511,616 B2, August 20, 2013, Solar Powered Excess Electron Emission Device.

[Vladimirov2005] Vladimirov, et al.: Physics and Applications of Complex Plasmas, Imperial College Press, 2005.

[Wait2010] K. W. Wait, P. J. Jackson, and L. S. Smoot, "Self locomotion of a spherical rolling robot using a novel deformable pneumatic method," Proc. - IEEE Int. Conf. Robot. Autom., pp. 3757–3762, 2010.

[Whipple1981] Whipple, E. C., "Potentials on Surfaces in Space," Rep. Prog. Phys, Vol. 44, No. 11, 1981, pp. 1197–1250.

[Yoshida2009] Yoshida, K., "Achievements in Space Robotics," IEEE Robotics & Automation Magazine 16(4): 20–28, December 2009.

[Yu2016] W. Yu, D. Han, and J. J. Wang, "Numerical Modeling of Dust Dynamics Around Small Asteroids," AIAA SPACE 2016 Conference and Exposition, Long Beach, CA, AIAA Paper 2016-5447, 2016.